

AD _____

Award Number: DAMD17-99-1-9191

TITLE: Molecular Mechanisms of Estrogen and Antiestrogen Resistance

PRINCIPAL INVESTIGATOR: Robert R. Clarke, Ph.D.

CONTRACTING ORGANIZATION: Georgetown University Medical Center
Washington, DC 20057

REPORT DATE: July 2003

TYPE OF REPORT: Final

PREPARED FOR: U.S. Army Medical Research and Materiel Command
Fort Detrick, Maryland 21702-5012

DISTRIBUTION STATEMENT: Approved for Public Release;
Distribution Unlimited

The views, opinions and/or findings contained in this report are those of the author(s) and should not be construed as an official Department of the Army position, policy or decision unless so designated by other documentation.

20031216 053

REPORT DOCUMENTATION PAGE

Form Approved
OMB No. 074-0188

Public reporting burden for this collection of information is estimated to average 1 hour per response, including the time for reviewing instructions, searching existing data sources, gathering and maintaining the data needed, and completing and reviewing this collection of information. Send comments regarding this burden estimate or any other aspect of this collection of information, including suggestions for reducing this burden to Washington Headquarters Services, Directorate for Information Operations and Reports, 1215 Jefferson Davis Highway, Suite 1204, Arlington, VA 22202-4302, and to the Office of Management and Budget, Paperwork Reduction Project (0704-0188), Washington, DC 20503

1. AGENCY USE ONLY (Leave blank)			2. REPORT DATE July 2003	3. REPORT TYPE AND DATES COVERED Final (1 Jul 1999 - 30 Jun 2003)
4. TITLE AND SUBTITLE Molecular Mechanisms of Estrogen and Antiestrogen Resistance			5. FUNDING NUMBERS DAMD17-99-1-9191	
6. AUTHOR(S) Robert R. Clarke, Ph.D.				
7. PERFORMING ORGANIZATION NAME(S) AND ADDRESS(ES) Georgetown University Medical Center Washington, DC 20057 E-Mail: clarker@georgetown.edu			8. PERFORMING ORGANIZATION REPORT NUMBER	
9. SPONSORING / MONITORING AGENCY NAME(S) AND ADDRESS(ES) U.S. Army Medical Research and Materiel Command Fort Detrick, Maryland 21702-5012			10. SPONSORING / MONITORING AGENCY REPORT NUMBER	
11. SUPPLEMENTARY NOTES				
12a. DISTRIBUTION / AVAILABILITY STATEMENT Approved for Public Release; Distribution Unlimited			12b. DISTRIBUTION CODE	
13. ABSTRACT (Maximum 200 Words) This is an Academic (Career Development) Award. Consistent with this award, the PI continues to "...appraise critically the state of the science in a particular aspect of breast cancer research and to forge new avenues of investigation." In this application, the studies are focused on antiestrogen resistance. With respect to the career development aspects, several original studies and reviews relevant to this application have been published, others have been submitted for publication. We continue to apply state-of-the-art technologies to addressing resistance, including the development of novel approaches to data mining and analysis. The studies of interferon regulatory factor-1 (IRF-1) continue. We have now completed the initial studies of the IRF-1 dominant negative IRF-1 construct. Immunohistologic methods for correlative studies on human breast tissues for nucleophosmin, NFkB, IRF-1 and X-box binding protein -1 (hXBP-1) have been completed on an initial study population. Several applications for funding arising directly from these studies have been submitted to NIH and DOD.				
14. SUBJECT TERMS Estrogens, antiestrogens, hormone resistance, gene expression microarrays, tissue microarrays			15. NUMBER OF PAGES 67	
			16. PRICE CODE	
17. SECURITY CLASSIFICATION OF REPORT Unclassified	18. SECURITY CLASSIFICATION OF THIS PAGE Unclassified	19. SECURITY CLASSIFICATION OF ABSTRACT Unclassified	20. LIMITATION OF ABSTRACT Unlimited	

NSN 7540-01-280-5500

Standard Form 298 (Rev. 2-89)
 Prescribed by ANSI Std. Z39-18
 298-102

FOREWORD

Opinions, interpretations, conclusions and recommendations are those of the author and are not necessarily endorsed by the U.S. Army.

 Where copyrighted material is quoted, permission has been obtained to use such material.

 Where material from documents designated for limited distribution is quoted, permission has been obtained to use the material.

 Citations of commercial organizations and trade names in this report do not constitute an official Department of Army endorsement or approval of the products or services of these organizations.

X In conducting research using animals, the investigator(s) adhered to the "Guide for the Care and Use of Laboratory Animals," prepared by the Committee on Care and use of Laboratory Animals of the Institute of Laboratory Resources, national Research Council (NIH Publication No. 86-23, Revised 1985).

X For the protection of human subjects, the investigator(s) adhered to policies of applicable Federal Law 45 CFR 46.

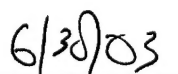
N/A In conducting research utilizing recombinant DNA technology, the investigator(s) adhered to current guidelines promulgated by the National Institutes of Health.

N/A In the conduct of research utilizing recombinant DNA, the investigator(s) adhered to the NIH Guidelines for Research Involving Recombinant DNA Molecules.

N/A In the conduct of research involving hazardous organisms, the investigator(s) adhered to the CDC-NIH Guide for Biosafety in Microbiological and Biomedical Laboratories.



PI - Signature



Date

Table of Contents

Cover.....	1
SF 298.....	2
Foreword.....	3
Table of Contents.....	4
Introduction.....	5
Body.....	5
Key Research Accomplishments.....	8
Reportable Outcomes.....	8
Conclusions.....	13
References.....	
Appendices.....	14

INTRODUCTION

This was an Academic Award (Career Development Award). The purpose of this application was to free additional time for the Principal Investigator to *“..appraise critically the state of the science in a particular aspect of breast cancer research and to forge new avenues of investigation.”* The PI continues to apply new, state-of-the-art technologies to identify key endocrine-regulated molecular pathways to apoptosis/proliferation. By identifying key components of these pathways, we may be able to predict response to first-line and crossover antiestrogenic therapies, and/or provide novel therapeutic strategies for antiestrogen resistant tumors.

BODY

This is an Academic Award, for which a detailed research plan was not required. Since the award is to support academic development, the aims are not finite, *i.e.*, restricted only to the time frame or resources provided through this type of award. Furthermore, unlike a R01-style application, the amount of work proposed represents the efforts of a number of individuals and funded grants already active within the PI’s laboratory, and both ongoing and future collaborations with other laboratories. Consistent with this, the proposed work requires substantially more than the time and financial resources provided by a single R01. Without describing the work in this manner, it was unclear how we could address the requirements of this new award category. The aims, amount of work proposed (which must, *e.g.*, go beyond the three year limit to satisfy the award requirements) and time frames were presented, in the original application, with these issues in mind. To prevent duplication and to limit the size of this report, published data are provided in the reprints, rather than being recapitulated in the text, and very preliminary data are described but not shown.

Aim 1: We will expand the MCF7/LCC1 and MCF7/LCC9 databases to a minimum of 30,000 tags/database. We also expect to establish a 30,000 tag database for MCF-7 cells growing with and without 17 β -estradiol. Completion of all four databases will require longer than the three year period, since we also plan to perform functional studies on candidate genes identified from our comparisons of the MCF7/LCC9 and MCF7/LCC1 databases. For the purposes of this application’s duration, we would consider this aim to have been successfully completed once the MCF7/LCC1 and MCF7/LCC9 databases have each reached a size of 30,000 tags. Time: years 1-3.

1. We have completed the initial study and the manuscript was published last year in *Cancer Research* - a reprint is included in the appendix (Gu *et al.* *Cancer Res* 62: 3428-3437, 2002).

Aim 2: We will continue to investigate the functional relevance of those genes/proteins that receive sufficient priority. This will include transient transfection studies with promoter-reporter constructs (for transcription modulating factors) and stable transfactions to assess functional relevance. We also will investigate clinical relevance by exploring expression in breast tumor biopsies, and correlating expression (or lack thereof) with established prognostic variables, *e.g.*, lymph node status, ER expression, S-phase/proliferation, tumor grade, disease free and overall survival and response to endocrine and cytotoxic chemotherapies. For the purposes of this application’s duration, we would consider this aim to have been successfully completed if we can confirm the roles of *NPM*, *NF κ B*, *CRE/hXBP-1* and the *IRF-1* polymorphism. Time: years 1-3.

We have continued our studies focusing on the human X-box binding protein-1 (hXBP-1) and interferon regulatory factor-1 (IRF-1). We have successfully overexpressed hXBP-1 in both MCF-7 and T47D cells and have selected both pooled populations and individual clones of overexpressing cells. We have confirmed overexpression in the MCF-7 cells and will do so shortly in the T47D cells. These models will be used to study further the role of hXBP-1 in endocrine resistance and in affecting breast cancer cell biology in general.

We have made substantial progress with the putative tumor suppressor IRF-1, particularly with our dominant negative (dnIRF-1). Our data now show that we can specifically separate the cell cycle arrest effects of ICI 182,780 (Faslodex; Fulvestrant) from the proapoptotic effects in antiestrogen sensitive cells. Proapoptotic effects of ICI 182,780 are fully ablated in the presence of dnIRF-1, whereas the cell cycle effects are unaffected by dnIRF-1. We have also determined that the regulation of IRF-1 mRNA is endocrine regulated, being inhibited by estradiol and induced by ICI 182,780 in sensitive cells (MCF-7 and T47D). This endocrine regulation is lost in antiestrogen resistant cells. These effects are fully consistent with the ability of IRF-1 to induce a caspase cascade. Of notable importance, the effect, which appears mediated by estrogen receptors, does not affect responsiveness to cytotoxic drugs that also signal to apoptosis through IRF-1, *i.e.*, these drugs still induce apoptosis through IRF-1 mediated signaling.

1. These data were used to support a R01 application to NIH on IRF-1 and endocrine resistance and an IDEA application to DOD on IRF-1 and cytotoxic drug responsiveness.

2. We have completed a draft of the studies of IRF-1 on endocrine resistance, a manuscript on IRF-1 and cytotoxic drug responsiveness is in preparation.

Table: Correlation of IRF-1, XBP-1, and NF κ B expression from tissue microarrays. *Numbers are p-values. (-) = inverse correlation, (+) = direct correlation. IRF-1c = cytoplasmic staining; IRF-1n = nuclear staining; NS=not significant.

	ER α	PgR	IRF-1c	IRF-1n	NF κ B
PgR	0.001 (+)	-	-	-	-
IRF-1c	0.079 (+)	NS	-	-	-
IRF-1n	NS	0.014 (+)	0.088 (-)	-	-
NF κ B	NS	NS	0.002 (+)	0.034 (-)	-
XBP-1	NS	NS	0.001 (+)	0.082 (-)	0.018 (+)

We have also now completed an initial study of the patterns of expression of the nucleophosmin (NPM), IRF-1, hXBP-1 and NF κ B proteins in breast cancer. Using tissue microarrays of 480 cores from 54 breast carcinomas and standard indirect immunoperoxidase procedures for immunohistochemistry, we first confirmed the known co-expression of ER and PgR (see Table). Since IRF-1 is a transcription factor with tumor suppressor activity, we might expect activated protein to be in the nucleus (IRF-1n) and inactive protein to be in the cytosol (IRF-1c) and an inverse expression between IRF-1n and survival factors such as NF κ B and IRF-1. Coexpression of survival/mitogenic activities also might be expected. While some correlations are of borderline significance, we find IRF-1n inversely correlated, and IRF-1c positively correlated, with both NF κ B and XBP-1. We also find coexpression of NF κ B and XBP-1. These data are broadly consistent with the hypothetical gene signaling network we have implicated in driving antiestrogen resistance.

3. These data were used to support an IDEA application to DOD to study the expression patterns of these proteins in cases from the Scottish Adjuvant Tamoxifen Trial.

4. Dr. Yuelin Zhu (postdoctoral fellow) received a prestigious Merck Senior Fellow Award from the Endocrine Society (June, 2003) for his poster presenting this work

Aim 3: We will continue to integrate the emerging experimental data into our molecular transduction schemes, and amend these as appropriate. Clearly, this will require substantial ongoing effort to integrate the studies from the more broad-based projects, *e.g.*, SAGE and gene array, with the more focused and functional studies, *e.g.*, those specifically addressing the function of *NPM* and *IRF-1*. Time: years 1-3.

We continue to increase our collaborations with the informatics group at Catholic University of America, which has recently expanded to include researchers at Virginia Tech) and develop new algorithms for studying the transcriptomes of endocrine sensitive and resistant breast cancers.

1. The method described in the previous report has been published (Wang *et al.*, *IEEE Trans Inf Technol Biomed*, 6: 29-37, 2002) - a reprint is included in the appendix.

2. The method for collecting breast biopsies for microarray studies, which was described in the previous report, has been published (Ellis *et al.*, *Clin Cancer Res*, 8: 1155-1166, 2002) - a reprint is included in the appendix.

We also have published a new method for analyzing gene expression microarray data.

3. Liu, *et al.*, *Stat Med*, 21: 3465-3474, 2002 - a reprint is included in the appendix.

We also continue our studies of P-glycoprotein, and have recently published a study of progesterone analogue inhibitors of this efflux pump and an extensive review of P-glycoprotein mediated drug resistance.

4. Leonessa, F., Kim, J.-H., Ghiorghis, A., Kulawiec, R., Hammer, C., Talebian, A. & Clarke R. "C-7 Analogs of progesterone as potent inhibitors of the P-Glycoprotein efflux pump." *J Med Chem*, 45: 390-398, 2002.

5. Leonessa, F. & Clarke, R. "ABC transporters and drug resistance in breast cancer." *Endocr Related Cancer*, 10: 43-73, 2003.

Each of the above aims represent ongoing studies within the PI's laboratory and each will continue beyond the limitations of this award. We will continue to evaluate new methodologies and adapt our approaches and integrative studies in the light of published work from other laboratories. ***In this latter regard, the award specifically allowed the PI to spend more time critically appraising the state of science in the area of resistance to estrogens and antiestrogens in breast cancer.***

Key Research Accomplishments (bulleted)

- Published several manuscripts and reviews on breast cancer, estrogen, antiestrogens and drug resistance (listed below).
- Used data from the studies described in the final report to support two successful breast cancer applications to NIH (as PI: a prestigious Bioengineering Research Partnership award to fund the molecular characterization of breast cancer - R01-CA096483 and as co-PI on a program project to study the effects of the timing of dietary exposure on mammary gland development and breast cancer susceptibility - U54-CA100970).
- Used data from the studies described in the final report to support a successful technology development R21/R33 to NIH (R21/R33-EB000830 Computational decomposition of composite molecular signatures).
- Used data from the studies described in the final report and appended publications to support new applications to NIH and DOD. Thus, An R21/R33 and an R01 have been submitted to NIH and a CTR preproposal was successfully submitted to DOD (full proposal is due in august, 2003).
- Completed a pilot study applying tissue microarrays to human breast cancers and shown the coexpression of several key components of our putative signaling network.
- Submitted a major review (by invitation) on antiestrogen resistance to the journal *Oncogene*.

Reportable Outcomes

Reportable outcomes are presented as A. Manuscripts, Abstracts and Presentations; B. Other Professional Activities; C. Degrees; and D. Funding Applied for Based on Work Supported by this Award.

A. Manuscripts, Abstracts and Presentations

Consistent with the goals of allowing the PI to spend time reevaluating his field, the PI has recently published a major review entitled "Cellular and Molecular Pharmacology of Antiestrogen Action and Resistance" in the peer review journal *Pharmacological Reviews*. A copy of this review and other published articles are included in the appendix. "In press" articles are not included in the appendix.

Manuscripts (published since last annual report)

1. Johnson, M., Kenney, N., Hilakivi-Clarke, L., Singh, S., Chepko, G., Newbold, R., **Clarke, R.**, Sholler, P.F., Lirio, A.A., Foss, C., Trock, B., Paik, S., Stoica, A. & Martin, M.B. "Cadmium mimics the effects of estrogen *in vivo* in the uterus and mammary gland." *Nature Med*, in press.

2. Gu, Z., Lee, Y.R., Skaar, T.C., Bouker, K.B., Welch, J.N., Lu, J., Liu, A., Davis, N., Wang, Y. **& Clarke, R.** "Association of interferon regulatory factor-1, nucleophosmin, nuclear factor- κ B and cAMP response element binding with acquired resistance to Faslodex (ICI 182,780)." *Cancer Res*, 8: 1155-1166, 2002.
3. Ellis, M., Davis, N., Coop, A., Liu, M., Schumaker, L., Lee, R.Y., Srikanchana, R., Russell, C., Singh, B., Miller, W.R., Stearns, V., Pennanen, M., Tsangaris, T., Gallagher, A., Liu, A., Zwart, A., Hayes, D.F., Lippman, M.E., Wang, Y. **& Clarke, R.** "Development and validation of a method for using breast core needle biopsies for gene expression microarray analyses." *Clin Cancer Res*, 8: 1155-1166, 2002.
4. Hilakivi-Clarke, L.A., Cho, E., Cabanes, A., DeAssis, S., Olivo, S., Helferich, W., Lippman, M.E. **& Clarke, R.** "Modulation of pregnancy estrogen levels by maternal dietary exposure to genistein or n-3 polyunsaturated fatty acids and breast cancer risk among female offspring." *Clin Cancer Res*, 8: 3601-3610, 2002.
5. Liu, A., Zhang, Y., Gehan, E. & **Clarke, R.** "Block principal components analysis with application to gene microarray data classification." *Stat Med*, 21: 3465-3474, 2002.
4. Leonessa, F. & **Clarke, R.** "ABC transporters and drug resistance in breast cancer." *Endocr Related Cancer*, 10: 43-73, 2003.
5. Wang, Y., Lu, J., Lee, R. & **Clarke, R.** "Iterative normalization of cDNA microarray data." *IEEE Trans Inf Techol Biomed*, 6: 29-37, 2002.
6. Leonessa, F., Kim, J.-H., Ghiorghis, A., Kulawiec, R. Hammer, C., Talebian, A. & **Clarke R.** "C-7 Analogs of progesterone as potent inhibitors of the P-Glycoprotein efflux pump." *J Med Chem*, 45: 390-398, 2002.
7. Poola, I., **Clarke, R.**, Dewitty, R. & Lafalle, L.D. "Constitutively active and dominant negative ER α isoforms are elevated and ER β is decreased during breast carcinogenesis in African American women." *Cancer*, 94: 615-623, 2002.
8. Welch, J.N. & **Clarke, R.** "ErbB-2 expression and drug resistance in cancer." *Signal*, 3: 4-9, 2002.
9. Zhang, J., Huang, K., Khan, J., Li, K., Bhujwalla, Z., **Clarke, R.**, Gu, Z., Szabo, Z., Xuan, J., & Wang, Y. Computational decomposition of molecular signatures. *Proc Intl Conf Diagnostic Imaging Analysis*, IEEE Press, in press.
10. Wang, Z., Zhang, J., Lu, J., Lee, R., Kung, S.-Y., Clarke R. & Wang Y. Discriminatory mining of gene expression microarray data. *J Signal Process Systems*, in press.
11. Hilakivi-Clarke, L.A., Cabanes, A., Olivo, S., Kerr, L., Bouker, K.B. & **Clarke, R.** "Do estrogens always increase breast cancer risk?" *J Steroid Biochem Mol Biol*, 80: 163-174, 2002.

Award Number: DAMD17-99-1-9191

Principal Investigator: Robert Clarke, Ph.D., D.Sc.

Title: Molecular Mechanisms of Estrogen and Antiestrogen Resistance (Academic Award)

Contracting Organization: Georgetown University School of Medicine, Washington, DC 20057

12. **Clarke, R.** & Dickson, R.B. "Animal models of endocrine responsive and unresponsive breast cancers". In: "*Endocrine Management of Breast Cancer*", Eds: Robertson, J.F.R., Nicholson, R.I. & Hayes, D.F., Martin Dunitz, Ltd, London, U.K., 191-208, 2002.
13. **Clarke, R.**, Liu, M.C., Bouker, K.B., Gu, Z., Lee, R.Y., Zhu, Y., Skaar, T.C., Gomez, B., O'Brien, K., Wang, Y., Hilakivi-Clarke, L.A. "Antiestrogen resistance in breast cancer and the role of estrogen receptor signaling." *Oncogene*, in press.
14. **Clarke, R.** "Human breast cancer xenografts as models of the human disease". In: "*Tumor Models in Cancer Research*", Ed: Teicher, B.A., Humana Press, Inc., New Jersey, pp453-470, 2002.

Abstracts

1. Bouker, K.B., Skaar, T.C., Fernandez, D. **& Clarke, R.** "Antiestrogens regulate IRF-1 expression in sensitive but not resistant breast cancer cells." *Proc Am Assoc Cancer Res* 43: 761, 2002.
2. Zhu, Y., Bouker, K., Skaar, T., Zwart, A., Gomez, B., Hewitt, S., Singh, B., Liu, A. **& Clarke, R.** "High throughout tissue microarray assessment of expressions of progression-related genes - NFKB, nucleophosmin, X-box binding protein-1 and IRF-1 in breast cancer." *Proc Am Assoc Cancer Res* 43: 762, 2002.
3. O'Brien, K.A., Lee, R. **& Clarke, R.** BCL-2 expression and retinoid resistance in breast cancer cell lines." *Proc 85th Annual Meeting Endocrine Society* 414, 2003.
4. Zwart, A., Lee, R.Y., Zhang, J., Wang, J., Wang, Y. **& Clarke, R.** "mRNA profiles from MCF-7 variants are used to predict antiestrogen resistance/responsive phenotypes." *Proc 85th Annual Meeting Endocrine Society* 146, 2003.
5. Lee, R.Y., O'Brien, K.A., Skaar, T.C., Wang, Z., Zhang, Z., Wang, Y. **& Clarke, R.** "Characterization of a novel MCF-7 variant resistant to 4-hydroxyphenyl retinamide and crossresistant to 9-cis-retinoic acid." *Proc 85th Annual Meeting Endocrine Society* 169, 2003.
6. Zhu, Y., Bouker, K., Skaar, T., Gomez, B., Hewitt, S., Singh, B., Liu, A. **& Clarke, R.** "High throughput tissue microarray study of antiestrogen related genes in human breast cancers." *Proc 85th Annual Meeting Endocrine Society* 140, 2003.
7. Lee, R.Y., O'Brien, K.A., Skaar, T.C., Wang, Z., Zhang, Z., Wang, Y. **& Clarke, R.** The gene expression pattern from a novel 9-cis-retinoic acid resistant MCF-7 variant can predict retinoid resistant/responsive phenotype using computational bioinformatics." *Proc 85th Annual Meeting Endocrine Society* 170, 2003.

Award Number: DAMD17-99-1-9191

Title: Molecular Mechanisms of Estrogen and Antiestrogen Resistance (Academic Award)

Contracting Organization: Georgetown University School of Medicine, Washington, DC 20057

Principal Investigator: Robert Clarke, Ph.D., D.Sc.

Presentations

1. Department of Pathology, Wayne State University, Detroit, MI, **U.S.A.** (2003)
2. 12th Breast Cancer Think Tank, St Maarten, Maho Bay, **Dutch Antilles** (2002)
3. Centre de Recherche en Endocrinologie Moléculaire et Oncologique, University of Laval, Québec City, Québec, **Canada** (2001)

B. Other Professional Activities

Study Section Memberships and Other Grant Reviews

1. Appointed Chair, N.I.H. Grant Review Study Section NIH ZAT1 SEP DB (01) Basic Science study section (National Center for Complementary and Alternative Medicine) - 2002-date.
2. Member, American Institute for Cancer Research grant review study section "Panel I" (1990-date).
3. Member, U.S. Army Medical Research and Materiel Command Clinical and Experimental Therapeutics-1 study section (1999-date).
4. Member, Cancer Research Foundation of America's grant review panel (1998-date).
5. Member, N.I.H. Grant Review Study Section ZCA GRB-V (01) that reviewed the Specialized Programs Of Research Excellence (SPORE) applications in Skin Cancer (2003).
6. Member, N.I.H. Grant Review Study Section ZCA SRRB-C Innovative Technologies for the Molecular Analysis of Cancer (2002).
7. Member, N.I.H. Grant Review Study Section NIH ZAT1 E (02) Basic Science for the National Center for Complementary and Alternative Medicine (2001).

Election to Professional Societies

The PI was appointed to the Editorial Board of ***Cancer Genomics and Proteomics*** (new journal in 2003)

The PI was appointed to the Editorial Board of the ***Journal of Steroid Biochemistry and Molecular Biology*** (appointed in 2002)

The PI also was appointed as an Associate Editor of ***Cancer Research*** (noted in previous reports for this award).

Award Number: DAMD17-99-1-9191

Principal Investigator: Robert Clarke, Ph.D., D.Sc.

Title: Molecular Mechanisms of Estrogen and Antiestrogen Resistance (Academic Award)

Contracting Organization: Georgetown University School of Medicine, Washington, DC 20057

The PI was elected as a Fellow of the Royal Society of Medicine (U.K.) in 2001 based on overall contribution to medical research (this is not a medical qualification), including the publications resulting from the work covered in this award.

C. Degrees

In 1999, the Principal Investigator was awarded the degree of Doctor of Science by his *alma mater*, The Queen's University of Belfast (United Kingdom). The D.Sc. degree is awarded for a thesis containing significant research in breast cancer published since award of a Ph.D. degree. In the U.K. and many other countries, a DSc is considered a "higher" degree than a Ph.D. (noted in previous reports for this award).

D. Funding Applied for Based on Work Supported by this Award

In direct support of this application, the PI successfully submitted an IDEA award to the DOD to fund studies into identifying the molecular mechanisms of antiestrogen resistance. In his role as mentor, the PI assisted and encouraged one of his predoctoral fellows to apply to the DOD for funding to study the role of EGF-receptor signaling in resistance to systemic therapies in breast cancer. This also was successfully funded. These applications were described in the first annual report. The following grants have been awarded since the first annual report.

1. **Principal Investigator:** N.I.H. R01-CA096483: "Molecular Analysis of Breast Cancer - Bioengineering Research Partnership Award" This award funds a Bioengineering Research Partnership to study the molecular profiling of recurrent and nonrecurrent breast cancers using several of the technologies described in this report and appended publications.
2. **Co-Principal Investigator** (Principal Investigator; Leena A. Hilakivi-Clarke, Ph.D.): N.I.H. U54-CA100970: "Timing of dietary exposure and breast cancer risk." Dr. Clarke runs a Biostatistics and Microarray Core, co-directs the Administrative Core, and is a coinvestigator on Project-1. This is a cooperative agreement similar to a Program Project Grant to study the effects of the timing of estrogenic and other exposures on the susceptibility of the mammary gland to carcinogenesis.
3. **Principal Investigator:** American Institute for Cancer Research 03A100: "Vitamin E and antiestrogen responsiveness in breast cancer". AICR is considered by NIH to provide peer-reviewed support similar to NIH (as is ACS, DOD, NSF).
4. **Principal Investigator - subcontract:** (Principal Investigator of host grant; Yue Wang, Ph.D.): N.I.H. R21/R33-EB000830: "Computational decomposition of composite molecular signatures". This is an R21/R33 award to study algorithms for the *in silico* partial volume correction of complex tissues (breast biopsies); essentially an *in silico* method for microdissection in gene expression microarray studies.
5. **Principal Investigator:** USAMRMC: IDEA Award BC990358 "Molecular characterization of resistance." This award funds gene microarray analysis of antiestrogen responsive and resistant human breast cancer cell lines.

Award Number: DAMD17-99-1-9191

Principal Investigator: Robert Clarke, Ph.D., D.Sc.

Title: Molecular Mechanisms of Estrogen and Antiestrogen Resistance (Academic Award)

Contracting Organization: Georgetown University School of Medicine, Washington, DC 20057

6. **Co-Principal Investigator:** N.I.H. R21/R33-CA893231: "Intelligent mapping of gene expression profiles" for the further development of supervised/unsupervised data analysis by standard Finite Normal Mixture Modeling using Akaike Information Criterion and Minimal Description Length analyses. This was originally funded as the R21 phase of a R21/R33 - the R33 phase was recently funded by NCI.
7. **Principal Investigator:** NIH SBIR R41-GM61401-01A1 (Subcontract): "Development of multi-receptor LC stationary phases" to study the development of novel methods for identifying P-glycoprotein substrates. Total funds awarded for this subcontract: \$59,800. Principal Investigator: William P. Purcell, PhD; President and CEO, Molecular Design International, Inc. This study was successfully completed.

Conclusions

We have made considerable progress in addressing our proposed aims during the period of the entire award. The time made available to the PI through this Academic Award has resulted in several relevant publications and reviews, the ability to attract significant additional funding related to the research, and the generation of preliminary data that could lead to further publications/grants in the coming years. The PI also continues to participate in other related professional activities. For example, during this award the PI was promoted to full professor with tenure and used the time freed by this award to complete and successfully submit his D.Sc. thesis. He also was appointed to three additional editorial boards, including *Cancer Research*, and was appointed as chair of a NIH Study Section (ZATI SEP DB 01 Basic Science). These professional appointments and continued level of productivity would not have been achieved had this award not been forthcoming.

APPENDICES

AWARD NUMBER: DAMD17-99-1-9191

TITLE: Molecular mechanisms of estrogen and antiestrogen resistance

PRINCIPAL INVESTIGATOR: Robert Clarke, Ph.D., D.Sc.

CONTRACTING ORGANIZATION: Georgetown University Medical Center

Cadmium mimics *in vivo* the effects of estrogen *in vivo* in the uterus and mammary gland

Michael Johnson^{1,5}, Nicholas Kenney^{2,5}, Adriana Stoica^{1,5}, Leena Hilakivi-Clarke¹, Baljit Singh¹, Gloria Chepko¹, Robert Clarke¹, Peter F Sholler¹, Apolonio A Lirio¹, Colby Foss³, Ronald Reiter¹, Bruce Trock¹, Soonmyoung Paik⁴ & Mary Beth Martin¹

It has been suggested that environmental contaminants that mimic the effects of estrogen contribute to disruption of the reproductive systems of animals in the wild, and to the high incidence of hormone-related cancers and diseases in Western populations. Previous studies have shown that functionally, cadmium acts like steroid estrogens in breast cancer cells as a result of its ability to form a high-affinity complex with the hormone binding domain of the estrogen receptor^{1,2}. The results of the present study show that cadmium also has potent estrogen-like activity *in vivo*. Exposure to cadmium increased uterine wet weight, promoted growth and development of the mammary glands and induced hormone-regulated genes in ovariectomized animals. In the uterus, the increase in wet weight was accompanied by proliferation of the endometrium and induction of progesterone receptor (PgR) and complement component C3. In the mammary gland, cadmium promoted an increase in the formation of side branches and alveolar buds and the induction of casein, whey acidic protein, PgR and C3. *In utero* exposure to the metal also mimicked the effects of estrogens. Female offspring experienced an earlier onset of puberty and an increase in the epithelial area and the number of terminal end buds in the mammary gland.

To determine whether *in vivo* exposure to an environmentally relevant dose of cadmium results in estrogen-like activity in target organs, female rats were ovariectomized on postnatal day 28 and allowed to rest for 3 weeks. Rats were then given a single intraperitoneal dose of cadmium (5 µg per kg body weight, or ~27 nmol/kg). The antiestrogen ICI-182,780 was administered intraperitoneally at a dose of 500 µg per kg per d. As a positive control, rats received a pellet of estradiol releasing 60 µg per kg per d. The uterine response was measured 4 d after treatment and the mammary gland response was measured 4 and 14 d later. As expected, there was a 3.8-fold increase in uterine wet weight in the estradiol-treated animals (Table 1). In the cadmium-treated animals, there was a 1.9-fold increase in uterine wet weight that was blocked by the antiestrogen. A similar increase in uterine wet weight was also observed when the animals were given a single intraperitoneal 10-µg/kg dose of cadmium (1.7-fold increase)

or when the animals were ovariectomized on day 40 (1.8-fold increase). Histological examination showed that the cadmium-induced increase in uterine wet weight was due to a mitogenic response and not due to toxicity (Fig. 1). In the ovariectomized control animals, the endometrial lining was flat to cuboidal. No vacuolation or stromal inflammation was observed. In addition, no mitoses were observed in either the endometrial or stromal cells. In the estradiol-treated animals, the endometrial lining showed epithelial hyperplasia and hypertrophy. The endometrial cells were taller and had abundant granular cytoplasm. The surrounding stroma was hypercellular and was infiltrated by numerous eosinophils. Cadmium-treated animals also showed hyperplasia and hypertrophy [AU: Referr to figures here]. In addition, the cells showed abundant subnuclear and supranuclear vacuolation. The stroma was more cellular in the cadmium-treated animals than in the ovariectomized animals and was less cellular than in the animals treated with estradiol. No stromal infiltrate was noted in the cadmium-treated animals. Both estradiol- and cadmium-treated animals showed rare mitoses in the endometrial cells. The ability of the antiestrogen to block the effects of cadmium suggests that the effects of the metal are mediated by the estrogen receptor. There was no evidence of toxicity in the liver or kidney, organs sensitive to the toxic effects of the metal (data not shown), and there was no effect on whole body weight.

Ovarian steroids also have a central role in the growth and development of the mammary gland (reviewed in refs. 3,4). In the rat, estrogens stimulate ductal and stromal proliferation and the secretion of prolactin, which, in turn, regulates lobuloalveolar development. To determine whether cadmium mimics the effects of estrogens in the mammary gland, epithelial density was measured on days 4 and 14 after treatment (Table 1 and data not shown). In the ovariectomized control animals, the mammary gland consisted of a simple ductal network with low epithelial density. After exposure to estradiol, there was a 50% increase in epithelial density on day 4 and 14, the result of an increase in mammary ducts and secretory lobuloalveolar structures. In animals exposed to cadmium, there was also a 50% increase in epithelial density by day 4 and a 30% increase by day 14. The cadmium-induced augmentation was due to a rise in quaternary branching of the ducts as well as an increase in lobuloalveolar structures. In

¹Department of Oncology, Lombardi Cancer Center, Georgetown University, Washington, DC 20007, USA. ²Department of Biology, Hampton University, Hampton, Virginia 23668, USA. ³Department of Chemistry, Georgetown University, Washington, DC 20007, USA. ⁴University of Pittsburgh, Pittsburgh, Pennsylvania 15238, USA. ⁵These authors contributed equally to this work. Correspondence should be addressed to M.B.M. (martinmb@georgetown.edu).

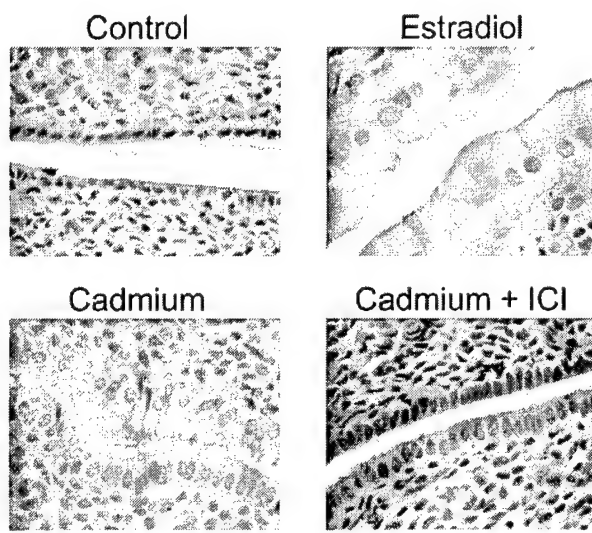


Figure 1 Histological effects of cadmium in the uteri of ovariectomized rats treated with cadmium, estradiol or ICI-182,780 (ICI). Sections were stained with H&E ($\times 200$).

rats treated with the antiestrogen, the epithelial density was not significantly different from control rats but there were fewer secretory structures in the glands of antiestrogen-treated rats [AU:OK?] on day 4, with a more pronounced effect observed on day 14. The antiestrogen also blocked the effects of cadmium on epithelial density and secretory structures, suggesting that the response of the mammary gland to cadmium is mediated by the estrogen receptor. To assess whether cadmium induced a secretory differentiation of the gland, the expression of casein and whey acidic protein were also examined on day 14 (data not shown). In control rats, the mammary gland was devoid of casein, whereas animals treated with estradiol for 14 d synthesized significant amounts of the protein. Casein was found in the ductal lumen, alveolar cells and alveolus. Rats exposed to a single dose of cadmium also synthesized significant amounts of casein. The protein was localized in luminal cells, alveolar cells, alveolus and ductal lumen, with most of the casein immunolocalized in the cytoplasm. Expression of whey acidic protein was also detected but was not as abundant. The ability of cadmium to induce the synthesis of both casein and whey acidic protein indicates that the metal induces milk protein synthesis in the mammary gland.

To determine whether cadmium also mimics the effects of estradiol on gene expression, we measured the amounts of PgR and complement protein C3 mRNA (Fig. 2). In the uterus, estradiol treatment resulted in a 3-fold increase in PgR mRNA and a 124-fold increase in C3 mRNA. Similarly, treatment with cadmium induced a 2-fold increase in PgR mRNA and a 12-fold increase in complement C3 mRNA ($P < 0.001$). In the mammary gland, estradiol induced a 42- and 416-fold increase in PgR mRNA and C3 mRNA, respectively, and cadmium induced a 9-fold increase in PgR mRNA and a 16-fold

increase in C3 mRNA ($P < 0.001$). The increase in PgR and C3 mRNA expression in both organs was blocked by the antiestrogen, providing additional evidence that the effects of cadmium are mediated by the estrogen receptor.

The amount of cadmium [AU: Please refer to Fig. 2] in the uterus and mammary gland was also determined using anodic stripping voltammetry, an electrochemical technique that offers detection limits in the sub-parts-per-billion range⁵. Cadmium was not detected in the organs of control animals but was detectable in most organs of the metal-treated animals. However, the amount of cadmium was too low to accurately quantitate. When detectable in the uterus or mammary gland, the amount of the cadmium was approximately 10^{-2} pg per g tissue (10^{-5} parts per billion).

In utero exposure to estrogens and estrogen-like substances causes early onset of puberty^{6,7} and alters mammary gland development in female offspring^{6,8,9}. To assess the estrogenic effects of cadmium after *in utero* exposure, pregnant rats were given two injections of cadmium intraperitoneally at a dose of either 0.5 or 5 μ g per kg body weight on days 12 and 17 of gestation. Cadmium did not alter pregnancy weight gain, number of pups per litter or birth weights (data not shown). On postnatal day 35, however, female offspring exposed to the lower dose of cadmium had significantly increased body weights (135.8 ± 2.4 g, mean \pm s.e.m.) compared with control offspring (120 ± 2.6 g; $F_{(2,15)} = 13.8$, $P < 0.001$). This temporary increase in weight is consistent with *in utero* exposure to estrogenic compounds¹⁰. Also consistent with *in utero* exposure to low doses of estrogens⁶, there was no difference in uterine wet weight (either crude or adjusted for body weight) between control animals and animals exposed to cadmium (data not shown). *In utero* exposure to cadmium also induced an earlier onset of vaginal opening^{6,7}. Vaginal opening occurred on average on day 30.6 ± 0.6 in control animals, and on day 27.2 ± 1.1 ($P < 0.05$) and day 26.7 ± 1.1 ($P < 0.05$) in animals exposed to cadmium doses of 0.5 and 5 μ g/kg, respectively.

The effects of *in utero* exposure to cadmium on mammary gland development were assessed on postnatal day 35 during the rapid growth phase of the gland. As with perinatal exposure to estrogenic compounds⁶, *in utero* exposure to [AU:OK?] cadmium increased the parenchymal area of the mammary gland and the number of terminal

Table 1 Effects of cadmium on uterine wet weight and mammary gland density in ovariectomized animals

	Uterine weight (day 4)		Mammary gland density		Body weight Grams
	Grams	Fold increase	Day 4	Day 14	
Control	0.075 (± 0.0069 ; $n = 17$)		54.3 (± 2.5 ; $n = 17$)	75.4 (± 1.9 ; $n = 9$)	187 ($n = 9$)
Cadmium	0.14* (± 0.0111 ; $n = 21$)	1.9	82.8*** (± 4.0 ; $n = 20$)	99.8*** (± 2.9 ; $n = 14$)	189 ($n = 12$)
ICI-182,780	0.048 (± 0.0027 ; $n = 13$)	0.64	69.7 (± 3.7 ; $n = 8$)	72.7 (± 2.2 ; $n = 8$)	182 ($n = 10$)
Cadmium + ICI-182,780	0.046 (± 0.0035 ; $n = 11$)	0.61	69.0 (± 5.4 ; $n = 8$)	72.2 (± 2.8 ; $n = 8$)	182 ($n = 8$)
Estradiol	0.284** (± 0.0168 ; $n = 22$)	3.8	84.1*** (± 3.2 ; $n = 20$)	112.6*** (± 6.9 ; $n = 11$)	172 ($n = 10$)

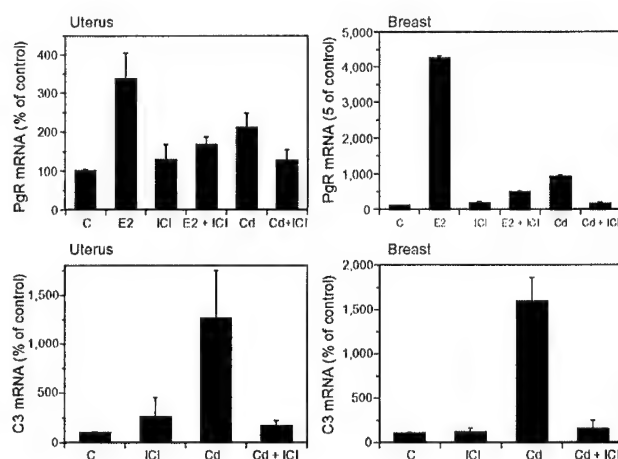
Uterine wet weight and mammary gland density in ovariectomized rats treated with cadmium, estradiol or ICI-182,780. Uterine wet weights and epithelial density are shown as mean \pm s.e.m. *, $P = 0.0001$ compared with control; **, $P < 0.0001$ compared with control. Epithelial density data were analyzed by one-way ANOVA ($F_{(4,68)} = 12.41$, $P < 0.001$ for day 4; $F_{(4,46)} = 20.73$, $P < 0.001$ for day 14). ***, $P < 0.05$ (significantly different from controls).

Figure 2 Effects of cadmium on the expression of PgR and C3 in ovariectomized animals treated with cadmium, estradiol or ICI-182,780. Total RNA was quantified using a real-time PCR assay. Data represent mean \pm s.d. of values from three independent experiments done in duplicate. C, control; E2, estradiol; ICI, ICI-182,780; Cd, cadmium. [AU: Are any of these significant? If so, add * and p values.]

end buds and decreased the number of alveolar buds⁶. The mammary epithelial area was significantly larger, at 70.7 ± 5.2 [AU: UNITS?] and 66.5 ± 7.7 [AU: UNITS?] (mean \pm s.e.m.) in rats exposed to cadmium doses of 0.5 and 5 $\mu\text{g}/\text{kg}$, respectively, compared with 45.5 ± 4.2 [AU: UNITS?] in control rats (Fig. 3a). The mammary glands of rats exposed to the lower dose of cadmium also contained significantly more terminal end buds (12.5 ± 1.0) than control rats (9.4 ± 0.2 ; Fig. 3b). Both doses of cadmium reduced the number of alveolar buds in the mammary gland from 15.0 ± 3.9 in control rats to 7.5 ± 1.5 in rats exposed to the metal (Fig. 3c). The ability of cadmium to mimic the *in utero* effects of estrogens provides additional support that environmentally relevant doses of the metal have potent estrogen-like activities.

To date, most animal studies that have examined the toxic and carcinogenic effects of cadmium have used doses [AU: OK AS EDITED?] in the range of 1–5 mg/kg ($\sim 5\text{--}25 \mu\text{mol}/\text{kg}$)^{11,12}. To mimic human exposure, we used a 1,000-fold lower [AU: ‘FOLD LOWER’ IS AMBIGUOUS—PLEASE GIVE A PERCENTAGE] dose of cadmium, similar to dietary exposures according to the World Health Organization—recommended Provisional Tolerable Weekly Intake of 7 μg per kg body weight per week. [AU: Add reference.] In the United States, Germany, the United Kingdom and Sweden, dietary cadmium exposure is estimated to range from 0.12 to 0.49 μg per kg body weight per d, with the highest exposure occurring in children 1–6 years of age^{13–19}. Cigarette smoking is also an important source of exposure, contributing 2–4 μg of cadmium per pack per d (refs. 20,21).

Exposure to cadmium is also influenced by its long half-life, estimated to range from 10 to 30 years²¹, which may account for its significant accumulation in the body. In newborns, the amount of cadmium is negligible, but by age 30 the body burden can reach 30 mg. In nonsmokers, the concentration of cadmium in the kidney is $\sim 15\text{--}20 \mu\text{g}$ per g tissue, whereas in smokers, the concentration doubles to $30\text{--}40 \mu\text{g}$ per g tissue. High concentrations of cadmium are also present in breast fat of healthy women and breast cancer patients ($20\text{--}30 \mu\text{g}$ per g tissue)²². In stark contrast to human breast tissue, the mammary glands of experimental animals contained approximately 0.01 pg per g tissue. Although present in extremely low amounts, cadmium had profound effects on the growth and development of the gland, suggesting that exposure to the metal may be a potential risk factor for breast cancer. However, the only epidemiological study to



suggest a link between cadmium exposure and breast cancer risk²³ is a hypothesis-generating case-control study based on death certificates coded for occupation and industry. After excluding homemakers, a job exposure matrix was used to estimate the probability of risk for occupational exposure to cadmium and found an odds ratio of 1.07–1.13 among white women and 1.5–2.3 among black women. Further studies are required to substantiate these findings.

The data presented in this study provide strong evidence that cadmium is a potent nonsteroidal estrogen *in vivo*. The ability of environmentally relevant amounts of cadmium to mimic the effects of estradiol suggests that the metal may represent a new class of endocrine disrupters^{1,2,24}. Not all bivalent cations activate the estrogen receptor, however. Zinc, for example, is a bivalent cation that binds to cysteines in the DNA binding domain to form zinc fingers, but does not interact with the hormone binding domain or activate the receptor¹.

METHODS

Animals. Female Sprague-Dawley rats (Harlan) were ovariectomized by the vendor at the age of 28 d and the animals were allowed to recover for 3 weeks before treatment with cadmium, estradiol or the antiestrogen ICI-182,780. Cadmium chloride (Sigma) was dissolved in sterile PBS and administered as a single intraperitoneal injection at a dose of 5 μg per kg body weight ($\sim 27 \text{ nmol}/\text{kg}$). An estradiol 30-d release pellet (Innovative Research of America) was implanted subcutaneously. The antiestrogen ICI-182,780 (Tocris) was dissolved in peanut oil and given intraperitoneally at a dose of 500 μg per kg per d. Animals were killed either 4 or 14 d later and the effects on histology and gene expression were examined.

Pregnant rats were obtained on day 10 of gestation and were individually housed in standard Plexiglas cages. Pregnant animals were injected intraperitoneally with either 0.5 or 5 $\mu\text{g}/\text{kg}$ cadmium or vehicle on days 12 and 17 of

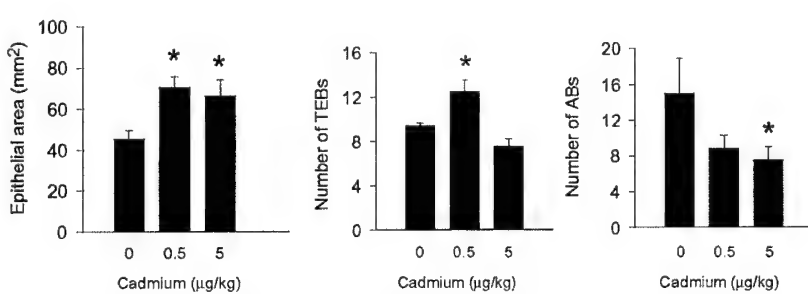


Figure 3 Effect of *in utero* exposure to cadmium on the mammary gland in female offspring. (a–c) Effects of *in utero* exposure to cadmium on mammary epithelial area (a), number of terminal end buds (TEBs; b) and number of alveolar buds (ABs; c). Values represent the mean of six animals per group \pm s.e.m. Data were analyzed by one way ANOVA: $F_{(2,15)} = 5.2$, $P < 0.02$ for epithelial area; $F_{(2,14)} = 11.6$, $P < 0.001$ for TEBs; and $F_{(2,14)} = 2.7$, $P < 0.01$ for ABs. *, $P < 0.05$ (significantly different from controls).

gestation. Two days after birth, the female offspring were cross-fostered. Ten female pups were housed with a lactating dam and were weaned on postnatal day 22. Thereafter, animals were housed in groups of three to five. Vaginal opening was determined by an investigator that was blinded to treatment [AU: OK AS EDITED?]. Data were analyzed by one-way ANOVA followed by Fisher LSD method. These studies were approved by the Georgetown University Animal Care and Use Committee.

Mammary whole mounts. After the animals were sacrificed, the inguinal mammary glands were removed and fixed in ethanol-glacial acetic acid (3:1, vol/vol). The glands were then stained with carmine alum, dehydrated and cleared with xylenes. Mammary epithelial density was determined by outlining a 2.05-cm² section of the midregion of the fourth inguinal gland using NIH Image (National Institutes of Health) [AU: OK?]. In all treatments, epithelial density was inversely proportional to light intensity. Images were then transferred to a Macintosh Power Station and processed using Adobe Photoshop Software. In the *in utero* exposed animals, the terminal end buds and alveolar buds were counted and the area was measured.

Immunohistochemistry. For immunohistochemical examination of casein and whey acidic protein synthesis, 5-μm sections were deparaffinized, washed in Tris-buffered saline (pH 7.6) containing 0.6% Tween 20 (TBS-T; Bio-Rad) and treated with 3% hydrogen peroxide. The sections were then washed and incubated with 10% BSA in TBS-T for 1 h. Sections were again washed in TBS-T and incubated for 2 h at room temperature with antibodies to mouse pancreatic casein (gift from G. Smith, National Cancer Institute) or mouse whey acidic protein (gift from L. Henninghausen, National Institute of Diabetes and Digestive and Kidney Diseases). Peroxidase staining was done using mouse Vectastain kit ABS (Vector Laboratories). [AU: PLEASE INCLUDE A SENTENCE ABOUT WHY YOU USED MOUSE ANTIBODIES (AND WHY IT'S OK) TO DETECT RAT PROTEINS.]

Real-time PCR. Total RNA was extracted from tissue with RNA STAT-60 (Tel-Test) and analyzed using the Platinum qRT-PCR Thermoscript One-Step System (Invitrogen). The reaction was run in the presence of 300 nM of specific primers and 200 nM of fluorescently labeled probes for PgR, C3 and GAPDH, the constitutive control. For the detection of PgR, we used the upper primer 5'-CTCAATGGCTCCCTCAG-3', the lower primer 5'-TGAATCTGGCTCAGTAGTT-3' and the 5-carboxyfluorescein (FAM)-labeled probe 5'-CTCAAGGACAGCCTGCCCCA-3'. For complement C3, we used the upper primer 5'-CTCAGTGACCAAGTGCAGA-3', the lower primer 5'-TCACGATCAGGTGTTCTCAG-3' and the FAM-labeled probe 5'-TTCTCCTGCAAGGACCCCG-3' for quantitation. For GAPDH, we used the upper primer 5'-GAACATCATCCCTGCATCCA-3', the lower primer 5'-CCAGTGAGCTTCCCGTTCA-3' and the Cy5-labeled probe 5'-CTTGGCCCACAGCCTTGGCAGC-3' for measurement of the constitutive control. The reaction conditions were 45 min at 54 °C and 5 min at 95 °C, followed by 50 cycles of 30 s at 95 °C, 30 s at 54 °C and 30 s at 68 °C. Fluorescent data were collected during the 68 °C step using the iCycler iQ Detection System (Bio-Rad). Serial dilutions of RNA from the uterus and mammary gland of an estrogen-treated rat were used as a standard. The data were normalized for GAPDH expression.

Anodic stripping voltammetry assay. The amount of cadmium was determined using an anodic stripping voltammetry assay. In this assay, the tissue were ashed in a muffle furnace at 450 °C for 12–24 h. The ash was then digested with trace metal-grade nitric acid (Fischer), the nitric acid was removed by evaporation to near dryness and the sample was dissolved in distilled water containing mercuric nitrate. The sample was placed in an electrochemical cell containing a working electrode made of glassy carbon, a platinum counter electrode and a pseudoreference electrode made of platinum. The metal analytes were then preconcentrated in the mercury film that forms on the working electrode. After the preconcentration step, the working electrode voltage was scanned in the positive direction at 50–100 mV/s. The oxidative current peak corresponding to cadmium was compared with a standard curve to determine the amount of cadmium in the tissue sample. PARC 270 Electrochemical Analysis Software (EG&G) was used for data analysis and manipulation.

ACKNOWLEDGMENTS

We thank M.E. Lippman for helpful discussions, R. Newbold for helpful discussions and critical reading of the manuscript, and A. Murray, I. Onojafe, G. Montenegro, A. Foxworth, D. Raval and W. Jefferson for technical assistance. This work was supported by National Institutes of Health grant CA70708, Cancer Research Foundation of America, The Susan G. Komen Foundation and an anonymous donation. Support for tissue culture, animal care and histopathology core facilities was provided by P50-CA58185 and P30-CA51008.

COMPETING INTERESTS STATEMENT

The authors declare that they have no competing financial interests.

Received 20 May; accepted 25 June 2003

Published online XX Month 2003; doi:10.1038/nm

1. Garcia-Morales, P. *et al.* Effect of cadmium on estrogen receptor levels and estrogen-induced responses in human breast cancer cells. *J. Biol. Chem.* **269**, 16896–16901 (1994).
2. Stoica, A., Katzenellenbogen, B.S. & Martin, M.B. Activation of estrogen receptor-alpha by the heavy metal cadmium. *Mol. Endocrinol.* **14**, 545–553 (2000).
3. Russo, I.H. & Russo, J. Mammary gland neoplasia in long-term rodent studies. *Environ. Health Perspect.* **104**, 938–967 (1996).
4. Vonderhaar, B.K. [AU: WHAT WAS THE NAME OF THE CHAPTER?] in *Breast Cancer: Cellular and Molecular Biology* (eds. Lippman, M.E. & Dickson, R.B.) 251–294 (Kluwer, Boston, 1988).
5. Heineman, W.R., Mark, H.B., Wise, J.A. & Roston, D.A. [AU: PLEASE GIVE CHAPTER TITLE] in *Laboratory Techniques in Electroanalytical Chemistry* (eds. Kissinger, P.T. & Heineman, W.R.) [AU: PLEASE GIVE PAGE NUMBERS] (Marcel Dekker, New York, 1984).
6. Hilakivi-Clarke, L. *et al.* A maternal diet high in n-6 polyunsaturated fats alters mammary gland development, puberty onset, and breast cancer risk among female offspring. *Proc. Natl. Acad. Sci. USA* **94**, 9372–9377 (1997).
7. Rothschild, T.C., Calhoun, R.E. & Boylan, E.S. Effects of diethylstilbestrol exposure *in utero* on the genital tracts of female ACl rats. *Exp. Mol. Pathol.* **48**, 59–76 (1988).
8. Tamooka, T. & Bern, H.A. Growth of mouse mammary glands after neonatal sex hormone treatment. *J. Natl. Cancer Inst.* **69**, 1347–1352 (1982).
9. Hilakivi-Clarke, L., Cho, E., Raygada, M. & Kenney, N. Alterations in mammary gland development following neonatal exposure to estradiol, transforming growth factor alpha, and estrogen receptor antagonist ICI 182,780. *J. Cell Physiol.* **170**, 279–289 (1997).
10. Sharpe, R.M., Fisher, J.S., Millar, M.M., Jobling, S. & Sumpter, J.P. Gestational and lactational exposure of rats to xenoestrogens results in reduced testicular size and sperm production. *Environ. Health Persp.* **103**, 1136–1143 (1995).
11. IARC International Agency for Research on Cancer Monographs. International Agency for Research for Cancer, Lyon, France (1993). [AU: PAGE NUMBERS, AUTHOR, TITLE?]
12. Waalkes, M.P. Cadmium carcinogenesis in review. *J. Inorg. Biochem.* **79**, 241–244 (2000).
13. Gartell, M.J., Craun, J.C., Podrebarac, D.S. & Gunderson, E.R. Pesticides, selected elements and other chemicals in adult total diet samples. October 1980–March 1982. *J. Assoc. Anal. Chem.* **69**, 146–161 (1986).
14. Gartell, M.J., Craun, J.C., Podrebarac, D.S. & Gunderson, E.R. Pesticides, selected elements and other chemicals in infant and toddler total diet samples. October 1980–March 1982. *J. Assoc. Anal. Chem.* **69**, 123–145 (1986).
15. Moschandreas, D.J. *et al.* Exposure apportionment: ranking food items by their contribution to dietary exposure. *J. Expo. Anal. Environ. Epidemiol.* **12**, 233–243 (2002).
16. Wilhelm, M., Wittsiepe, J., Schrey, P., Budde, U. & Idel, H. Dietary intake of cadmium by children and adults from Germany using duplicate portion sampling. *Sci. Total Environ.* **285**, 11–19 (2002).
17. Muller, M., Anke, M., Illing-Gunther, H. & Thiel, C. Oral cadmium exposure of adults in Germany: 2. Market basket calculations. *Food Addit. Contam.* **15**, 135–141 (1998).
18. Ysart, G. *et al.* 1997 UK Total Diet Study—dietary exposures to aluminium, arsenic, cadmium, chromium, copper, lead, mercury, nickel, selenium, tin and zinc. *Food Addit. Contam.* **17**, 775–785 (2000).
19. Jarup, L., Berglund, M., Elinander, C.G., Nordberg, G. & Vahter, M. Health effects of cadmium exposure—a review of the literature and a risk estimate. *Scand. J. Work Environ. Health* **24** (suppl. 1), 1–51 (1998).
20. Health assessment document of cadmium (EPA-600/8-81, NTIS Pub. PB82-115163). US Environmental Protection Agency, Office of Research and Development (1981).
21. International Agency for Research on Cancer. IARC monographs on the evaluation of carcinogenic risk of chemicals to man (cadmium, nickel, some epoxides, miscellaneous industrial chemicals and general considerations on volatile anaesthetics). [AU: PAGE NUMBERS OR OTHER SERIES INFORMATION?] (World Health Organization, Geneva, 1976).
22. Antila, E., Mussalo-Rauhamaa, H., Kantola, M., Atroshi, F. & Westermark, T. Association of cadmium with human breast cancer. *Sci. Total Environ.* (Netherlands) **186**, 251–256 (1996).
23. Cantor, K.P., Steward, P.A., Brinton, L.A. & Dosemeci, M. Occupational exposures and female breast cancer mortality in the United States. *J. Occup. Med.* (1994).
24. Martin, M.B. *et al.* Estrogen-like activity of metals in MCF-7 breast cancer cells. *Endocrinology* **144**, 2425–2436 (2003).

Association of Interferon Regulatory Factor-1, Nucleophosmin, Nuclear Factor- κ B, and Cyclic AMP Response Element Binding with Acquired Resistance to Faslodex (ICI 182,780)¹

Zhiping Gu,² Richard Y. Lee, Todd C. Skaar,³ Kerrie B. Bouker, James N. Welch, Jianping Lu, Aiyyi Liu, Yuelin Zhu, Natalie Davis, Fabio Leonessa,⁴ Nils Brünner,⁵ Yue Wang, and Robert Clarke⁶

Vincent T. Lombardi Cancer Center and Department of Oncology, Georgetown University School of Medicine, Washington, DC 20007 [Z. G., R. Y. L., T. C. S., K. B. B., J. N. W., A. L., Y. Z., N. D., F. L., R. C.]; Department of Electrical Engineering and Computer Science, The Catholic University of America, Washington, DC 20064 [J. L., Y. W.]; and Finsen Laboratory, Copenhagen, Denmark [N. B.]

ABSTRACT

To identify genes associated with survival from antiestrogens, both serial analysis of gene expression and gene expression microarrays were used to explore the transcriptomes of antiestrogen-responsive (MCF7/LCC1) and -resistant variants (MCF7/LCC9) of the MCF-7 human breast cancer cell line. Structure of the gene microarray expression data was visualized at the top level using a novel algorithm that derives the first three principal components, fitted to the antiestrogen-resistant and -responsive gene expression data, from Fisher's information matrix. The differential regulation of several candidate genes was confirmed. Functional studies of the basal expression and endocrine regulation of transcriptional activation of implicated transcription factors were studied using promoter-reporter assays.

The putative tumor suppressor interferon regulatory factor-1 is down-regulated in resistant cells, whereas its nucleolar phosphoprotein inhibitor nucleophosmin is up-regulated. Resistant cells also up-regulate the transcriptional activation of cyclic AMP response element (CRE) binding and nuclear factor κ B (NF κ B) while down-regulating epidermal growth factor receptor protein expression. Inhibition of NF κ B activity by ICI 182,780 is lost in resistant cells, but CRE activity is not regulated by ICI 182,780 in either responsive or resistant cells. Parthenolide, a potent and specific inhibitor of NF κ B, inhibits the anchorage-dependent proliferation of antiestrogen-resistant but not antiestrogen-responsive cells. This observation implies a greater reliance on their increased NF κ B signaling for proliferation in cells that have survived prolonged exposure to ICI 182,780.

These data from serial analysis of gene expression and gene microarray studies implicate changes in a novel signaling pathway, involving interferon regulatory factor-1, nucleophosmin, NF κ B, and CRE binding in cell survival after antiestrogen exposure. Cells can up-regulate some estrogen-responsive genes while concurrently losing the ability of antiestrogens to regulate their expression. Signaling pathways that are not regulated by estrogens also can be up-regulated. Thus, some breast cancer cells may survive antiestrogen treatment by bypassing specific growth inhibitory signals induced by antagonist-occupied estrogen receptors.

Received 8/31/01; accepted 5/2/02.

The costs of publication of this article were defrayed in part by the payment of page charges. This article must therefore be hereby marked *advertisement* in accordance with 18 U.S.C. Section 1734 solely to indicate this fact.

¹ Supported in part by Public Health Service awards 5R01-CA/AG58022, 5P50-CA58185 (to R. C.), 5R33-CA83231 (to Y. W.) from the National Cancer Institute; Department of Defense Awards DAMD17-99-9189 (to K. B. B.), DAMD17-99-1-9191, BC010619, and BC990358 (to R. C.) from the United States Army Medical Research and Materiel Command; and the American Cancer Society IRG-97-1520-01 (to T. C. S.). Technical services also were provided by the Flow Cytometry and Cell Sorting, and Macromolecular Shared Resources funded through Public Health Service Award 2P30-CA51008 (Vincent T. Lombardi Cancer Center Support Grant).

² Present address: Celera Genomics, 45 West Gude Drive, Rockville, MD 20850.

³ Present address: Indiana University, Department of Medicine, Indianapolis, IN 46202.

⁴ Present address: Laboratory of Clinical Investigation, National Institute on Aging, NIH, 5600 Nathan Shock Drive, Baltimore, MD 21224.

⁵ Present address: United States Patent and Trade Mark Office, Crystal Plaza 3, Washington, DC 20231.

⁶ To whom requests for reprints should be addressed, at Room W405A Research Building, Vincent T. Lombardi Cancer Center, Georgetown University School of Medicine, 3970 Reservoir Road, NW, Washington, D.C. 20007. Phone: (202) 687-3755; Fax: (202) 687-7505; E-mail: clarke@georgetown.edu.

INTRODUCTION

ERs⁷ are nuclear transcription factors, their activities being affected by the nature of the ligand bound and the pattern of genes/proteins expressed within cells (cellular context; Ref. 1). Antiestrogens compete with endogenous estrogens for activation of ER, and induce both cell cycle arrest and apoptosis in responsive cells (2). Neither the genes regulated by antiestrogens that signal to apoptosis nor those genes that confer an acquired antiestrogen resistance have been identified. Nonetheless, antiestrogenic drugs are effective in both premenopausal and postmenopausal breast cancer patients, and in the metastatic and adjuvant settings (3). The most widely used antiestrogen in current clinical practice is the triphenylethylene TAM. Clinical experience with this drug likely now exceeds 10 million patient years. When patients with metastatic disease are selected for treatment based on the ER and PgR content of their tumors, responses are seen in up to 75% of tumors expressing both receptors (2). TAM also reduces the incidence of ER-positive breast cancers in high risk women (4).

Other antiestrogens have emerged recently, most notably the benzothiophene Raloxifene and the steroidal ICI 182,780 (Faslodex). Both drugs appear to have significant clinical activity and may have better toxicological profiles when compared with TAM (2). Faslodex has significant activity in TAM-resistant patients (5), consistent with data obtained previously with TAM-resistant human breast cancer cells selected *in vitro* (6).

Despite the utility of antiestrogens, most tumors that initially respond to these drugs will recur and require alternative systemic therapies (2). Unfortunately, the precise mechanisms that confer resistance remain unknown. Change to an antiestrogen-stimulated phenotype has been described in some animal models (6, 7). This phenotype may occur in up to 20% of breast cancer patients but a loss of responsiveness to antiestrogens may be the more common phenotype (2). The expression of mutant ER proteins and splice variants has been reported but the functional role of these in endocrine resistance remains unclear (2). Most tumors acquiring antiestrogen resistance do so while retaining expression of ER (8). Thus, whereas lack of ER expression is a major form of *de novo* antiestrogen resistance, other mechanisms must be active in most instances of acquired resistance (2). The persistent expression of ER in tumors with acquired resistance suggests that some cells expressing this phenotype may either require ER expression and/or reflect the altered expression of otherwise estrogen-regulated genes.

Because ER-mediated transcription is directly affected by antiestrogens, we initially hypothesized that antiestrogen resistance might include perturbations in the patterns of expression and/or regulation of

⁷ The abbreviations used are: ER, estrogen receptor; CRE, cyclic AMP response element; CCS-IMEM, improved minimal essential medium supplemented with 5% charcoal calf stripped serum; EGF-R, epidermal growth factor receptor; IRF-1, interferon regulatory factor-1; NPM, nucleophosmin; PgR, progesterone receptor; SAGE, serial analysis of gene expression; TAM, Tamoxifen; XBP-1, X-box binding protein-1; FACS, fluorescence-activated cell sorting; NF κ B, nuclear factor κ B; EGR-1, early growth response factor-1; TNF α , tumor necrosis factor α .

a subset of all of the ER-regulated genes (1). To address this hypothesis, we first generated a novel series of human breast cancer variants from the MCF-7 human breast cancer cell line. These cells have different growth requirements for estrogen and exhibit differential sensitivities to TAM and ICI 182,780 (9–11). In this study, we focus on MCF7/LCC1 cells (estrogen-independent, TAM-responsive, and ICI 182,780 responsive) and MCF7/LCC9 cells (estrogen-independent, ICI 182,780 resistant, and TAM cross-resistant; Ref. 11). Because the cells exhibit comparable cell cycle profiles⁸ and are both MCF-7 variants, we can exclude the altered expression of genes related solely to differences in both genetic background and cell cycle distribution. A direct comparison of these respective transcriptomes should identify genes associated with survival from long-term antiestrogen exposure.

Several techniques are now available to explore the transcriptomes of tumors and experimental models. However, the most effective approach remains a matter of debate (12). Studies in breast cancer have been limited, most simply attempting to identify the genes expressed in breast cancers. For example, a recent study by Perou *et al.* (13) explored data from excisional breast biopsies from 42 individuals. Gene clusters, identified by exploration of the data structure, include those associated with ER, HER-2, and IFN-induced genes. A similar cluster of IFN-regulated genes was identified in the breast cancer cell lines included in the NIH drug screening program (14). Studies comparing the gene expression profiles of specific breast cancer phenotypes include an examination of histologically different samples from single breast cancer lesion (15) and a preliminary analysis of a TAM-stimulated xenograft model (16). None of these reports directly addressed either the function or potential role of the specific genes identified. We have used two different but complementary approaches, SAGE and gene expression microarrays. These approaches would not be expected to provide identical data because not all of the genes identified by SAGE are on the microarrays, some genes identified on the cDNA arrays may be confounded by cross-hybridization to homologous RNAs, and the ability to detect significant differences between the SAGE databases is affected by the relative abundance of the tags and the size of the databases. We approached both technologies as means to sample the transcriptomes of MCF7/LCC1 and MCF7/LCC9 cells, and to generate data that would allow us to begin testing our hypothesis implicating estrogen-regulated genes in antiestrogen resistance. We now show that cells can survive prolonged antiestrogen treatment by altering the expression, patterns of regulation, and functional activation of specific estrogen-regulated genes.

MATERIALS AND METHODS

Cell Lines. MCF7/LCC1 cells were derived from the estrogen-dependent MCF-7 human breast cancer cell line after selection for growth in ovariectomized nude mice (9, 17). MCF-7/LCC9 cells were obtained by an *in vitro* stepwise selection of the estrogen-independent but antiestrogen-responsive MCF7/LCC1 cells against the steroidal antiestrogen ICI 182,780 (Faslodex). MCF7/LCC9 cells are ICI 182,780 resistant and TAM cross-resistant, express ER and PgR, and exhibit an estrogen-independent but responsive phenotype (11). MCF7/LCC1 and MCF7/LCC9 cells were routinely passaged in Improved Minimal Essential Medium without phenol red (Biofluids, Bethesda, MD) supplemented with 5% CCS-IMEM. Serum was stripped of endogenous estrogens as described previously and is estimated to contain ≤ 10 fM estrogen (18). Vehicle for all of the hormone/antihormone treatments was ethanol (final concentration $<0.1\%$ v/v). All of the cell cultures were maintained at 37°C in a humidified 5% CO₂:95% air atmosphere and shown to be free of contamination with *Mycoplasma* species as determined by solution hybridization to

Mycoplasma-specific, radiolabeled, RNase riboprobes (Gen-Probe Inc., San Diego, CA).

SAGE Analyses. SAGE was performed as described previously (19). Polyadenylic acid mRNA was harvested from cells using biotin labeled-oligonucleotidyl acid magnetic beads (Promega PolyATract System 1000 kit; Promega, Madison, WI) and treated with DNase I enzyme to remove any contaminating DNA. mRNA (5 μ g) was converted to double-stranded cDNA using the Life Technologies, Inc. cDNA Synthesis kit (Life Technologies, Inc., Rockville, MD). Biotinylated cDNA was completely cleaved with Nia III and the 3'-end digested fragments extracted with magnetic streptavidin beads. The cDNA was evenly divided and ligated, one half to linker A and the other half to linker B (19). Cleavage of the cDNA by BsmF1 produced 11–13 bp oligo DNA tags with linkers, which were blunt-ended with T4 polymerase. Linkers A and B were ligated together to form ditags, which were then amplified by PCR using primers to linkers A and B. Ditags (22–26 bp) were gel purified and ligated into concatenated polytags. The polytags were purified and cloned into the SphI-digested pZeo1 vector, which was transferred to competent TOP10F' cells by electroporation. Positive clones were selected overnight at 37°C for growth on low-salt Luria-Bertani bacterial plates supplemented with Luria-Bertani-Zeocin (50 μ g/ml) and isopropyl β -D-thiogalactopyranoside (1 mM). Colonies were screened for plasmids containing appropriate inserts by size fractionating PCR products, obtained using M13 forward and reverse primers, in agarose gels. PCR products containing concatamers of >600 bp were purified and sequenced.

Characteristics of the SAGE databases are shown in Table 1. We compared the MCF7/LCC1 and MCF7/LCC9 databases, using the SAGE version 1.00 software (kindly provided by Dr. K. W. Kinzler, Johns Hopkins University, Baltimore, MD), to identify putatively differentially expressed genes. Only a representative sample of these can be presented. The genes presented in Table 2 were primarily selected based on: (a) fold difference ≥ 2 -fold; (b) that the Tags compared should represent ≤ 2 genes; and (c) that a Tag found in either the MCF7/LCC1 and/or MCF7/LCC9 SAGE libraries must represent $\geq 0.10\%$ of the database. Evidence that a gene was already known to be expressed in breast cancers also was considered. None of these criteria were considered an absolute requirement for gene selection. Whereas 2-fold was selected as the cutoff, biologically critical events can be controlled by genes that exhibit a fold regulation as small as 50% (20). As described recently by Man *et al.* (21), χ^2 analyses were used to compare the proportions of specific tags in each database.

RNA Isolation, Generation of Probes, and Hybridization of Gene Microarrays. Each probe was generated from an independent cell culture, each culture being grown on a different day but using identical cell culture conditions. Six MCF7/LCC1 and five MCF7/LCC9 cell cultures were used. RNA was isolated from proliferating, subconfluent monolayers of each cell line using the TRIzol reagent (Life Technologies, Inc., Grand Island, NY). RNA quality was determined by standard spectroscopic and gel electrophoresis analyses.

Probes for the Clontech Atlas gene microarrays (Clontech, Palo Alto, CA) were made as described by the manufacturer. Briefly, 1 μ g of DNase-treated mRNA was primed with the Clontech cDNA Synthesis Primer mix. The product was reverse transcribed into radiolabeled cDNA with [γ -³²P]dATP (Amersham Life Science Inc., Arlington Heights, IL), and the reaction incubated at 50°C for 25 min and terminated by adding 0.1 M EDTA (pH 8.0). Radiolabeled cDNA was purified and eluted through a NucleoSpin Extraction Column (centrifuged at 14,000 rpm). The cDNA probe was denatured with 1

Table 1 Characteristics of the SAGE libraries from MCF7/LCC1 and MCF7/LCC9 cells

Characteristics of SAGE libraries	Tags ^a	Gene hits
Tags sequenced from MCF7/LCC1 cells	12,816 ^b	5,783
Tags sequenced from MCF7/LCC9 cells	11,109 ^b	1,170
Number of Tags identified	10,518	208
Number of known Tags ^c	7,221	38
Number of unknown Tags	3,297	10

^a Number of Tags representing a corresponding number of gene hits, e.g., 5,783 Tags are specific for single genes, whereas 208 Tags could identify up to 3 genes each.

^b Number of Tags in each SAGE database.

^c Includes expression sequence tags.

⁸ R. Clarke, unpublished observations.

Table 2 Differentially expressed genes identified in the MCF7/LCC1 and MCF7/LCC9 SAGE libraries

Putative gene ^a	Unigene no.	MCF7/LCC1	MCF7/LCC9	Difference ^b	P ^c	Gene function
N-ras-related gene	Hs.260523	2	20	10-fold	<0.001	G-protein
Cathepsin D	Hs.343475	7	34	5-fold	<0.001	Protease involved in tumor invasion
XBP-1	Hs.149923	7	25	4-fold	<0.001	Transcription factor
Prefoldin 5	Hs.288856	6	21	4-fold	0.002	Chaperone for unfolded proteins
HSP-27	Hs.76067	23	55	2-fold	0.001	Stress response protein
Vit B-12-binding protein	Hs.2012	17	37	2-fold	0.002	Vitamin-binding protein
NPM	Hs.9614	10	14	1.5-fold	>0.05	Oncogenic nucleolar protein
L14	Hs.738	13	2	6-fold	0.021	Ribosomal protein
Death-associated protein-6	Hs.336916	11	2	6-fold	0.049	Apoptosis-associated protein
EF- γ	Hs.2186	22	6	4-fold	0.014	Translation elongation factor
Ferritin, heavy polypeptide-1	Hs.62954	54	16	3-fold	<0.001	Iron-binding protein

^a The gene designations are considered putative, although the identity of most genes designated in this fashion have been shown to be correct. These genes include those Tags where: (a) the fold difference is ≥ 2 -fold; (b) the Tag could represent ≤ 2 genes; and (c) represents 0.1% of either the MCF7/LCC1 and/or MCF7/LCC9 SAGE library.

^b Predicted fold difference in gene expression between MCF7/LCC1 vs. MCF7/LCC9 cells.

^c Obtained by χ^2 analyses; P estimated to 3 significant figures.

^d NPM (not statistically significant) is shown because we know it to be both estrogen regulated and associated with TAM treatment in patients.

1 M NaOH and 10 mM EDTA, and incubated at 68°C for 20 min. *c*₀-1 DNA and 1 M NaH₂PO₄ (pH 7.0) were added to the denatured probe, and incubated at 68°C for an additional 10 min.

Each Atlas Array (Clontech) was prehybridized with 5 ml of ExpressHyb buffer (Clontech) and 0.5 mg of denatured DNA from sheared salmon testes at 68°C for 30 min with continuous agitation. The cDNA probe, prepared as described above, was then added and allowed to hybridize overnight. The array was washed four times with 2× SSC containing 1% (w/v) SDS for 30 min at 68°C and once with 0.1× SSC containing 0.5% (w/v) SDS for 30 min at 68°C. One final wash was performed with 2× SSC for 5 min at room temperature. The Atlas Array was sealed in plastic and signals detected by phosphorimage analysis using a Molecular Dynamics Storm phosphorimager (Molecular Dynamics, Sunnyvale, CA). Each filter was used only once.

Measuring NPM and EGF-R Protein Levels. Established methods were used for performing and quantifying Western analyses of NPM (22, 23). Briefly, 10 μ g of protein was loaded onto an SDS-PAGE gel and fractionated under reducing conditions [5% (v/v) β -mercaptoethanol]. To account for within-gel differences, samples were loaded in a random sequence onto each gel. Proteins were blotted onto nitrocellulose membrane and the blots probed with an anti-NPM monoclonal antibody (kindly provided by Dr. Pui-Kwong Chan, Baylor College of Medicine, Houston, TX; Ref. 24). After transfer to the membranes, equal protein loading was confirmed by staining the nitrocellulose with Ponceau S as is widely reported (22, 23, 25). Any material remaining in the gels were stained by Coomassie Blue. This approach provides an adequate and appropriate estimate for equivalence of protein loading (22, 23, 25). Immunoreactivity was visualized using a horseradish peroxidase-linked goat antimouse IgG and the enhanced chemiluminescence detection system (Amersham Life Science Inc.). Chemiluminescence was densitometrically measured using a Quantity One Scanning and Analysis System (pdi, Huntingdon, NY).

EGF-R is expressed at low levels in MCF-7 cells and cannot readily be detected/quantified by Western blot. Consequently, we measured immunofluorescently labeled EGF-R protein by FACS. For each cell line, EGF-R immunofluorescence was performed by rinsing 5×10^6 cells once in PBS and pelleting cells by centrifugation at 1000 rpm for 5 min at room temperature. Cell pellets were resuspended in 100 μ l of an anti-EGF-R mouse monoclonal antibody that recognizes the extracellular domain of the receptor (EGF-R antibody-1; NeoMarkers, Lab Vision Corp., Fremont, CA; 200 μ g/ml diluted 1:50 in PBS), and incubated at room temperature for 1 h. Cell pellets were then resuspended in 1:50 dilution of R-phycoerythrin-conjugated goat antimouse IgG-2a (CALTAG Laboratories, Burlingame, CA) and incubated in the dark for 30 min. After rinsing in PBS, cells were again pelleted, fixed by resuspending in 1% paraformaldehyde, and fluorescence measured by FACS. Control cells were treated either with secondary antibody alone or with no antibody. FACS was performed on a FACStar^{Plus} flow cytometer (Becton-Dickinson, Mountain View, CA) at 488 nm.

RNase Protection Analysis of IFN Regulatory Factor-1 mRNA Expression. Total RNA was isolated using the TRIzol reagent (Life Technologies, Inc.) according to the manufacturer's instructions. The IRF-1 riboprobe was made by *in vitro* transcription of a 360-bp fragment of the IRF-1 cDNA. The 36B4 loading control riboprobe was similarly obtained from a 220-bp fragment

of the 36B4 cDNA (17). Riboprobes were labeled by the addition of [³²P]UTP (Amersham Life Sciences Inc.) in the transcription buffer. To achieve bands for the two genes with similar intensities, the 36B4 riboprobe was made with a specific activity of ~20% that of the IRF-1 riboprobe. The RNase protection assays were performed as described previously (26). Briefly, total RNA (30 μ g), the IRF-1 riboprobe, and the 36B4 riboprobe were hybridized overnight at 50°C. After digestion with RNase A, the protected fragments were size fractionated on 6% acrylamide Tris-borate EDTA-urea minigels (Novex, San Diego, CA). The gels were dried and the respective signals quantified by phosphorimager analysis (Molecular Dynamics).

Estimation of the Transcriptional Activation of CREs and NF κ B. Two commercially available promoter-reporter assays were used to measure NF κ B and CRE transcriptional activities. Experiments were performed as described by the manufacturer (Stratagene, La Jolla, CA). Briefly, firefly luciferase reporter constructs, under the control of the appropriate enhancer elements and *trans*-activator constructs, were provided in the PathDetect *in vivo* signal transduction pathway *cis*-reporting system (Stratagene). Cells were grown to 90% confluence in 5% CCS-IMEM medium and seeded at 8×10^4 cells into each well of 24-well tissue culture dishes. After incubation for 12–24 h, cells were transiently transfected with the appropriate plasmids using the Qiagen Superfect transfection reagent as described by the manufacturer (Qiagen, Valencia, CA). The ratio of plasmid to Superfect reagent was 250 ng:1 μ l, with a transfection time of 2.5 h.

Estrogen (5 nM) and ICI 182,780 treatments (10 nM) were administered for 48 h after transfection in CCS-IMEM. Transfected cells were harvested and firefly luciferase activity measured using the Stratagene assay system. Activity is expressed in relative light units from a 20- μ l sample as detected by luminometry. Each measurement is from duplicate samples, independent experiments being repeated on different days. Normalization of transfection efficiency was made to the *Renilla* luciferase reporter construct, under the control of the cytomegalovirus promoter (Promega). The *Renilla* luciferase assay was performed using the Promega Dual-luciferase reporter assay system.

Assessment of Growth Response to Parthenolide. MCF7/LCC1 and MCF7/LCC9 cells were plated in 96-well tissue culture plates and incubated for 24 h in 0.2 ml of 5% CCS-IMEM. Medium was removed and replaced with fresh 5% CCS-IMEM containing either vehicle (0.1% DMSO) or parthenolide (300 nM and 600 nM). Cells were refed every third day with the appropriate cell culture medium. Cell growth was determined on day 6, using a crystal violet assay where dye uptake is directly related to cell number (27). Cells were incubated for 30 min with crystal violet stain [0.5% (w/v) crystal violet in 25% (v/v) methanol] at 25°C. Unincorporated stain was removed with deionized water and the cells allowed to dry at room temperature. Incorporated dye was extracted into 0.1 ml of 0.1 M sodium citrate in 50% (v/v) ethanol for 10–15 min at room temperature. Absorbance was read at 570 nm using a Molecular Devices *V*_{max} kinetic microplate reader.

Statistical Analyses and Analysis of Gene Expression Microarray Data. *t* tests were used to compare control and experimental groups as appropriate for the RNase protection, Western blot, promoter-reporter, and cell proliferation assays. All of the tests were two-tailed, with statistical significance established at $P \leq 0.05$, unless stated otherwise.

For the gene array studies, background signal was estimated locally and

subtracted from the signal obtained from its target cDNA, producing the background-corrected data. These corrections were done using the algorithms in Pathways 4.0 (Research Genetics Inc., Huntsville, AL). Background-corrected data were normalized to account for differences in probe-specific activity, hybridization, and other variables among replicates (28). Normalization was accomplished using the mean value of all of the background-corrected signals on each array.

Different approaches have been used to analyze data from gene array studies. Some methods are simply based on fold-regulation (29), others are more statistically based (16, 30), and/or apply an informatics-based exploration of data structure (31, 32). The optimal approach remains a subject of considerable debate (30). As with most gene microarray studies, our data set is high in dimensionality (597 dimensions) but the number of replicates is limited by the resource-intensive nature of the technology. The relatively few replicates limits the applicability of normal mixture models and other analyses that can operate in high dimensional data space (33, 34) and often generates noisy data sets.

Previously, we have reported a hierarchical visualization algorithm that can reveal all of the major aspects of the multimodal data points, which concurrently exist in a high dimensional gene expression space (35, 36). Using this algorithm, our data can be projected from 597 dimensions to two or three dimensions (multidimensional scaling). This is accomplished by respectively deriving the first three principal components fitted to the antiestrogen responsive (MCF7/LCC1) and resistant (MCF7/LCC9) gene expression data (Fig. 1). Thus, we evaluate the data structure subsets visually and assess whether these contain differentially expressed genes that may contribute to the respective phenotypes.

Because we can visualize data structure, our next priority was to identify a simple, supervised approach for reducing the dimensionality of the data without affecting its structure. Thus, we applied geometric and simple descriptive statistical approaches to the normalized data before and after a logarithmic transformation of these data. As noted previously, the distribution of the expression data for each gene is unknown (30), and it is unclear whether these violate the normal distribution required for parametric analyses. Indeed, it seems likely that the distribution assumption required will be normal for some genes and not for others. Whereas most investigators analyze data transformed by a logarithmic function, those genes with values that appear normally

distributed before transformation may no longer have this distribution once transformed.

To be inclusive, we used simple statistics (*t* tests) to explore the data. The inflated type-1 error from multiple comparisons should overestimate (false positive) significant differences. We considered this preferable to a high incidence of false-negative estimates, which would lead to the exclusion of potentially informative genes. The inclusion of uninformative genes (false negatives) is less problematic at this stage of the exploration. We used Student's *t* test, a *t* test for unequal variance (assumes normal distribution) and the nonparametric (distribution-free) Wilcoxon signed rank test. Logarithm transformed and nontransformed data were explored. This approach is similar to using a *F* test as described recently by Hedenfalk *et al.* (37).

t test results were evaluated and candidate genes selected with which to reconstruct a lower dimensional data set that should retain most of the information apparent in the top level visualization. However, the *t* test results were only one of several criteria used to guide gene selection, and only a subset of those genes that appear to be differentially regulated are presented. These genes were selected by comparing the results of *t* tests on logarithm transformed and untransformed data, fold-regulation (~2-fold or greater was selected because this difference is likely to be confirmed in independent analyses), the distribution of the background-corrected and normalized data for each gene (some genes appeared strongly differentially regulated but did not generate statistically significant differences because of heterogeneity in the data), and the probable relevance to breast cancer of each gene.

Where the gene subsets (reduced dimensional data) provide a reasonable description of the entire expression data, the replicate profiles of the resistant and responsive cells should exist in separable data space (35, 36). Furthermore, if the profiles are adequately defined by a small, rational gene subset, some of its members likely represent differentially expressed and functionally relevant genes. We acknowledge that our approach is limited, and is probably only applicable to simple comparisons within related cell culture models.

RESULTS

Genes Implicated by SAGE. The data in Table 1 show the number of different genes identified. Most genes were commonly expressed, and were not differentially expressed between the MCF7/LCC1 and MCF7/LCC9 cells. A selection of the genes identified by SAGE, and predicted to be differentially expressed in MCF7/LCC1 and MCF7/LCC9 SAGE databases, is shown in Table 2. Presentation of all of the genes expressed and/or differentially expressed is beyond the scope of a single, focused study.⁹ The criteria applied for gene selection are described in "Materials and Methods." NPM was included because we already know it to be both estrogen regulated (23) and indirectly associated with TAM treatment in patients (38). Confirmation of the differential expression of NPM (see Table 2 and Fig. 2B) and altered CRE binding activity (the function of XBP-1; see Table 2 and Fig. 3B) indicate that these represent reasonable criteria for gene selection. Currently, the XBP-1 and NPM are the only genes from the SAGE database comparisons for which we have attempted to confirm differential expression/activation.

Comparing the SAGE databases identifies several genes that are up-regulated in MCF7/LCC9 cells compared with MCF7/LCC1 cells. These genes include *XBP-1*, *NPM*, *cathepsin D*, *HSP-27*, and *n-ras*. Increased CRE activity is indicated by the up-regulation of XBP-1, which regulates gene transcription through these response elements (39). XBP-1 is involved in regulating the expression of several tissue-specific genes including tissue inhibitor of metalloproteinases, osteopontin, and osteocalcin (40). Significantly, both Perou *et al.* (13) and West *et al.* (41) recently identified XBP-1 as being associated with ER gene expression clusters in human breast tumor biopsies. NPM is induced by estrogen in MCF-7 cells and is up-regulated in estrogen-independent cells (23). NPM also provokes an autoimmune

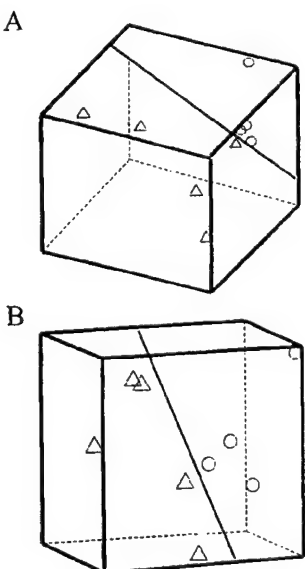
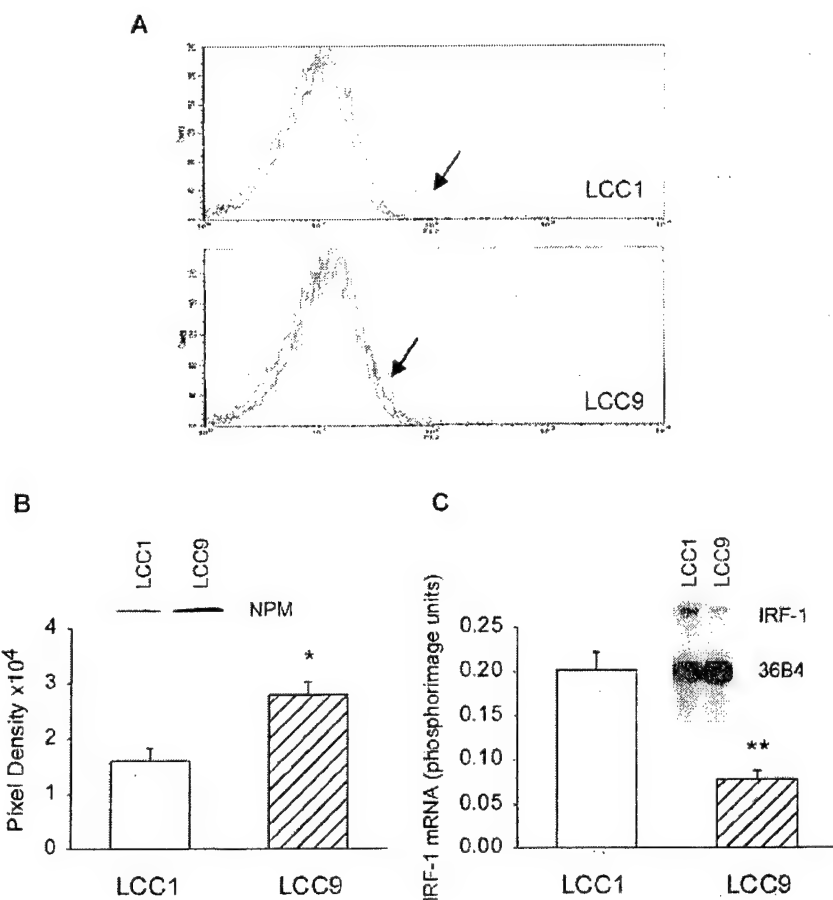


Fig. 1. Visual representations of the structure of the multidimensional gene microarray data. *A*, three-dimensional representation of 597 dimensions (\triangle , MCF7/LCC1; \circ , MCF7/LCC9) where the top three principal components capture 81.2% of the cumulative variance in the data. *B*, three-dimensional representation of 7 dimensions (data from Table 3) where the top three principal components capture 98.9% of the cumulative variance in the data. Axes represent the first three principal components derived from the gene expression data (79, 80). Plots are rotated to provide the optimal visualization. In both plots, a plane is shown demonstrating the linear separability of the MCF7/LCC1 ($n = 5$) and MCF7/LCC9 ($n = 4$) gene expression profiles.

⁹ http://clarkelabs.georgetown.edu/gu_et_al/gu_et_al_links.htm.

Fig. 2. Confirmation of the differential expression of NPM, EGF-R, and IRF-1 in MCF7/LCC1 and MCF7/LCC9 cells. *A*, EGF-R protein immunofluorescence as measured by FACS (representative figure of three experiments). Arrows indicate EGF-R signal, other signals are controls (no antibody; primary antibody but no secondary antibody). Axes are abscissa = fluorescence; ordinate = cell counts. *B*, NPM protein as measured by Western blotting ($*P \leq 0.02$) and represented as a percentage of control (MCF-7 cells growing in CCS-IMEM); bars, \pm SE. Insert = representative Western blot. *C*, IRF-1 mRNA as measured by RNase protection ($**P = 0.005$, three independent replicate experiments) and expressed in phosphorimager units; bars, \pm SE. Insert = representative analysis; 36B4 is a ribosomal gene (loading control).



response in breast cancer patients, the magnitude of which is associated with TAM therapy (38).

The altered expression of cathepsin D is consistent with our data published previously, showing increased secretion of this protein in several of our hormone-independent MCF-7 variants (42). Cathepsin D expression in breast tumors also is associated, at least in some studies, with a poor prognosis (43). HSP-27 expression has been implicated in refining the diagnosis of suspicious fine-needle aspirates of breast tissues (44). Vitamin B12 binding proteins are expressed in breast tumors (45), and vitamin B12 deficiency is a likely risk factor for breast cancer (46). Altered expression of the *n-ras*-related gene is consistent with the elevated *ras* signaling reported in some breast cancer cell lines and tumors (47).

SAGE also identified genes expressed at higher levels in the parental, antiestrogen-responsive cells (MCF7/LCC1) when compared with MCF7/LCC9 cells. These include ferritin, death-associated protein-6, and the eukaryotic elongation factor- γ . Ferritin is expressed in breast cancers, and breast tumor-derived ferritin may be a more useful tumor marker than measuring levels of ferritin in serum (48).

Structure of the Gene Microarray Data. It has been suggested that the cost required to perform gene microarray studies can be reduced by combining RNA populations from several replicates and performing a single hybridization on an Atlas array (16). However, we found heterogeneity among replicate experiments, which often remained after normalization. Logarithmic transformation of these data reduced this heterogeneity but not to the point where a single replicate could be used to obtain an adequate description of the data. Consequently, multiple replicates are required to provide a more reliable

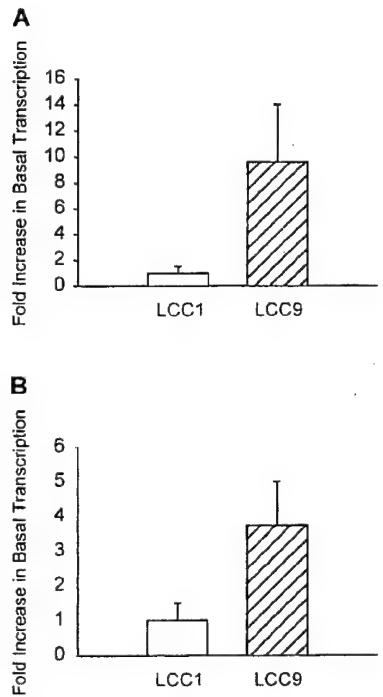


Fig. 3. Basal transcriptional activity of NF- κ B and CRE in MCF7/LCC1 and MCF7/LCC9 cells. *A*, NF- κ B. *B*, CRE. Data represent mean and are expressed as fold induction relative to MCF7/LCC1; bars, \pm SE. All cells were grown in the absence of estrogens (CCS-IMEM).

Table 3. Representative list of differentially expressed genes identified by gene microarray analyses

Gene ^a	Unigene no.	MCF7/LCC1 ^b	MCF7/LCC9	Gene function
NF κ B	Hs.75569	1	2	Transcription factor involved in cell survival signaling
SOD	Hs.75428	1	2	Enzyme involved in detoxifying oxygen radicals
EGR-1	Hs.326035	3	1	Transcription factor
EGFR	Hs.77432	2	1	Growth factor receptor
IRF-1	Hs.80645	2	1	Transcription factor involved in signaling to cell cycle arrest and apoptosis
TNF α	Hs.241570	2	1	Cytokine
TNF-R1	Hs.159	2	1	Cytokine receptor involved in signaling to apoptosis

^a Abbreviations are SOD, superoxide dismutase; TNF-R1, tumor necrosis factor receptor 1.

^b Data are represented as level of expression relative to the other cell line. Data are based on the mean values for each gene (6 microarrays of MCF7/LCC1; 5 microarrays of MCF7/LCC9). Values are expressed to the nearest integer.

estimate of the putative gene expression profiles. These observations on filter microarrays are consistent with recent reports for glass slide-based and oligonucleotide array-based gene expression microarrays (49, 50).

Fig. 1*A* is a visual representation of the multidimensional data (597 dimensions) in three dimensions. This visualization allows for an inspection of the data structure, and the likely comparability of the replicates among each other and between the two experimental groups (antiestrogen-responsive MCF7/LCC1 and antiestrogen-resistant MCF7/LCC9). For this top level visualization, the replicate gene expression profiles for MCF7/LCC1 and MCF7/LCC9 exist within linearly separable regions of the gene expression data space after elimination of one outlier array from each experimental group. The top three principal components capture 81.2% of the cumulative variance in the data (597 dimensions). Thus, the data structure is consistent with differences in the gene expression profiles as predicted by the known differential antiestrogen responsiveness of the two variants.

Genes Implicated by Gene Microarray Studies. The data in Table 3 show the fold-differences in expression of selected genes identified in the Clontech Atlas gene microarray studies selected using the criteria described in "Materials and Methods." The selection was not intended to describe fully the data set, only to assist in an initial exploration of the data. This small but rational subset of genes could be additionally evaluated in focused studies to confirm the differential expression patterns and establish potential functional relevance. Furthermore, if members of this subset were truly differentially expressed, we could begin to understand how cells perceive antiestrogens and adapt to this selective pressure.

To determine whether these genes are broadly representative of the differences between the gene expression profiles of MCF7/LCC1 and MCF7/LCC9 cells, we generated a three-dimensional projection from the seven-dimensional gene expression data space (Fig. 1*B*). This was necessary because we used several criteria to construct the subset, including some genes where fold-regulation or distribution of the data were given more weight than formal statistical significance. Consequently, we could not assume that we had maintained the linear separability of the data, at the top level, as seen in all 597 dimensions.

We might not expect this small subset of expression data (<2% of the information) to prove as effective in representing the respective phenotypes as the full data set (597 genes). Nonetheless, as for the 597-dimension visualization, after elimination of outlier data the seven-dimensional MCF7/LCC1 and MCF7/LCC9 profiles remain in linearly separable, three-dimensional data space. The top three principal components capture 98.9% of the cumulative variance in the

data (seven-dimensions). This observation suggests that these data contain information that contributes to the differences in the molecular profiles of these two variants, that these genes may contribute to the respective biological phenotypes, and that additional studies of their potential functional relevance are warranted.

Genes expressed at a higher level in the MCF7/LCC1 cells include EGF-R, EGR-1, IRF-1, and both TNF α and its R1 receptor (TNF-R1). A well-established inverse relationship exists between the expression of EGF-R and ER in breast tumors (51). EGF-R can induce expression of EGR-1 (52), and expression of both genes is lower in MCF7/LCC9 cells. EGR-1 is a transcription factor with proapoptotic activity (53) that can block NF κ B function (54) and repress TGF- β receptor expression (29). EGR-1 expression is down-regulated in 7,12-dimethylbenz(a)anthracene-induced mammary adenocarcinomas in rats (55). IRF-1 is an IFN-regulated transcription factor that functions as a tumor suppressor gene (56, 57) and is induced by TNF α (58). A TNF α -mediated pathway for signaling to apoptosis occurs in MCF7 human breast cancer cells (59, 60), and measuring serum TNF concentrations may be a useful prognostic marker in breast cancer patients (61). Furthermore, HER-2/neu can block resistance to TNF α -induced apoptosis in breast cancer cells, using a mechanism that involves activation of NF κ B (62). We have previously implicated overexpression of superoxide dismutase in resistance to TNF α in MCF7 cells (63). Superoxide dismutase appears to be up-regulated in MCF7/LCC9 cells (Table 3) and in TAM-stimulated MCF7 xenografts (64). NF κ B (p65/RelA) appears expressed at higher levels in MCF7/LCC9 cells. NF κ B is overexpressed in ER-negative breast cancer cells (65) and has an important role in the development of the normal mammary gland (66).

NPM, EGF-R, and IRF-1 Are Differentially Expressed in MCF7/LCC1 and MCF7/LCC9 Cells. The data in Table 2 and Table 3 predict differential expression of NPM, EGF-R, and IRF-1 between MCF7/LCC1 and MCF7/LCC9 cells. To confirm these observations, we measured the levels of the EGF-R (immunofluorescence) and NPM proteins (Western blot) and IRF-1 mRNA (RNase protection). The data in Fig. 2*A* show that MCF7/LCC9 cells express lower amounts of EGF-R than MCF7/LCC1 cells. NPM protein expression is significantly increased in MCF7/LCC9 cells compared with MCF7/LCC1 cells (Fig. 2*B*; $P < 0.02$), consistent with the predicted data from the SAGE analyses (Table 2) and our previous studies (23, 38). The higher levels of IRF-1 mRNA, seen in the antiestrogen-responsive MCF7/LCC1 cells in Table 3, are confirmed by RNase protection analysis (Fig. 2*C*; $P = 0.005$). Both the gene microarray and RNase protection analyses show an ~2-fold higher level of IRF-1 expression in MCF7/LCC1 cells, when compared with the antiestrogen-resistant MCF7/LCC9 cells.

Transcriptional Regulatory Activities of NF κ B and CRE Are Increased in MCF7/LCC9 Cells. The increased expression of NF κ B (gene expression microarray) and XBP-1 (SAGE) imply increased transcriptional activation of promoters containing NF κ B and CRE response elements, respectively. We confirmed these observations directly, using commercially available promoter-reporter assays to measure transcriptional activities. The data in Fig. 3 show that the basal activity of both promoters is increased in MCF7/LCC9 cells; ~10-fold for NF κ B and 4-fold for CRE ($P < 0.02$). The increase in transcriptional activation of the NF κ B constructs is greater than that predicted by the gene array data, but mRNA, protein, and protein/DNA binding activities can be poor predictors of the functional activation of some transcription factors (67). This prediction is not problematic for XBP-1, where the 4-fold increase in mRNA expression identified by SAGE (Table 2) compares well with the 4-fold increase in basal transcriptional activation (Fig. 3*B*).

We next assessed whether ICI 182,780, the antiestrogen used to

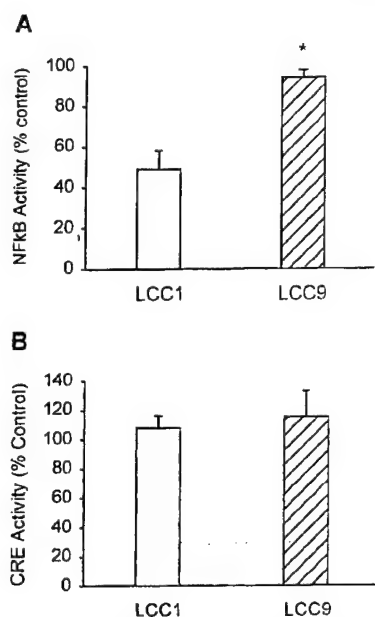


Fig. 4. Regulation of NF κ B and CRE transcription by ICI 182,780 in MCF7/LCC1 and MCF7/LCC9 cells. *A*, NF κ B (* $P \leq 0.001$, MCF7/LCC1 versus MCF7/LCC9). *B*, CRE (not significant). NF κ B and CRE data are represented as mean of transcriptional activation expressed as a percentage of controls (vehicle-treated cells of the same cell line); bars, \pm SE. Cells were grown in CCS-IMEM and treated with 10 nM ICI 182,780 for 48 h before measuring reporter gene expression.

generate the MCF7/LCC9 cells, could regulate the transcriptional activities of NF κ B and CRE. Whereas ICI 182,780 inhibits NF κ B activity in the MCF7/LCC1 cells (TAM- and ICI 182,780-responsive), this regulation is lost in the TAM and ICI 182,780 cross-resistant MCF7/LCC9 cells (Fig. 4*A*). In contrast, ICI 182,780 treatment does not alter the transcriptional regulatory activities of the CRE promoter in any of these variants (Fig. 4*B*).

MCF7/LCC9 Cells Are Specifically Responsive to an Inhibitor of NF κ B Activity. The increased activation of NF κ B and loss of its estrogenic regulation in MCF7/LCC9 cells suggests that these cells might now be partly dependent on NF κ B signaling for survival/growth. Consequently, we compared the growth response of MCF7/LCC1 and MCF7/LCC9 cells to parthenolide, a potent and specific inhibitor of NF κ B that can inhibit the inhibitor of NF κ B kinase repressor of NF κ B (68, 69) and also binds NF κ B in a highly stereospecific manner to block DNA binding (70). Parthenolide produces a dose-dependent inhibition of MCF7/LCC9 cells, with an apparent IC₅₀ of \sim 600 nM (Fig. 5). In contrast, parthenolide does not significantly affect growth of MCF7/LCC1 cells at these concentrations. MCF7/LCC9 cells are significantly more dependent on the transcriptional regulatory activities of NF κ B than their ICI 182,780-responsive parental cells ($P < 0.01$ for MCF7/LCC9 versus MCF7/LCC1 at both 300 nM and 600 nM parthenolide).

DISCUSSION

We have begun to identify the molecular changes associated with cell survival after prolonged ICI 182,780 treatment in breast cancer cells. Whereas we have not attempted to confirm the altered expression of all implicated genes, some expression patterns are consistent with the activities we have confirmed. Here we discuss only those genes for which altered mRNA, protein, and/or transcriptional activation have been confirmed, and that are known to interact with each other in various cellular models, *i.e.*, IRF-1, NPM, NF κ B, and CRE.

IRF-1 can function as a tumor suppressor and can signal to apoptosis through both p53-dependent and p53-independent pathways (71). These observations may partly reflect the ability of IRF-1 to induce a caspase cascade through activation of either caspase 1 (ICE; Ref. 72) and/or caspase 7 (73). Caspase 1 is involved in regulating apoptosis in normal mammary epithelial cells (74), and overexpression of caspase 1 is lethal in MCF-7 human breast cancer cells (75). Preliminary data from our laboratory demonstrate that overexpression of IRF-1 inhibits anchorage-dependent colony formation and that the rate of cell proliferation in MCF-7 cells is inversely related to the level of IRF-1 expression (76). These data suggest that the down-regulation of IRF-1 in MCF7/LCC9 cells may protect these cells from IRF-1-induced inhibition of proliferation and/or induction of apoptosis.

NPM can function as an oncogene, its overexpression fully transforming NIH 3T3 cells in a standard assay for oncogenic potential (77). We have shown that levels of autoantibodies to NPM increase in breast cancer patients 6 months before their recurrence. Consistent with an estrogenic/antiestrogenic regulation of NPM, the levels of these autoantibodies are lower in breast cancer patients that have received TAM (38). The increased NPM expression in MCF7/LCC9 cells compared with MCF7/LCC1 cells may reflect oncogenic potential of NPM, an activity potentially related to its ability to inhibit IRF-1 function (see below).

NF κ B has been implicated in resistance to cytotoxic drugs and can function as a survival factor in various cell types (78). Several aspects of normal mammary gland development appear dependent on NF κ B activity (66), perhaps partly reflecting its estrogenic regulation (65). Elevated NF κ B activity arises early during neoplastic transformation in the rat mammary gland (79). Widely expressed in breast cancer cells and tumors, elevated NF κ B activity is associated with estrogen-independence (65, 66). Currently, NF κ B is the only protein known to induce BRCA2 expression (80). ICI 182,780 cannot suppress the increased NF κ B activity in MCF7/LCC9 cells, despite inhibiting this function in ICI 182,780-responsive cells (MCF7/LCC1). The functional relevance of this observation was tested directly using parthenolide, which both specifically binds NF κ B and blocks degradation of the endogenous NF κ B inhibitor I κ B, resulting in the inhibition of NF κ B transcriptional regulatory activities (68, 70). This activity of parthenolide has been used to evaluate the functional role of NF κ B in several recent studies (68, 69, 81, 82). MCF7/LCC9 cells are significantly more sensitive to growth inhibition by parthenolide than their MCF7/LCC1 parental cells. This

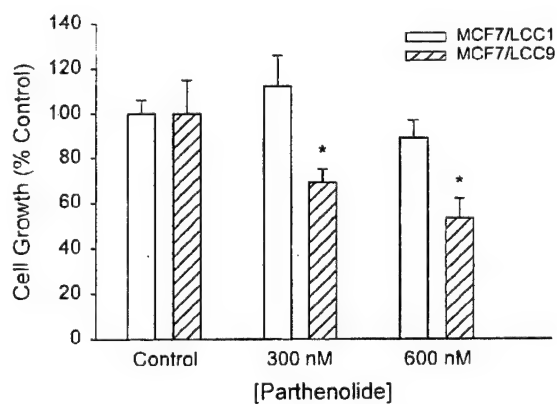


Fig. 5. Response to inhibition of NF κ B activity by parthenolide. Data represent mean of four determinations, where absorbance in each treated population is expressed as a percentage of the absorbance in control cells (vehicle treated cells of the same cell line). * $P \leq 0.01$ MCF7/LCC1 versus MCF7/LCC9. Cells were grown in CCS-IMEM without (control; vehicle only) or with parthenolide supplementation (300 nM; 600 nM).

observation is consistent with a greater functional reliance on NF κ B activation for cell growth/survival, and implies that one option for surviving antiestrogen exposure is the up-regulation of an estrogen-regulated survival factor(s) concurrent with the loss of its ER-mediated regulation. Furthermore, parthenolide is now in clinical trials, and our data suggest that it may prove useful in combination with Faslodex or other antiestrogens to either increase responsiveness and/or delay the appearance of resistant disease.

XBP-1 has been identified recently in clusters of genes associated with ER-positive breast tumors in two independent studies (13, 41), and its expression is increased in MCF7/LCC9 cells. XBP-1 is a transcription factor that binds and activates CRE (39). The importance of CRE-regulated events is widely reported in many cell types (83, 84). These events include a likely role in signal transduction either at or downstream of ER and PgR (85). The relevance of increased CRE activity in MCF7/LCC9 cells is additionally supported by recent evidence that CRE-decoy oligonucleotides inhibit the growth of MCF-7 cells (86). We detected a 4-fold increase in CRE transcriptional activation in MCF7/LCC9 cells. Importantly, ICI 182,780 cannot regulate CRE activity in either MCF7/LCC1 (ICI 182,780-responsive) or MCF7/LCC9 (resistant) cells. These data imply an additional option available to breast cancer cells, a switch to signaling pathways that are normally independent of ER-mediated signaling.

IRF-1, NPM, NF κ B, and CRE are known to affect cell proliferation, apoptosis, and/or carcinogenesis. Two critical protein-protein interactions directly link the IRF-1, NF κ B, and NPM proteins. Direct binding occurs between IRF-1 and NPM (77), and between IRF-1 and NF κ B (87, 88). In both cases, the interactions with IRF-1 have important effects on gene transcription and cell signaling. NPM binding inhibits the transcription regulatory activities of IRF-1 (77). A coordinated perturbation in the regulation of these two genes has occurred in the MCF7/LCC9 cells; NPM is up-regulated and IRF-1 is down-regulated. Thus, overexpression of NPM could additionally reduce the remaining lower levels of IRF-1, potentially blocking/eliminating its ability to initiate an apoptotic caspase cascade through caspase 1 and/or caspase 7. Such an effect would likely also eliminate the ability of IRF-1 to induce p21^{cip1/waf1} (89) and cooperate with wild-type p53 in signaling to apoptosis (56, 57). Changes in the amount of available IRF-1 will directly affect the number of IRF-1:NF κ B heterodimers available to regulate an additional series of genes. Whereas NF κ B will compete with NPM for IRF-1 binding, their relative affinities for IRF-1 are unknown, and the preferred IRF-1 heterodimer remains to be established. IRF-1:NF κ B protein-protein interactions or other cooperative interactions are implicated in the induction of ATF-2/jun (90), RANTES (91), VCAM-1 (88), interleukin 6 (92), and MHC class 1 genes (87). A functional IFN- β enhanceosome has been described that includes IRF-1, NF κ B, and ATF2/jun (93). The importance of both IRF-1 and NF κ B in IFN-induced signaling may contribute to the ability of IFNs to increase responses to antiestrogens (94–96).

CRE activation also may interact with the pathways regulated by IRF-1, NF κ B, and NPM interactions. Delgado *et al.* (97) described a cyclic AMP-dependent pathway that inhibits IRF-1 transactivation. Thus, the increased CRE activity in MCF7/LCC9 cells may explain, in part, the lower IRF-1 mRNA levels seen both in the gene expression arrays and in the IRF-1 RNase protection studies.

The concurrent changes in NPM, IRF-1, NF κ B, and CRE suggest a novel integrated signaling pathway that may involve the ability of NPM and CRE to inhibit IRF-1 initiation of a caspase cascade to apoptosis, the altered ability of cells to induce genes dependent on IRF-1:NF κ B, and an increased activation of survival pathways that involve both NF κ B and CRE. Studies to additionally establish the

nature, function, and regulation of this putative pathway are currently in progress, including an overexpression of NF κ B in sensitive cells and a dominant-negative approach in resistance cells. Because we looked only at cells that survived long-term antiestrogen exposure, the ability of the changes implicated in the present study to protect from an initial or short term exposure have yet to be determined. For example, cells may or may not survive an initial antiestrogenic exposure by the same mechanisms that allow for long-term survival. Irrespective of whether these other genes are functionally involved, their patterns of expression may be important in better predicting the 25% of ER+/PgR+, 55% of ER-/PgR+, and 66% of ER+/PgR- breast tumors that do not respond to antiestrogens (2).

It is not possible, in a single focused study, to define all of the potentially differentially expressed genes nor to establish their functional relevance firmly. Because the number of cellular models studied is small, additional functional studies where expression of the candidate genes is induced or repressed are in progress. Nonetheless, our data imply that breast cancer cells have highly plastic transcriptomes, with access to several signal transduction pathways for regulating the choice to differentiate, proliferate, or die. For example, MCF7/LCC9 cells have taken several possible interactive/interdependent approaches to circumvent the growth inhibitory effects of antiestrogens. This plasticity in gene expression patterns is consistent with the marked heterogeneity apparent in the clinical disease (2, 98).

In summary, our data suggest that one molecular profile associated with surviving prolonged antiestrogen exposure may include loss of ER-mediated signaling to apoptosis through IRF-1. This lost signaling is achieved both by down-regulation of IRF-1 and a coordinated up-regulation of its inhibitor NPM, and possibly another protein partner NF κ B. Up-regulation of CRE activities also is implicated in this molecular profile. Other patterns of gene expression may provide alternative routes to the resistant phenotype or in cells that acquire a TAM-stimulated phenotype (2). The identification of these molecular profiles and signaling pathways may ultimately allow us to understand ER-regulated signaling, facilitate the development of novel treatment strategies, and allow clinicians to better identify antiestrogen-responsive and -resistant breast tumors.

ACKNOWLEDGMENTS

We thank Dr. K. W. Kinzler and his colleagues at Johns Hopkins University, Baltimore, MD, for their assistance in establishing the SAGE protocols and for providing their SAGE data analysis software.

REFERENCES

- Clarke, R., and Brünnner, N. Acquired estrogen independence and antiestrogen resistance in breast cancer: estrogen receptor-driven phenotypes? *Trends Endocrinol. Metab.*, **7**: 25–35, 1996.
- Clarke, R., Leonessa, F., Welch, J. N., and Skaar, T. C. Cellular and molecular pharmacology of antiestrogen action and resistance. *Pharmacol. Rev.*, **53**: 25–71, 2001.
- Early Breast Cancer Trialists' Collaborative Group. Tamoxifen for early breast cancer: an overview of the randomized trials. *Lancet*, **351**: 1451–1467, 1998.
- Fisher, B., Costantino, J. P., Wickerham, D. L., Redmond, C. K., Kavanagh, M., Cronin, W. M., Vogel, V., Robidoux, A., Dimitrov, M., Atkins, J., Daly, M., Wieand, S., Tan-Chiu, E., Ford, L., and Wolmark, N. Tamoxifen for prevention of breast cancer: report of the National Surgical Adjuvant Breast and Bowel Project P-1 study. *J. Natl. Cancer Inst.*, **90**: 1371–1388, 1998.
- Howell, A., DeFriend, D. J., Robertson, J. F. R., Blamey, R. W., Anderson, L., Anderson, E., Sutcliffe, F. A., and Walton, P. Pharmacokinetics, pharmacological and anti-tumor effects of the specific anti-oestrogen ICI 182780 in women with advanced breast cancer. *Br. J. Cancer*, **74**: 300–308, 1996.
- Gottardis, M. M., and Jordan, V. C. Development of tamoxifen-stimulated growth of MCF-7 tumors in athymic mice after long-term antiestrogen administration. *Cancer Res.*, **48**: 5183–5187, 1988.
- Osborne, C. K., Coronado, E. B., and Robinson, J. P. Human breast cancer in athymic nude mice: cytostatic effects of long-term antiestrogen therapy. *Eur. J. Cancer Clin. Oncol.*, **23**: 1189–1196, 1987.

8. Johnston, S. R. D., Saccanti-Jotti, G., Smith, J. E., Newby, J., and Dowsett, M. Change in oestrogen receptor expression and function in tamoxifen-resistant breast cancer. *Endocr. Related Cancer*, **2**: 105–110, 1995.

9. Clarke, R., Brünner, N., Katzenellenbogen, B. S., Thompson, E. W., Norman, M. J., Koppi, C., Paik, S., Lippman, M. E., and Dickson, R. B. Progression from hormone dependent to hormone independent growth in MCF-7 human breast cancer cells. *Proc. Natl. Acad. Sci. USA*, **86**: 3649–3653, 1989.

10. Brünner, N., Frandsen, T. L., Holst-Hansen, C., Bei, M., Thompson, E. W., Wakeling, A. E., Lippman, M. E., and Clarke, R. MCF7/LCC2: A 4-hydroxytamoxifen resistant human breast cancer variant which retains sensitivity to the steroidal antiestrogen ICI 182, 780. *Cancer Res.*, **53**: 3229–3232, 1993.

11. Brünner, N., Boysen, B., Jirus, S., Skaar, T. C., Holst-Hansen, C., Lippman, J., Frandsen, T., Spang-Thomsen, M., Fuqua, S. A. W., and Clarke, R. MCF7/LCC9: an antiestrogen resistant MCF-7 variant in which acquired resistance to the steroidal antiestrogen ICI 182, 780 confers an early cross-resistance to the non-steroidal antiestrogen tamoxifen. *Cancer Res.*, **57**: 3486–3493, 1997.

12. Marx, J. DNA arrays reveal cancer in its many forms. *Science (Wash. DC)*, **289**: 1670–1672, 2000.

13. Perou, C. M., Sorlie, T., Eisen, M. B., Van de R., M., Jeffrey, S. S., Rees, C. A., Pollack, J. R., Ross, D. T., Johnsen, H., Akslen, L. A., Fluge, O., Pergamenschikov, A., Williams, C., Zhu, S. X., Lønning, P. E., Borresen-Dale, A. L., Brown, P. O., and Botstein, D. Molecular portraits of human breast tumours. *Nature (Lond.)*, **406**: 747–752, 2000.

14. Ross, D. T., Scherf, U., Eisen, M. B., Perou, C. M., Rees, C., Spellman, P., Iyer, V., Jeffrey, S. S., Van de R., M., Walther, M., Pergamenschikov, A., Lee, J. C., Lashkari, D., Shalon, D., Myers, T. G., Weinstein, J. N., Botstein, D., and Brown, P. O. Systematic variation in gene expression patterns in human cancer cell lines. *Nat. Genet.*, **24**: 227–235, 2000.

15. Sgroi, D. C., Teng, S., Robinson, G., LeVangie, R., Hudson, J. R., and Elkhoul, A. G. *In vivo* gene expression profile analysis of human breast cancer progression. *Cancer Res.*, **59**: 5656–5661, 1999.

16. Hilsenbeck, S. G., Friedrichs, W. E., Schiff, R., O'Connell, P., Hansen, R. K., Osborne, C. K., and Fuqua, S. A. W. Statistical analysis of array expression data as applied to the problem of tamoxifen resistance. *J. Natl. Cancer Inst.*, **91**: 453–459, 1999.

17. Brünner, N., Boulay, V., Fojo, A., Freter, C., Lippman, M. E., and Clarke, R. Acquisition of hormone-independent growth in MCF-7 cells is accompanied by increased expression of estrogen-regulated genes but without detectable DNA amplifications. *Cancer Res.*, **53**: 283–290, 1993.

18. Darbre, P., Yates, J., Curtis, S., and King, R. J. B. Effect of estradiol on human breast cancer cells in culture. *Cancer Res.*, **43**: 349–354, 1983.

19. Velezlescu, V. E., Zhang, L., Vogelstein, B., and Kinzler, K. W. Serial analysis of gene expression. *Science (Wash. DC)*, **270**: 484–487, 1995.

20. Yan, H., Dobbie, Z., Gruber, S. B., Markowitz, S., Romans, K., Giardello, F. M., Kinzler, K. W., and Vogelstein, B. Small changes in expression affect predisposition to tumorigenesis. *Nat. Genet.*, **30**: 25–26, 2002.

21. Man, M. Z., Wang, X., and Wang, Y. POWER SAGE: comparing statistical tests for SAGE experiments. *Bioinformatics (Oxf.)*, **16**: 953–959, 2000.

22. Harlow, E., and Lane, D. (eds.). *Antibodies. A Laboratory Manual*. Cold Spring Harbor, NY: CSH, 1988.

23. Skaar, T. C., Prasad, S. C., Sharaeh, S., Lippman, M. E., Brünner, N., and Clarke, R. Two-dimensional gel electrophoresis analyses identify nucleophosmin as an estrogen regulated protein associated with acquired estrogen-independence in human breast cancer cells. *J. Steroid Biochem. Mol. Biol.*, **67**: 391–402, 1998.

24. Chan, P. K., Chan, W.-Y., Yung, B. Y. M., Cook, R. G., Aldrich, M., Ku, D., Goldknopf, I. L., and Busch, H. Amino acid sequence of a specific antigenic peptide of protein B23. *J. Biol. Chem.*, **261**: 14335–14341, 1986.

25. Klein, D., Kern, R. M., and Sokol, R. Z. A method for quantification and correction of proteins after transfer to immobilization membranes. *Biochem. Mol. Biol. Int.*, **36**: 59–66, 1995.

26. Clarke, R., Brünner, N., Katz, D., Glanz, P., Dickson, R. B., Lippman, M. E., and Kern, J. The effects of a constitutive production of TGF- α on the growth of MCF-7 human breast cancer cells *in vitro* and *in vivo*. *Mol. Endocrinol.*, **3**: 372–380, 1989.

27. Frandsen, T. L., Boysen, B. E., Jirus, S., Spang-Thomsen, M., Dane, K., Thompson, E. W., and Brünner, N. Experimental models for the study of human cancer cell invasion and metastasis. *Fibrinolysis*, **6**(Suppl. 4): 71–76, 1992.

28. Wang, Y., Lu, J., Lee, R. Y., and Clarke, R. Iterative normalization of cDNA microarray data. *IEEE Trans. Inf. Technol. Biomed.*, **6**: 29–36, 2002.

29. Du, B., Fu, C., Kent, K. C., Bush, H., Jr., Schulick, A. H., Kreiger, K., Collins, T., and McCaffrey, T. A. Elevated Egr-1 in human atherosclerotic cells transcriptionally represses the transforming growth factor- β type II receptor. *J. Biol. Chem.*, **275**: 39039–39047, 2000.

30. Witte, J., and Friedman, H. P. Searching for evidence of altered gene expression: a comment on statistical analysis of microarray data. *J. Natl. Cancer Inst.*, **91**: 400–401, 1999.

31. Ermolacova, O., Rastogi, M., Pruitt, K. D., Schuler, G. D., Bittner, M. L., Chen, Y., Simon, R., Meltzer, P., Trent, J. M., and Boguski, M. S. Data management and analysis for gene expression arrays. *Nat. Genet.*, **20**: 19–23, 1998.

32. Golub, T. R., Slonim, D. K., Tamayo, P., Huard, C., Gaasenbeek, M., Mesirov, J. P., Coller, H., Loh, M. L., Downing, J. R., Caligiuri, M. A., Bloomfield, C. D., and Lander, E. S. Molecular classification of cancer: class discovery and class prediction by gene expression monitoring. *Science (Wash. DC)*, **286**: 531–537, 1999.

33. Hinneburg, A., and Keim, D. A. Optimal grid-clustering: towards breaking the curse of dimensionality in high-dimensional clustering. *In* M. P. Atkinson, M. E. Orlowska, P. Valdoriez, S. B. Zdonik, and M. L. Brodie (eds.). *Proceedings of the 25th Conference on Very Large Databases*, pp. 506–517. San Francisco: Morgan Kaufmann, 1999.

34. Liu, J., Wang, Y., Xuan, J., Kung, S. Y., Gu, Z., and Clarke, R. Discriminative mining of gene microarray data. *Proc. IEEE Neural Netw. Signal. Process.*, **II**: 218–227, 2001.

35. Wang, Y., Luo, L., Freedman, M. T., and Kung, S. Y. Probabilistic principal component subspaces: a hierarchical finite mixture model for data visualization. *IEEE Trans. Neural Netw.*, **II**: 635–646, 2000.

36. Wang, Y., Lin, S. H., Li, H., and Kung, S. Y. Data mapping by probabilistic modular networks and information theoretic criteria. *IEEE Trans. Signal Process.*, **46**: 3378–3397, 1998.

37. Hedenfalk, I., Duggan, D., Chen, Y., Radmacher, M., Bittner, M., Simon, R., Meltzer, P., Gusterson, B., Esteller, M., Kallioniemi, O. P., Wilfond, B., Borg, A., and Trent, J. Gene-expression profiles in hereditary breast cancer. *N. Engl. J. Med.*, **344**: 539–548, 2001.

38. Brankin, B., Skaar, T. C., Trock, B. J., Berris, M., and Clarke, R. Autoantibodies to numatrin: an early predictor for relapse in breast cancer. *Cancer Epidemiol. Biomark. Prev.*, **7**: 1109–1115, 1998.

39. Clauss, I. M., Chu, M., Zhao, J. L., and Glimcher, L. H. The basic domain/leucine zipper protein hXBp-1 preferentially binds to and transactivates CRE-like sequences containing an ACGT core. *Nucleic Acids Res.*, **24**: 1855–1864, 1996.

40. Clauss, I. M., Gravellies, E. M., Darling, J. M., Shapiro, F., Glimcher, M. J., and Glimcher, L. H. *In situ* hybridization studies suggest a role for the basic region-leucine zipper protein hXBp-1 in exocrine gland and skeletal development during mouse embryogenesis. *Dev. Dyn.*, **197**: 146–156, 1993.

41. West, M., Blanchette, C., Dressman, H., Huang, E., Ishida, S., Spang, R., Zuzan, H., Olson, J. A., Jr., Marks, J. R., and Nevins, J. R. Predicting the clinical status of human breast cancer by using gene expression profiles. *Proc. Natl. Acad. Sci. USA*, **98**: 11462–11467, 2001.

42. Thompson, E. W., Brünner, N., Torri, J., Johnson, M. D., Boulay, V., Wright, A., Lippman, M. E., Steeg, P. S., and Clarke, R. The invasive and metastatic properties of hormone-independent and hormone-responsive variants of MCF-7 human breast cancer cells. *Clin. Exp. Metastasis*, **11**: 15–26, 1993.

43. Rochefort, H., Liandet, E., and Garcia, M. Alterations and role of human cathepsin D in cancer metastasis. *Enzyme Protein*, **49**: 106–116, 1996.

44. Keeling, J., and McKee, G. T. Heat shock protein (HSP)27: a further refinement in the diagnosis of suspicious fine needle aspirates of breast. *Cytopathology*, **10**: 40–49, 1999.

45. Ogawa, K., Kudo, H., Kim, Y. C., Nakashima, Y., Ohshio, G., and Yamabe, H. Expression of vitamin B12 R-binder in breast tumors. An immunohistochemical study. *Arch. Pathol. Lab. Med.*, **112**: 1117–1120, 1988.

46. Wu, K., Helzlsouer, K. J., Cornstock, G. W., Hoffman, S. C., Nadeau, M. R., and Sellhub, J. A prospective study on folate, B12, and pyridoxal 5'-phosphate (B6) and breast cancer. *Cancer Epidemiol. Biomark. Prev.*, **8**: 209–217, 1999.

47. Clark, G. J., and Der, C. J. Aberrant function of the Ras signal transduction pathway in human breast cancer. *Breast Cancer Res. Treat.*, **35**: 133–144, 1995.

48. Gumer, G., Kirkali, G., Yenisey, C., and Tore, J. R. Cytosol and serum ferritin in breast carcinoma. *Cancer Lett.*, **67**: 103–112, 1992.

49. Kerr, M. K., and Churchill, G. A. Bootstrapping cluster analysis: assessing the reliability of conclusions from microarray experiments. *Proc. Natl. Acad. Sci. USA*, **98**: 8961–8965, 2001.

50. Novak, J. P., Sladek, R., and Hudson, T. J. Characterization of variability in large-scale gene expression data: implications for study design. *Genomics*, **79**: 104–113, 2002.

51. Dotzlaw, H., Miller, T., Karvelas, J., and Murphy, L. C. Epidermal growth factor gene expression in human breast cancer biopsy samples: relationship to estrogen and progesterone receptor gene expression. *Cancer Res.*, **50**: 4204–4208, 1990.

52. Tsai, J. C., Liu, L., Guan, J., and Aird, W. C. The egr-1 gene is induced by epidermal growth factor in ECV304 cells and primary endothelial cells. *Am. J. Physiol. Cell Physiol.*, **279**: C1414–C1424, 2000.

53. Das, A., Chendil, D., Dey, S., Mohiuddin, M., Mohiuddin, M., Milbradt, J. D., Rangnekar, V. M., and Ahmed, M. M. Ionizing radiation down-regulates p53 protein in primary Egr-1 $^{-/-}$ mouse embryonic fibroblast cells causing enhanced resistance to apoptosis. *J. Biol. Chem.*, 2000.

54. Chapman, N. R., and Perkins, N. D. Inhibition of the RelA(p65) NF- κ B subunit by Egr-1. *J. Biol. Chem.*, **275**: 4719–4725, 2000.

55. Huang, R. P., Fan, Y., de Belle, I., Niemeyer, C., Gottardis, M. M., Mercola, D., and Adamson, E. D. Decreased Egr-1 expression in human, mouse and rat mammary cells and tissues correlates with tumor formation. *Int. J. Cancer*, **72**: 102–109, 1997.

56. Tanaka, N., Ishihara, M., Kitagawa, M., Harada, H., Kimura, J., Matsuyama, T., Lamphier, M. S., Aizawa, S., Mak, T. W., and Taniguchi, T. Cellular commitment to oncogene-induced transformation or apoptosis is dependent on the transcription factor IRE-1. *Cell*, **77**: 829–839, 1994.

57. Tanaka, N., Ishihara, M., Kitagawa, M., Nozawa, H., Matsuyama, T., Mak, T. W., Aizawa, S., Tokino, T., Oren, M., and Taniguchi, T. Cooperation of the tumour suppressors IRE-1 and p53 in response to DNA damage. *Nature (Lond.)*, **382**: 816–818, 1996.

58. Mori, K., Stone, S., Khaodhia, L., Braverman, L. E., and DeVito, W. J. Induction of transcription factor interferon regulatory factor-1 by interferon- γ (IFN γ) and tumor necrosis factor- α (TNF α) in FRTL-5 cells. *J. Cell Biochem.*, **74**: 211–219, 1999.

59. Birow, M. E., Weldon, C. B., Tang, Y., Navar, G. L., Krajewski, S., Reed, J. C., Hammond, T. G., Clejan, S., and Beckman, B. S. Differences in susceptibility to tumor necrosis factor α -induced apoptosis among MCF-7 breast cancer cell variants. *Cancer Res.*, **58**: 4940–4946, 1998.

60. Egebäld, M., and Jaattela, M. Cell death induced by TNF or serum starvation is independent of ErbB receptor signaling in MCF-7 breast carcinoma cells. *Int. J. Cancer*, **86**: 617-625, 2000.

61. Sheen-Chen, S. M., Chen, W. J., Eng, H. L., and Chou, F. F. Serum concentration of tumor necrosis factor in patients with breast cancer. *Breast Cancer Res. Treat.*, **43**: 211-215, 1997.

62. Zhou, B. P., Hu, M. C., Miller, S. A., Yu, Z., Xia, W., Lin, S. Y., and Hung, M. C. HER-2/neu blocks tumor necrosis factor-induced apoptosis via the Akt/NF- κ B pathway. *J. Biol. Chem.*, **275**: 8027-8031, 2000.

63. Ziyad, A., Bernard, J., Clarke, R., Tursz, T., Brockhaus, M., and Chouaib, S. Human breast cancer cross-resistance to TNF and adriamycin: relationship to MDR1. Mn-SOD and TNF gene expression. *Cancer Res.*, **54**: 825-831, 1994.

64. Schiff, R., Reddy, P., Ahottupa, M., Coronado-Heinsohn, E., Grim, M., Hilsenbeck, S. G., Lawrence, R., Deneke, S., Herrera, R., Chamness, G. C., Fuqua, S. A., Brown, P. H., and Osborne, C. K. Oxidative stress and AP-1 activity in tamoxifen-resistant breast tumors *in vivo*. *J. Natl. Cancer Inst.*, **92**: 1926-1934, 2000.

65. Nakshatri, H., Bhat-Nakshatri, P., Martin, D. A., Goulet, R. J., and Sledge, G. W. Constitutive activation of NF- κ B during progression of breast cancer to hormone-independent growth. *Mol. Cell. Biol.*, **17**: 3629-3639, 1997.

66. Clarkson, R. W., and Watson, C. J. NF- κ B and apoptosis in mammary epithelial cells. *J. Mammary Gland Biol. Neoplasia*, **4**: 165-175, 1999.

67. van der Burg, B., Slager-Davidov, R., van der Leede, B. M., de Laat, S. W., and van der Saag, P. T. Differential regulation of AP-1 activity by retinoic acid in hormone-dependent and -independent breast cancer cells. *Mol. Cell. Endocrinol.*, **112**: 143-152, 1995.

68. Hehner, S. P., Hofmann, T. G., Droege, W., and Schmitz, M. L. The antiinflammatory sesquiterpene lactone parthenolide inhibits NF- κ B by targeting the I κ B kinase complex. *J. Immunol.*, **163**: 5617-5623, 1999.

69. Patel, N. M., Nozaki, S., Shortle, N. H., Bhat-Nakshatri, P., Newton, T. R., Rice, S., Gelfanov, V., Boswell, S. H., Goulet, R. J., Jr., Sledge, G. W., Jr., and Nakshatri, H. Paclitaxel sensitivity of breast cancer cells with constitutively active NF- κ B is enhanced by I κ B α super-repressor and parthenolide. *Oncogene*, **19**: 4159-4169, 2000.

70. Garcia-Pineres, A. J., Castro, V., Mora, G., Schmidt, T. J., Strunck, J., Pahl, H. L., and Merfort, I. Cysteine 38 in p65/NF- κ B plays a crucial role in DNA binding inhibition by sesquiterpene lactones. *J. Biol. Chem.*, **276**: 39713-39720, 2001.

71. Taniguchi, T. Transcription factors IRF-1 and IRF-2: Linking the immune responses and tumor suppression. *J. Cell. Physiol.*, **173**: 128-130, 1997.

72. Tamura, T., Ishihara, M., Lamphier, M. S., Tanaka, N., Oishi, J., Alzawa, S., Matsuyama, T., Mak, T. W., Taki, S., and Taniguchi, T. An IRF-1-dependent pathway of DNA damage-induced apoptosis in mitogen-activated T lymphocytes. *Nature (Lond.)*, **376**: 596-599, 1995.

73. Saneau, J., Hiscock, J., Delatré, O., and Wietzerbin, J. IFN- β induces serine phosphorylation of Stat-1 in Ewing's sarcoma cells and mediates apoptosis via induction of IRF-1 and activation of caspase-7. *Oncogene*, **19**: 3372-3383, 2000.

74. Boudreau, N., Sympon, C. J., Werb, Z., and Bissell, M. J. Suppression of ICE and apoptosis in mammary epithelial cells by extracellular matrix. *Science (Wash. DC)*, **267**: 891-893, 1995.

75. Kean, M. M., Ettenberg, S. A., Lowrey, G. A., Russell, E. K., and Lipkowitz, S. Fas expression and function in normal and malignant breast cell lines. *Cancer Res.*, **56**: 4791-4798, 1996.

76. Skaar, T. C., Bouker, K. B., and Clarke, R. Interferon regulatory factor-1 (IRF-1) in breast cancer. *Proc. Am. Assoc. Cancer Res.*, **41**: 428, 2000.

77. Kondo, T., Minamino, N., Nagamura-Inoue, T., Matsumoto, M., Taniguchi, T., and Tanaka, N. Identification and characterization of nucleophosmin/B23/nurratin which binds the anti-oncogenic transcription factor IRF-1 and manifests oncogenic activity. *Oncogene*, **15**: 1275-1281, 1997.

78. Wang, C. Y., Cusack, J. C., Jr., Liu, R., and Baldwin, A. S., Jr. Control of inducible chemoresistance: enhanced anti-tumor therapy through increased apoptosis by inhibition of NF- κ B. *Nat. Med.*, **5**: 412-417, 1999.

79. Kim, D. W., Sovak, M. A., Zanieski, G., Nonet, G., Romieu-Mourez, R., Lau, A. W., Hafer, L. J., Yaswen, P., Stampfer, M., Rogers, A. E., Russo, J., and Sonenschein, G. E. Activation of NF- κ B/Rel occurs early during neoplastic transformation of mammary cells. *Carcinogenesis (Lond.)*, **21**: 871-879, 2000.

80. Welsh, P. L., and King, M. C. BRCA1 and BRCA2 and the genetics of breast and ovarian cancer. *Hum. Mol. Genet.*, **10**: 705-713, 2001.

81. Blum, D., Torch, S., Nissou, M. F., and Verna, J. M. 6-hydroxydopamine-induced nuclear factor- κ B activation in PC12 cells. *Biochem. Pharmacol.*, **62**: 473-481, 2001.

82. Cavallini, L., Francesconi, M. A., Zoccarato, F., and Alexandre, A. Involvement of nuclear factor- κ B (NF- κ B) activation in mitogen-induced lymphocyte proliferation: inhibitory effects of lymphoproliferation by salicylates acting as NF- κ B inhibitors. *Biochem. Pharmacol.*, **62**: 141-147, 2001.

83. Habener, J. F. Cyclic AMP response element binding proteins: a cornucopia of transcription factors. *Mol. Endocrinol.*, **4**: 1087-1094, 1990.

84. Borrelli, E., Montmayeur, J. P., Foulkes, N. S., and Sascone-Corsi, P. Signal transduction and gene control: the cAMP pathway. *Crit. Rev. Oncog.*, **3**: 321-338, 1992.

85. Cho, H., Aronica, S. M., and Katzenellenbogen, B. S. Regulation of progesterone receptor gene expression in MCF-7 breast cancer cells: a comparison of the effects of cyclic adenosine 3', 5'-monophosphate, estradiol, insulin-like growth factor-I, and serum factors. *Endocrinology*, **134**: 658-664, 1994.

86. Lee, Y. N., Park, Y. G., Choi, Y. H., Cho, Y. S., and Cho-Chung, Y. S. CRE-transcription factor decoy oligonucleotide inhibition of MCF-7 breast cancer cells: cross-talk with p53 signaling pathway. *Biochemistry*, **39**: 4863-4868, 2000.

87. Drew, P. D., Franzoso, G., Becker, K. G., Bours, V., Carlson, L. M., Siebenlist, U., and Ozato, K. NF- κ B and interferon regulatory factor 1 physically interact and synergistically induce major histocompatibility class I gene expression. *J. Interferon Cytokine Res.*, **15**: 1037-1045, 1995.

88. Neish, A. S., Read, M. A., Thanos, D., Pine, R., Maniatis, T., and Collins, T. Endothelial interferon regulatory factor 1 cooperates with NF- κ B as a transcriptional activator of vascular cell adhesion molecule 1. *Mol. Cell. Biol.*, **15**: 2558-2569, 1995.

89. Coccia, E. M., Del Russo, N., Stellacci, E., Orsatti, R., Benedetti, E., Marzill, G., Hiscock, J., and Battistini, A. Activation and repression of the 2'-5'A synthetase and p21 gene promoters by IRF-1 and IRF-2. *Oncogene*, **18**: 2129-2137, 2000.

90. Escalante, C. R., Yic, J., Thanos, D., and Aggarwal, A. K. Structure of IRF-1 bound DNA reveals determinants of interferon regulation. *Nature (Lond.)*, **391**: 103-106, 1998.

91. Lee, A. H., Hong, J.-H., and Seo, Y. S. Tumor necrosis factor- α and interferon- γ synergistically activate the RANTES promoter through nuclear factor- κ B and interferon regulatory factor 1 (IRF-1) transcription factors. *Biochem. J.*, **350**: 131-138, 2000.

92. Saneau, J., Kaisho, T., Hirano, T., and Wietzerbin, J. Triggering of the human interleukin-6 gene by interferon- γ and tumor necrosis factor- α in monocytic cells involves cooperation between interferon regulatory factor-1, NF- κ B, and SP1 transcription factors. *J. Biol. Chem.*, **270**: 27920-27931, 1995.

93. Kim, T. K., and Maniatis, T. The mechanism of transcriptional synergy of an *in vitro* assembled interferon- β enhancerosome. *Mol. Cell. Biol.*, **1**: 119-129, 1997.

94. van den Berg, H. W., Leahy, W. J., Lynch, M., Clarke, R., and Nelson, J. Recombinant human interferon α increases oestrogen receptor expression in human breast cancer cells (ZR-75-1) and sensitises them to the anti-proliferative effects of tamoxifen. *Br. J. Cancer*, **55**: 255-257, 1987.

95. Lindner, D. J., and Borden, E. C. Effects of tamoxifen and interferon- β or the combination on tumor-induced angiogenesis. *Int. J. Cancer*, **71**: 456-461, 1997.

96. Buzzi, E., Brugia, M., Trippa, F., Rossi, G., Trivisonne, R., Giustini, L., Pinaglia, D., Capparella, V., and Sica, G. Natural interferon- β and tamoxifen in hormone-resistant patients with advanced breast cancer. *Anticancer Res.*, **15**: 2187-2190, 1995.

97. Delgado, M., Munoz-Elias, E. J., Gornariz, R. P., and Ganea, D. Vasointestinal polypeptide and pituitary adenylate cyclase-activating polypeptide prevent inducible nitric oxide synthase transcription in macrophages by inhibiting NF- κ B and IFN regulatory factor 1 activation. *J. Immunol.*, **162**: 4685-4696, 1999.

98. Clarke, R., Dickson, R. B., and Lippman, M. E. Hormonal aspects of breast cancer: growth factors, drugs and stromal interactions. *Crit. Rev. Oncol. Hematol.*, **12**: 1-23, 1992.

Iterative Normalization of cDNA Microarray Data

Yue Wang, Jianping Lu, Richard Lee, Zhiping Gu, and Robert Clarke

Abstract—This paper describes a new approach to normalizing microarray expression data. The novel feature is to unify the tasks of estimating normalization coefficients and identifying control gene set. Unification is realized by constructing a window function over the scatter plot defining the subset of constantly expressed genes and by affecting optimization using an iterative procedure. The structure of window function gates contributions to the control gene set used to estimate normalization coefficients. This window measures the consistency of the matched neighborhoods in the scatter plot and provides a means of rejecting control gene outliers. The recovery of normalizational regression and control gene selection are interleaved and are realized by applying coupled operations to the mean square error function. In this way, the two processes bootstrap one another. We evaluate the technique on real microarray data from breast cancer cell lines and complement the experiment with a data cluster visualization study.

Index Terms—Data normalization, dynamic programming, gene expression, gene microarray, linear regression.

I. INTRODUCTION

SPOTTED cDNA microarrays are emerging as a powerful and cost-effective tool for the large-scale analysis of gene expression. Using this technology, the relative expression levels in two or more mRNA populations derived from tissue samples can be assayed for thousands of genes simultaneously [1], [2]. Microarrays are potentially powerful tools for investigating the mechanism of drug action. Two recent studies have described the application of high-density microarrays to examine the effects of drugs on gene expression in yeast as a model system. A similar method applied to human breast cancer cells and tissues would have direct utility in the identification and validation of novel therapeutics. It is widely accepted that the pattern of genes expressed within a specific cell is essentially responsible for its phenotype. The most widely publicized use of gene microarrays has been in cancer research.

From a statistical point of view, sources of measurement error within an array, and variation between arrays, must be quantified and taken into account in order to make indirect comparisons among samples that have not been directly assayed on the same array. For example, gene microarrays vary with production batches, e.g., introducing variations in the amount of probe that hybridizes to areas of the support that do not contain target cDNAs, or the amount of the cDNA spotted onto the support

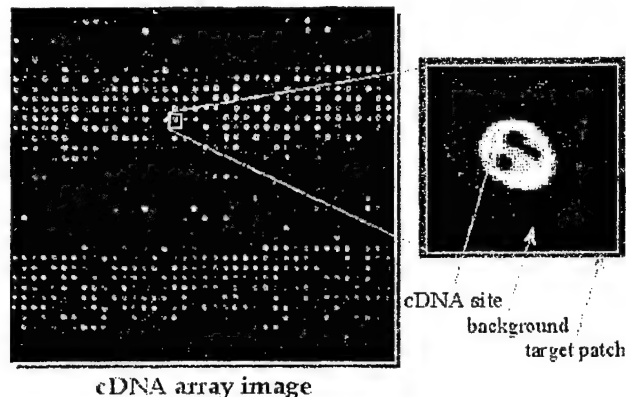


Fig. 1. Example of cDNA microarray image.

surface. The specific activity of the probe will vary from probe to probe, often reflecting variations in the amount of signal produced by each molecule of label incorporated into the probe.

Two major data preprocessing operations are involved: background correction and interexperiment normalization. In background correction, local sampling of background can be used to specify a threshold that a true signal must exceed. It is even possible to accurately detect weak signals and extract a mean intensity above background for the target [3]. A typical cDNA array image is given in Fig. 1.

In carrying out comparisons of expression data using measurements from a single array or multiple arrays, the question of normalizing data arises. A reasonable assumption, adopted by most researchers, is that all experiments are carried out under conditions of a large excess of immobilized probe relative to labeled target. The kinetics of hybridization are therefore pseudofirst order, and interprobe competition is not a factor [3]. Under these assumptions, the linear differences arising from the exact amount of applied target, extent of target labeling, efficiencies of fluor excitation and emission, and detector efficiency can be compounded into a single variable. Two major strategies can be used to carry out normalization. One is based on a consideration of all of the genes in the sample, and the other on a designated subset expected to be unchanged over most circumstances, called the control gene set. In instances of closely related samples, global normalization (e.g., using all genes) will be a useful tool. As samples become more divergent, a good normalization may be achieved using a subset of constantly expressed genes (e.g., using only control genes) [3].

The work most closely related to our methodology was reported in [4]. The authors introduced a comparison of gene expression levels arising from cohybridized samples by taking ratios of average expression levels for individual genes. A novel method of image segmentation was presented to identify cDNA

Manuscript received March 28, 2001; revised September 14, 2001. This work was supported in part by the National Institutes of Health under Grants 5R21CA83231 and R01CA/AG58022.

Y. Wang and J. Lu are with the Department of Electrical Engineering and Computer Science, The Catholic University of America, Washington, DC 20064 USA.

R. Lee and R. Clarke are with the Lombardi Cancer Center, Georgetown University Medical Center, Washington, DC 20007 USA.

Z. Gu is with the Celera Genomics, Inc., Rockville, MD 20850 USA.

Publisher Item Identifier S 1089-7771(02)02009-5.

target sites, and a hypothesis test and confidence interval was developed to quantify the significance of observed differences in expression ratios. In particular, the probability density of the ratio and the maximum-likelihood estimator for the distribution were derived, and an iterative procedure for signal calibration was developed. In general, however, an integral of ratios is not the same as a ratio of integrals, and simple ratios of the data will not necessarily provide unbiased estimates of expression ratios. Alternatively, the mean value of all signals on the hybridized filter can be used for normalization, and further normalizations can be done to a reference hybridization [5]. Nonetheless, the optimal approach remains controversial.

II. METHOD AND ALGORITHM

In this paper, we adopt a somewhat different approach to the problem of normalizing microarray expression data. Rather than rejecting those control genes that give rise to a large normalization error, we attempt to iteratively correct them. In a nutshell, our idea is to bootstrap by alternating between estimating normalization coefficients and identifying control gene subset. The framework is furnished by constructing a window function over the scatter plot defining the subset of constantly expressed genes. Specifically, this window measures the consistency of the matched neighborhoods in the scatter plot and provides a means of rejecting control gene outliers. We evaluate the technique on real microarray data from breast cancer cell lines and complement the experiment with a data cluster visualization study.

Our goal is to generate a transformation that best maps the expression levels of floating data set onto their counterparts in a reference data set. Assume that data points $\{x_1, x_2, \dots, x_{n_c}\}$ and $\{y_1, y_2, \dots, y_{n_c}\}$ are the expression levels of the control or housekeeping genes from two microarray experiments, where n_c is the total number of control genes. In this paper, we use $\{x_i\}$ as the floating data set and $\{y_i\}$ as the reference data set. We further assume that the normalization can be accurately achieved through a linear regression mapping

$$y_i = ax_i + b \quad (1)$$

where a is the true ratio of the data and b is the bias correction of the data. Since there are two free parameters in the transformation, the estimation of their values requires a minimum of two data points that are known to be in correspondence. By considering noise effect, however, more control points are needed to produce an accurate estimate. This process is overconstrained and can be solved using least squares estimation. Clearly, a natural criterion is the minimum mean squared error between the two control data subsets. Based on the expression levels of the control genes, the mean squared error (MSE) can be written as

$$\epsilon = \frac{1}{n_c} \sum_{i=1}^{n_c} [y_i - (ax_i + b)]^2. \quad (2)$$

Thus, the search principle for estimating the optimal values of a and b is simply taking the partial derivatives of the MSE and

setting them to zero. It can be shown that the estimated linear regression coefficients a and b can be calculated by [6]

$$a = \frac{\sum_{i=1}^{n_c} (x_i - \mu_x)(y_i - \mu_y)}{\sum_{i=1}^{n_c} (x_i - \mu_x)^2} \quad (3)$$

$$b = \mu_y - a\mu_x \quad (4)$$

where μ_x and μ_y are the means of $\{x_i\}$ and $\{y_i\}$, respectively, given by

$$\mu_x = \frac{1}{n_c} \sum_{i=1}^{n_c} x_i, \quad \mu_y = \frac{1}{n_c} \sum_{i=1}^{n_c} y_i \quad (5)$$

and the normalization shall be performed for all of the data points in the floating data set based on (1).

The accuracy of the method highly depends on the selection of control genes. In addition to the predetermined control genes, including housekeeping genes, we shall add more control genes based on a reasonable heuristics that the genes that are nondifferentially expressed should be considered as control genes in normalization. Posed in this way, there is a basic "chicken-and-egg" problem [7]. Before a good control gene subset can be defined, expression levels of all genes need to be reasonably normalized. Yet, this normalization is, after all, the ultimate goal of computation.

We propose an iterative regression normalization algorithm to solve this problem. First, solely based on the predetermined control genes such as housekeeping genes, we will conduct an initial normalization to all data sets based on (1)–(5). Since an accurate data analysis requires several repetitive cDNA hybridizations in microarray studies [8], starting from the whole data set, we will then eliminate those genes from the control gene list whose expressions have a large standard deviation across replications, namely, outliers, according to the criterion given by

$$\mu_i = \frac{1}{m_i} \sum_{j=1}^{m_i} x_{i,j}, \quad \sqrt{\frac{1}{m_i} \sum_{j=1}^{m_i} \left(\frac{x_{i,j}}{\mu_i} - 1 \right)^2} \geq \epsilon_1 \quad (6)$$

for all genes, where m_i is the number of replications for gene i in the experiment, $x_{i,j}$ is the expression level of gene i in the j th replication, μ_i is the mean of replications, and ϵ_1 is a predetermined threshold.

In our experiment, ϵ_1 is determined as follows. For each of the genes, the replications are normalized by its mean and the normalized standard deviation is calculated. A mean standard deviation is then obtained by the sample average of the individual normalized standard deviations. Our experience has shown that ϵ_1 being two times of the mean standard deviation is appropriate and effective. It should be noted that this criterion will also eliminate differentially expressed genes from the control gene list. Thus, a gene will be selected as a control gene if its expression level pair across reference and floating experiments satisfies

$$\epsilon_2 \leq \sqrt{x_i^2 + y_i^2} \leq \epsilon_3 \quad \text{and} \quad \left| \frac{\log x_i}{\log y_i} - 1 \right| \leq \epsilon_4 \quad (7)$$

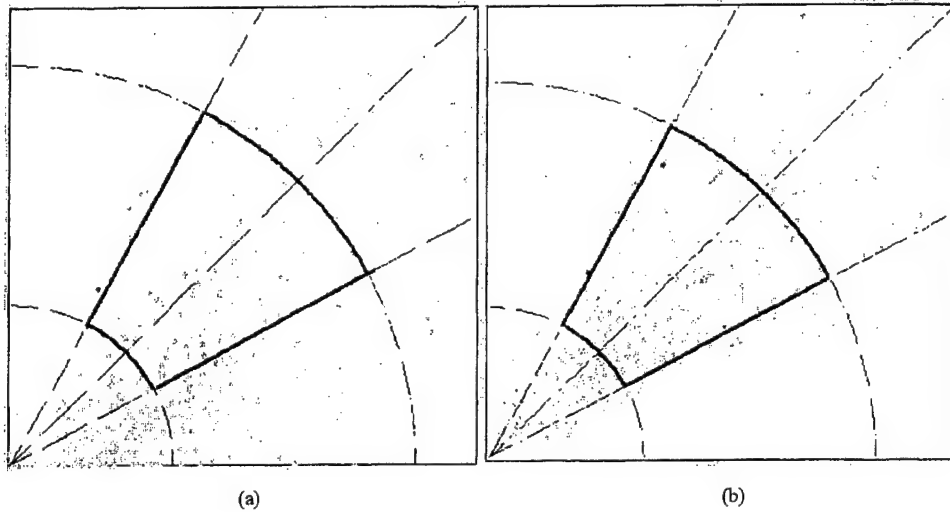


Fig. 2. Example of control gene selection window. (a) Before and (b) after normalization.

where ϵ_2 , ϵ_3 , and ϵ_4 are the empirically predetermined thresholds defining the subset of constantly expressed genes. It can be seen that (7) defines a window function over the scatter plot. A typical window function is illustrated in Fig. 2. In particular, as we have noted according to our experience, ratios can be very unstable when one (or both) of the signals is small or large. Thus, we further eliminate unstably expressed genes from the control gene list using the constraints defined by ϵ_2 and ϵ_3 . Clearly, ϵ_4 provides the boundaries of a constantly expressed gene subset.

The algorithm first generates the interim scatter plot of the data sets through the observations and the current parameter estimates [(1)] and then updates parameter estimates using a newly defined control gene subset [(3)–(5)]. The procedure cycles back and forth between these two steps until it reaches a stationary point where no significant change occurs to the content of the control gene subset. A summary of the major steps is given as follows.

- 1) Based on predetermined control genes including house-keeping genes, estimate initial values of $a^{(0)}$ and $b^{(0)}$ and perform an initial normalization using (3)–(5) and (1), where only one data set is used as a reference set and all other data sets are considered as floating sets and shall be normalized to the reference set.
- 2) Eliminate those genes from the control gene list whose expressions have a large standard deviation across replications, according to the criterion given by (6).
- 3) For each of experiment pairs, construct a new control gene subset by selecting additional control genes that satisfy (7).
- 4) Based on the newly constructed control gene subset, estimate interim values of $a^{(m)}$ and $b^{(m)}$ and perform data normalization for each of the floating data sets using (3)–(5) and (1), where m is the iteration index.
- 5) Repeat Steps 3) and 4) until the convergence ($a^{(\infty)} \rightarrow 1$ and $b^{(\infty)} \rightarrow 0$) is reached or no significant change occurs to the content of the control gene subset.

The philosophy for estimating normalization coefficients and identifying a control gene set is similar in spirit to the *self-organizing principle* [9], [10]. The structure of window function gates contributions to the control gene subset used to estimate normalization coefficients such that possible oscillation during algorithm convergence can be prevented. Specifically, the window function defines a neighborhood of scatter centroid to gating consistency contribution of the control gene subset to normalization. By making the value ϵ_4 of the topological window function decrease with time, the neighborhood is initially very large and shrinks slowly to its final desired size (e.g., a nearest neighbor structure). A popular choice for the dependence of ϵ_4 on discrete time m is the exponential decay [9]. In addition, the actual algorithm implementation concerns the issue of numerical stability. We have applied a simple dynamic programming technique to estimating normalization coefficients, called a factoring-shifting (FS) procedure.

The structure of window function gates contributions to the control gene subset used to estimate normalization coefficients such that possible oscillation during algorithm convergence can be prevented. Specifically, the window function defines a neighborhood of scatter centroid to gating consistency contribution of the control gene subset to normalization. By making the value ϵ_4 of the topological window function decrease with time, the neighborhood is initially very large and shrinks slowly to its final desired size (e.g., a nearest neighbor structure). A popular choice for the dependence of ϵ_4 on discrete time m is the exponential decay [9]. In addition, the actual algorithm implementation concerns the issue of numerical stability. We have applied a simple dynamic programming technique to estimating normalization coefficients, called a factoring-shifting (FS) procedure.

F-Step

$$a^{(k|m)} = \frac{\sum_{i=1}^{n_c} x_i^{(k|m)} y_i}{\sum_{i=1}^{n_c} [x_i^{(k|m)}]^2} \quad (8)$$

$$x_i^{(k'|m)} = a^{(k|m)} x_i^{(k|m)} \quad (9)$$

S-Step

$$b^{(k|m)} = \frac{1}{n_c} \sum_{i=1}^{n_c} [y_i - x_i^{(k'|m)}] \quad (10)$$

$$x_i^{(k+1|m)} = x_i^{(k'|m)} + b^{(k|m)} \quad (11)$$

where at each complete cycle of the procedure, we first use the “old” set of floating data to determine the normalization factor $a^{(k|m)}$ using (8) by setting $b = 0$ and simply rescale floating data values using (9). These interim results $x_i^{(k'|m)}$ are then used to obtain the normalization shift $b^{(k|m)}$ using (10) by setting

$a = 1$ and further generate "new" values $x_i^{(k+1|m)}$ of floating data using (11). The procedure cycles back and forth until the values of $a^{(\infty|m)}$ and $b^{(\infty|m)}$ reach their stationary points.

In relation to previous work, the concept of using linear regression analysis for microarray normalization can be traced back to [4] and was further developed in [12] for iterative regression in conjunction with control gene selection. Such approaches are based on several assumptions regarding the data and can be considered as special cases of our framework [5].

The primary assumption is that for either the entire collection of arrayed genes or some subset such as housekeeping genes, the shift of the measured expression averaged over the set is zero (e.g., $b = 0$) and the ratio of normalized expression pair averaged over the set should be one [e.g., $1/n_c \sum_{i=1}^{n_c} (y_i/ax_i) = 1$]. Under these assumptions, there are basically three major approaches for calculating the normalization factor a [5]. The first simply uses the mean value of all the background-corrected signals. Normalization can be separately performed for each of the data sets, without explicitly calculating a and selecting a reference data set [15]. Specifically, if a raw data pair is denoted by $(\{x_i\}, \{y_i\})$, normalization leads to $(\{x_i/\sum_{i=1}^{n_c} x_i\}, \{y_i/\sum_{i=1}^{n_c} y_i\})$. By multiplying the pair with $\sum_{i=1}^{n_c} y_i$, the result is equivalent to using (4), that is, $(\{ax_i\}, \{y_i\})$, where $a = \sum_{i=1}^{n_c} y_i / \sum_{i=1}^{n_c} x_i$ and $b = 0$. A second approach uses simplified linear regression analysis, called linear regression through the origin [6]. Consequently, a scatter plot of the normalized data set pair should have a slope of one [5]. By setting $b = 0$ in (1) and (2), the normalization factor is given by $a = \sum_{i=1}^{n_c} x_i y_i / \sum_{i=1}^{n_c} x_i^2$. A third approach relies on the assumption that, for control genes, the distribution of expression levels can be modeled and the mean of the ratio adjusted to one [4]. An iterative procedure was developed to estimate a by $1/n_c \sum_{i=1}^{n_c} (y_i/x_i)$, once again setting $b = 0$. It should be noticed that some heuristic approximations have been made in using these approaches, since, in general

$$\frac{\sum_{i=1}^{n_c} y_i}{\sum_{i=1}^{n_c} x_i} \neq \frac{\sum_{i=1}^{n_c} x_i y_i}{\sum_{i=1}^{n_c} x_i^2} \neq \frac{1}{n_c} \sum_{i=1}^{n_c} \frac{y_i}{x_i} \quad (12)$$

and

$$b \neq 0 \quad (13)$$

while our method is presented as a standard linear regression analysis without any approximation step.

III. EXPERIMENT AND DISCUSSION

In this section, we will provide experimental evaluation of our new normalization method. This investigation has two related strands. First, we will furnish examples demonstrating the use of an iterative normalization scheme on real microarray data. Here, we will use two different data sets. The first of these involves *within-class* normalization of data from LCC1 breast cancer cell lines across replications. The second example involves normalizing *between-class* breast cancer cell line data from LCC1 against LCC9, whose phenotypes are known to be different from LCC1.

In the second strand of our experiments, we will provide an algorithm accuracy analysis. Here, we confine ourselves to the linear regression variant of the normalization process. The aim is to experimentally compare our iterative algorithm with the performance of each of its components taken individually, thus to demonstrate that the combined processing of both control gene selection and transformation coefficient estimation yields significant advantages over existing methods. In addition, we would like to acknowledge that although the cell lines are not fully representative of solid tumors in humans, their patterns of gene expression profile are rich in information with respect to drug resistance.

We obtained gene expression profiles from two breast cancer cell lines. MCF7/LCC1 is an estrogen-independent but antiestrogen responsive variant of the MCF-7 human breast cancer cell line [14], [15]. An antiestrogen resistant variant (MCF7/LCC9) was obtained by stepwise selection of MCF7/LCC1 cells against the steroid antiestrogen ICI 182 780 (trade name: Faslodex). MCF7/LCC9 cells have many of the characteristics seen in antiestrogen-resistant human breast cancers and provide a novel model in which to study antiestrogen resistance [14].

Gene expression profiles were obtained using the AtlasTM Human Array cDNA expression microarrays (Clontech, Laboratories, Inc., Palo Alto, CA). These microarrays are produced on nylon filters and contain 588 target genes and nine housekeeping genes. Briefly, total RNA was obtained from independent cultures of MCF7/LCC1 and MCF7/LCC9 cells with the TRIzol reagent (Life Technologies, Grand Island, NY). One μ g of DNase-treated mRNA was primed with Clontech's cDNA Synthesis Primer mix and the product reverse transcribed into radiolabeled cDNA with $[-32P]$ dATP (Amersham Life Science Inc., Arlington Heights, IL). Probes were purified, denatured, and both C0t-1 DNA and 1 M NaH2PO4 (pH 7.0) added to the denatured probe. Each microarray was prehybridized with 5-ml ExpressHyb buffer and 0.5-mg denatured DNA from sheared salmon testes. Microarray filters were hybridized overnight with the appropriate $[-32P]$ -labeled cDNA probe. The array was extensively washed and sealed in plastic, with signals detected by phosphorimage analysis using a Molecular Dynamics Storm phosphorimager (Molecular Dynamics, Sunnyvale, CA). Digitization of these signals provided numerical values representing the signal for each gene.

Generally, it has been assumed that, under variable conditions, the expression of housekeeping genes remains unchanged. Hence, high-throughput differential expression data can rely on these genes for data normalization. However, recent data indicate deviation from this concept [11].

To assess the effectiveness of housekeeping genes in normalizing cDNA microarray data, a normalization based on single linear regression is performed using only the set of nine housekeeping genes suggested by CLONTECH. The scatter plots of normalization results are given in Fig. 3. Although log-log-based scatter plots are widely used, we have decided to use original scaled scatter plots since our numerical simulations have shown possible misleading perceptions from the "distorted" shape of actual data distribution. Particularly focusing on breast cancer, we have observed significant variations in

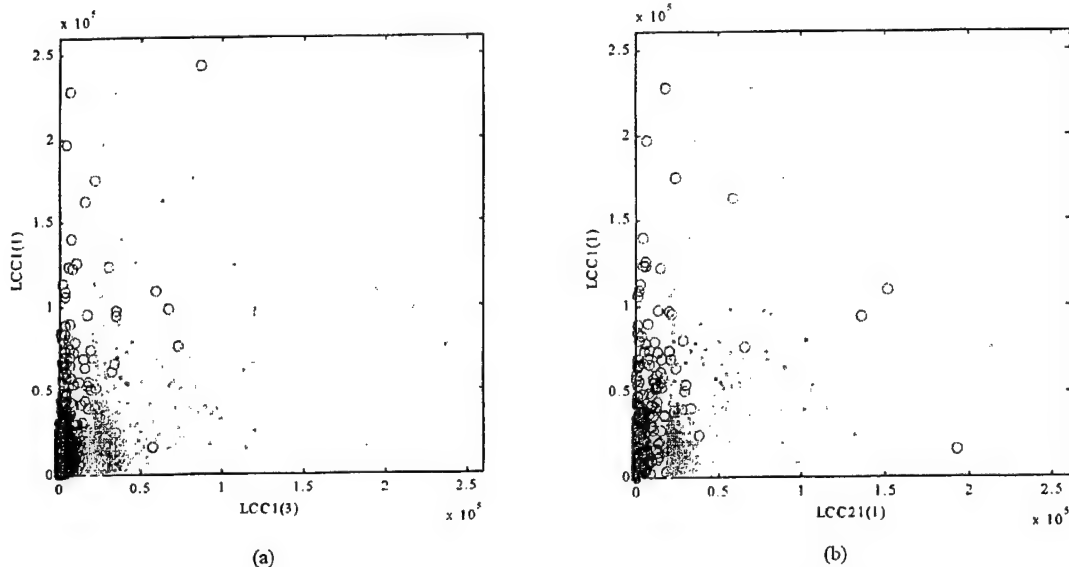


Fig. 3. (a) Scatter plot of *within-class* normalized microarray data based on nine housekeeping genes. (b) Scatter plot of *between-class* normalized microarray data based on nine housekeeping genes. (Circle: before normalization; dot: after normalization.)

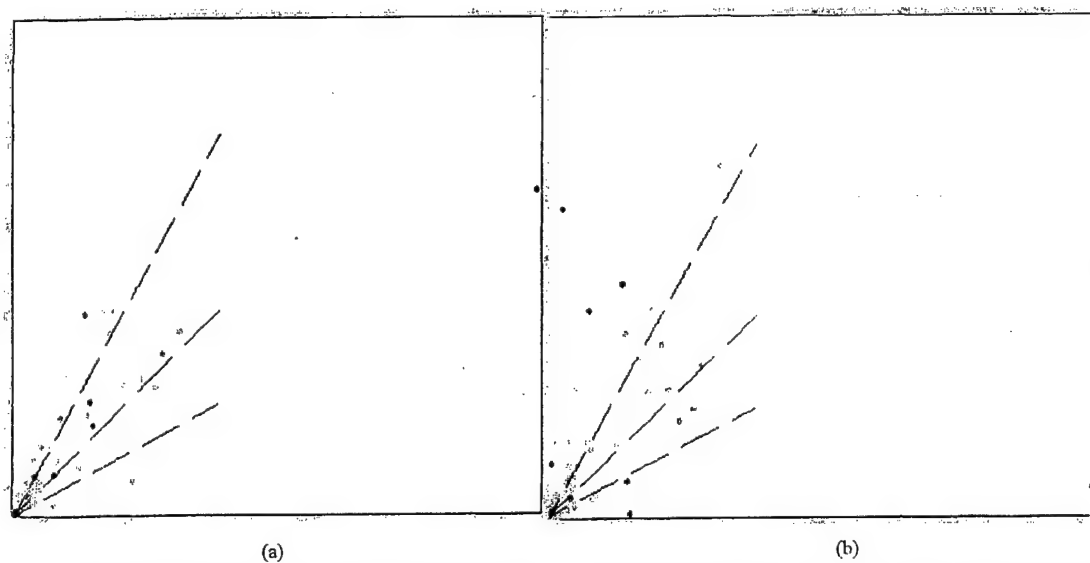


Fig. 4. Example of differential expression of housekeeping genes (red dots, where the dashed lines are the partition edges of the window functions). (a) *Within-class* and (b) *between-class*.

the expression of these housekeeping genes. For example, differential expression was observed between LCC1 and LCC9. See Fig. 4, where the data sets were normalized using the first method discussed above. This fact was observed from all of our experiments and shared by the same observation reported in [11]. Therefore, selection and use of housekeeping genes for normalization of differential expression data from various biological models should be approached with caution [11].

Since evaluation requires comparison with existing methods, we have implemented all three major approaches and applied these to the same data sets. In this experiment, all genes are considered as control genes and used in the calculation. Our measure of normalization accuracy is the MSE defined by (2) over the selected control gene set. The result of using the first

method is given in Fig. 5, where $a = \sum_{i=1}^{n_c} y_i / \sum_{i=1}^{n_c} x_i = 9.9$ and $b = 0$; an MSE of 8549 is reached. In the second method, normalization is based on a linear regression through the origin, i.e., $a = \sum_{i=1}^{n_c} x_i y_i / \sum_{i=1}^{n_c} x_i^2$ that is most close to the correct formulation. The corresponding result is shown in Fig. 6, where $a = 5.0$ and $b = 0$. A lower MSE of 3905 is obtained, consistent with our theoretical expectation. In Fig. 7, we show the normalization result using the third method, i.e., $a = 1/n_c \sum_{i=1}^{n_c} (y_i / x_i)$. As predicted, a biased estimate of the expression ratio is obtained, leading to a high MSE of 20 728 with $a = 18$.

These comparisons clearly indicate that the three existing approaches are not equivalent, as shown by both our experimental results and the theoretical justification of (12). To illustrate the

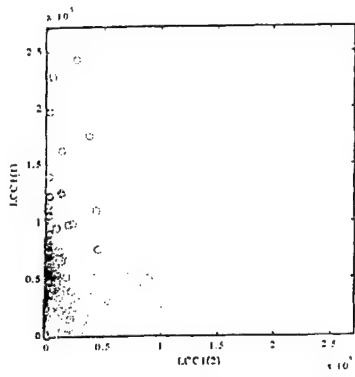


Fig. 5. Scatter plot of normalized microarray data using the existing method 1. (Circle: before normalization; dot: after normalization.)

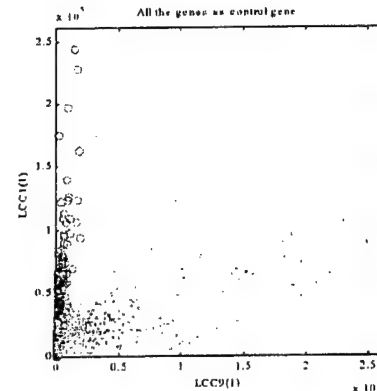


Fig. 8. Scatter plot of normalized *between-class* microarray data using the existing method 2. (Circle: before normalization; dot: after normalization.)

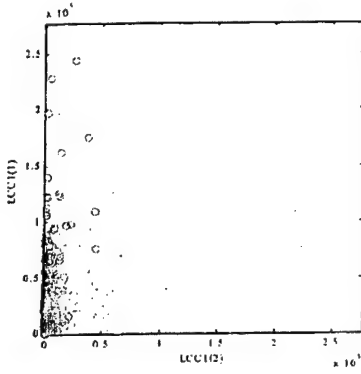


Fig. 6. Scatter plot of normalized microarray data using the existing method 2. (Circle: before normalization; dot: after normalization.)

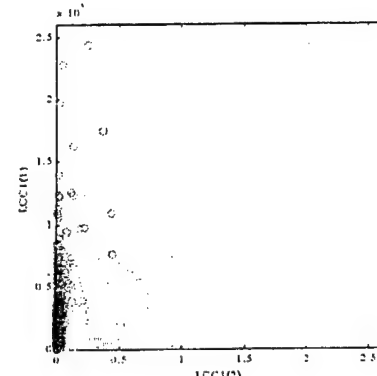


Fig. 9. Scatter plot of normalized *within-class* microarray data based on selected control gene subset using a static window function. (Circle: before normalization; dot: after normalization.)

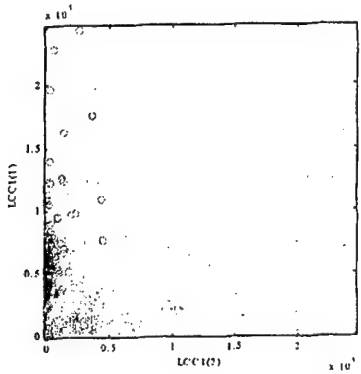


Fig. 7. Scatter plot of normalized microarray data using the existing method 3. (Circle: before normalization; dot: after normalization.)

impact of using the whole gene set as control gene set and using a dynamic programming technique on the normalization accuracy, we applied method 2 to the differential expression between LCC1 and LCC9. The scatter plot is given in Fig. 8. The corresponding MSE in this case is 6527, compared to the previous MSE of 3905. An increase in MSE suggests that, as samples become more divergent, a good normalization may be achieved using a subset of constantly expressed genes rather than a global normalization (e.g., using all genes) [3]. We then used the FS procedure to estimate both a and b . This additional step further

reduced the MSE to 6438, but this reduction is probably not significant.

To explore the effect of control gene selection, we first performed an initial linear regression using the whole gene set. Four different window functions were configured to select control gene subsets where $\epsilon_2 \leq r \leq \epsilon_3$ and ϕ is the sector angle of the window function. Based on the selected control genes, we then applied a single linear regression to normalizing *within-class* samples. A numerical comparison on the normalization accuracy of using different control gene subsets is conducted, as reported in Table I. The main feature to note from these results is that, for different window functions, a stable estimate of the scaling factor a is obtained, while the shifting offset b varies significantly from case to case. In addition, the MSEs of normalizations in all three cases are comparable (i.e., 5632~5796). The scatter plot of the best normalization result is shown in Fig. 9.

We further applied the same procedure to processing *between-class* samples and observed similar data characteristics. The scaling factor in this case is about $a = 44$, while b varies substantially. Not surprisingly, an increase in MSE is observed (i.e., 6754~7384). Numerical analysis with different window functions shows the capable nature of the approach, since the interim estimate of linear regression coefficient is very stable with a satisfactory low MSE. Indeed, the robustness of

TABLE I
NUMERICAL COMPARISONS OF NORMALIZATION RESULTS BASED ON A DESIGNATED SUBSET OF CONTROL GENES WITH DIFFERENT WINDOW CONFIGURATIONS

Window($\times 10^3$)	$r \in (1, 4), \phi = \frac{\pi}{16}$	$r \in (1, 4), \phi = \frac{\pi}{8}$	$r \in (3, 6), \phi = \frac{\pi}{8}$	$r \in (16, 29), \phi = \frac{\pi}{8}$
Coefficient	$a = 7.6, b = 8311$	$a = 7.7, b = 2885$	$a = 7.7, b = 803$	$a = 7.7, b = -11378$
MSE	5633	5676	5693	5796

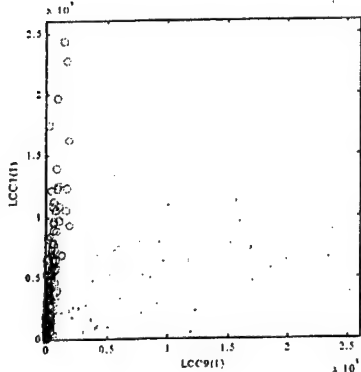


Fig. 10. Scatter plot of normalized *between-class* microarray data based on selected control gene subset using a static window function. (Circle: before normalization; dot: after normalization.)

the gene selection step has been successfully discovered in all our experiments. A typical scatter plot of *between-class* normalization results, using a window-based control gene selection, is given in Fig. 10.

Next, we provide an illustration of the iterative properties of our normalization algorithm. The sequence in our experiment shows the iterative recovery of the full linear regression matching. In this *within-class* case, $10000 < r < 24000$ and $\phi = \pi/2, \pi/4, \pi/8, \pi/16, \pi/32, \pi/48$. Each window shrinking step is mixed with one of the FS steps using the current set of recovered data points. The initial parameters are estimated based on the whole gene set. The normalization process converges to a good solution after six iterations. Figs. 11 and 12 show the scatter plots of initial and final normalization results. Once the algorithm has converged, the consistency of the control gene selection is significantly improved. Moreover, there are no erroneous matches between control genes for the last two adjacent iterations. The final control gene subset contains 37 genes. Finally, the MSE of 3892 is in good agreement with the corresponding results of the existing methods.

We next considered the iterative normalization for *between-class* samples. As a step toward improving the performance of microarray data normalization, we have put considerable effort into conducting various studies and developing reliable control gene selection and linear regression techniques. More precisely, we aim to perform an unsupervised normalization when confronted with unreliable housekeeping genes. Experience suggested that our newly proposed method can achieve this goal. We applied our algorithm to the differential expression between LCC1 and LCC9. In this *between-class* case, $10000 < r < 24000$ and $\phi = \pi/4, \pi/8, \pi/16, \pi/48$. As before, the initial parameters are estimated based on the whole gene set. The normalization process converges on a good solution after only four

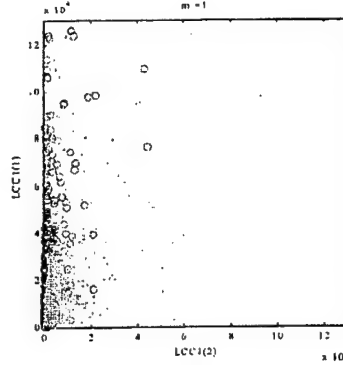


Fig. 11. Scatter plot of initial normalized *within-class* microarray data based on selected control gene subset using a dynamic window function. (Circle: before normalization; dot: after normalization.)

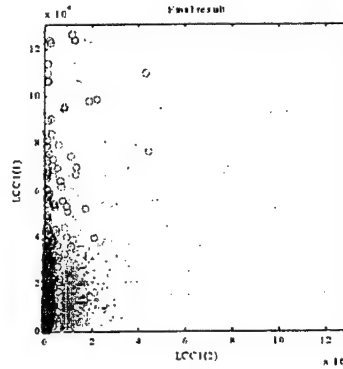


Fig. 12. Scatter plot of final normalized *within-class* microarray data based on selected control gene subset using a dynamic window function. (Circle: before normalization; dot: after normalization.)

iterations. Figs. 13 and 14 show the scatter plots of initial and final normalization results. The final control gene subset contains 43 genes, and a stable and satisfactory MSE of 6523 is reached.

Finally, we used our previously developed the VISDA algorithm to display the expression patterns of different cell line samples in the gene expression space [13]. All data were normalized using the new method. For a molecular analysis of breast cancer, the profile of microarray expression is the molecular signature of interest. The representation of each sample is described as a point in a d -dimensional gene expression space in which each axis represents the expression level of one gene. The presence of well-separated sample groups implies that the representations of samples within the same group are close to each other in this gene expression space but distant from those of other samples. Thus, the representations of phenotype-specific samples form clusters. Fig. 15 shows a

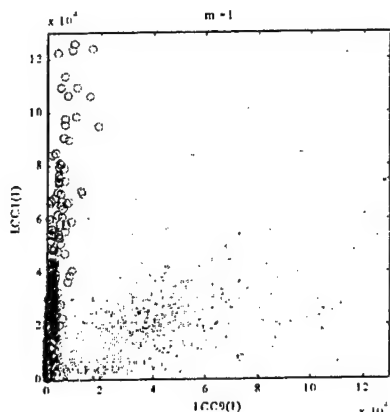


Fig. 13. Scatter plot of initial normalized *between-class* microarray data based on selected control gene subset using a dynamic window function. (Circle: before normalization; dot: after normalization.)

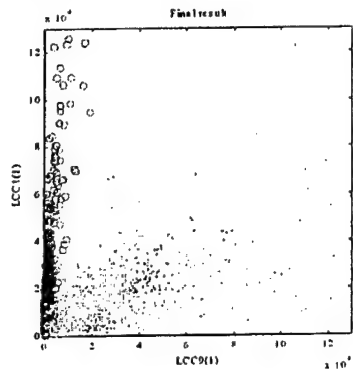


Fig. 14. Scatter plot of final normalized *between-class* microarray data based on selected control gene subset using a dynamic window function. (Circle: before normalization; dot: after normalization.)

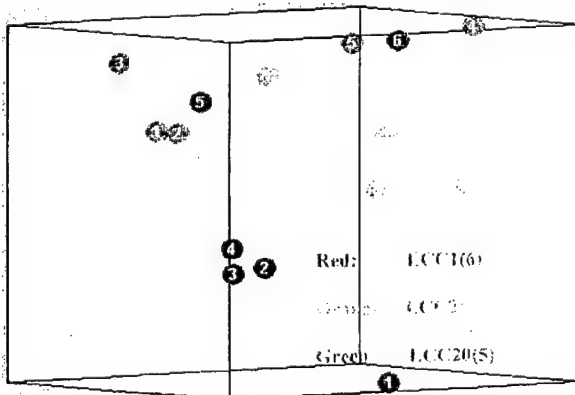


Fig. 15. Projection of 597-gene dimensions onto top three principal discriminant component spaces based on Fisher's scatter matrix measure of the separability of patterns. With an accurate data normalization, visual exploration reveals phenotype-specific sample clusters in gene expression space.

projected display of 597-gene dimensions into the top three principal discriminative component spaces, based on Fisher's scatter matrix [9]. With an accurate data normalization, visual exploration reveals three phenotype-specific sample clusters in gene expression space. Using the trace of Fisher's scatter

matrix as a measure of the separability of patterns, our new normalization method achieved an improved performance with respect to the existing methods.

One important consideration with the present approach is the measure of quality in data normalization [11]. This is not a glamorous area, but progress in it is critical for the future success of data normalization [12]. What is the correct control gene set for a direct normalization of *between-class* data sets? How effective was a particular normalization method? Did the succeeding analysis come to the correct conclusion? Benchmark criteria assignment in data normalization are very different and difficult [5]. We believe that in data normalization, there is currently no objective measure of quality, and so it is difficult to quantify the merit of a particular data normalization technique. The effectiveness of such a techniques is often highly data-dependent. However, we would expect this iterative normalization method to be an effective tool in many gene microarray applications.

REFERENCES

- [1] S. Kim, E. R. Dougherty, Y. Chen, K. Sivakumar, P. Meltzer, J. M. Trent, and M. L. Bittner, "Multivariate measurement of gene expression relationships," *Genomics*, vol. 67, pp. 201–209, 2000.
- [2] A. J. Carlisle, V. V. Prabhu, A. Elkahloun, J. Hudson, J. M. Trent, W. M. Linehan, E. D. Williams, M. R. Emmert-Buck, L. A. Loitt, P. J. Munson, and D. B. Krizman, "Development of a prostate cDNA microarray and statistical gene expression analysis package," *Mol. Carcin.*, vol. 28, pp. 12–22, 2000.
- [3] D. J. Duggan, M. L. Bittner, Y. Chen, P. Meltzer, and J. M. Trent, "Expression profiling using cDNA microarrays," *Nature*, vol. 21, pp. 10–14, January 1999.
- [4] Y. Chen, E. R. Dougherty, and M. L. Bittner, "Ratio-based decisions and the quantitative analysis of cDNA microarray images," *J. Biomed. Opt.*, vol. 2, pp. 364–374, 1997.
- [5] P. Hedge, R. Qi, K. Abernathy, C. Gay, S. Dharap, R. Gasparad, J. E. Hughes, E. Sneshad, N. Lee, and J. Quackenbush, "A concise guide to cDNA microarray analysis," *Biotechniques*, vol. 29, pp. 548–557, 2000.
- [6] J. H. Zar, *Biostatistical Analysis*, 4th ed. Upper Saddle River, NJ: Prentice-Hall, 1999.
- [7] A. D. J. Cross and E. R. Hancock, "Graph matching with a dual-step EM algorithm," *IEEE Trans. Pattern Anal. Machine Intell.*, vol. 20, no. 11, pp. 1236–1253, Nov. 1998.
- [8] M. T. Lee, F. C. Kuo, G. A. Whitmore, and J. Sklar, "Importance of replication in microarray gene expression studies: Statistical methods and evidence from repetitive cDNA hybridizations," *Proc. Nat. Acad. Sci.*, vol. 97, no. 18, pp. 9834–9839, Aug. 2000.
- [9] S. Haykin, *Neural Networks: A Comprehensive Foundation*, 2nd ed. Upper Saddle River, NJ: Prentice-Hall, 1999.
- [10] A. P. Dhawan, L. K. Arata, A. V. Levy, and J. Mantil, "Iterative principal axes registration method for analysis of MR-PET brain images," *IEEE Trans. Biomed. Eng.*, vol. 42, pp. 1079–1088, Nov. 1995.
- [11] S. T. Lott, "Array data normalization: Faith in housekeeping genes or regulation," in *3rd Annual Conf. Integrated Bioinformatics*, Zurich, Switzerland, Jan. 24–26, 2001.
- [12] D. B. Finkelstein, J. Golub, R. Ewing, F. Sterly, S. Somerville, and J. M. Cherry, "Iterative linear regression by sector: Renormalization of cDNA microarray data and cluster analysis weighted by cross homology," in *Critical Assessment of Techniques for Microarray Data Analysis*, Dec. 18–19, 2000.
- [13] Y. Wang, L. Luo, M. T. Freedman, and S.-Y. Kung, "Probabilistic principal component subspaces: A hierarchical finite mixture model for data visualization," *IEEE Trans. Neural Nets*, vol. 11, pp. 625–636, May 2000.
- [14] R. Clarke, F. Leonessa, J. N. Welch, and T. C. Skaar, "Cellular and molecular pharmacology of antiestrogen action and resistance," *Pharmacol. Rev.*, vol. 53, pp. 25–71, 2001.
- [15] Z. Gu, R. Lee, T. Skaar, J. Welch, K. Bouker, J. Lu, A. Liu, N. Davis, F. Leonessa, N. Brunner, Y. Wang, and R. Clarke, "Molecular profiles of antiestrogen resistance implicate NFkB, cAMP response element binding, nucleophosmin and interferon regulatory factor-1," *J. Nat. Cancer Inst.*, 2001, submitted for publication.

Development and Validation of a Method for Using Breast Core Needle Biopsies for Gene Expression Microarray Analyses¹

Matthew Ellis,² Natalie Davis, Andrew Coop, Minetta Liu, Lisa Schumaker, Richard Y. Lee, Rujirutana Srikanchana, Chris G. Russell, Baljit Singh, William R. Miller, Vered Stearns,³ Marie Pennanen, Theodore Tsangaris, Ann Gallagher, Aiyi Liu, Alan Zwart, Daniel F. Hayes,³ Marc E. Lippman,³ Yue Wang, and Robert Clarke⁴

Departments of Oncology [M. E., N. D., A. C., M. L., L. S., R. Y. L., V. S., A. G., A. Z., D. F. H., M. E. L., R. C.], Pathology [B. S.], Surgery [M. P., T. T.], Physiology and Biophysics [R. Y. L., R. C.], and Biostatistics and Biomathematics [A. L.], Georgetown University School of Medicine, Washington, DC 20007; Department of Electrical Engineering and Computer Science, The Catholic University of America, Washington, DC 20064 [R. S., Y. W.]; ResGen, part of the Invitrogen Corporation, Huntsville, Alabama 35801 [C. G. R.]; and Department of Oncology, University of Edinburgh, Western General Hospital, Edinburgh, Scotland, EH4 2XU United Kingdom [W. R. M.]

ABSTRACT

Purpose: Gene expression microarray technologies have the potential to define molecular profiles that may identify specific phenotypes (diagnosis), establish a patient's expected clinical outcome (prognosis), and indicate the likelihood of a beneficial effect of a specific therapy (prediction). We wished to develop optimal tissue acquisition, processing, and analysis procedures for exploring the gene expression profiles of breast core needle biopsies representing cancer and noncancer tissues.

Experimental Design: Human breast cancer xenografts were used to evaluate several processing methods for prospectively collecting adequate amounts of high-quality RNA

for gene expression microarray studies. Samples were assessed for the preservation of tissue architecture and the quality and quantity of RNA recovered. An optimized protocol was applied to a small study of core needle breast biopsies from patients, in which we compared the molecular profiles from cancer with those from noncancer biopsies. Gene expression data were obtained using Research Genetics, Inc. NamedGenes cDNA microarrays. Data were visualized using simple hierarchical clustering and a novel principal component analysis-based multidimensional scaling. Data dimensionality was reduced by simple statistical approaches. Predictive neural networks were built using a multilayer perceptron and evaluated in an independent data set from snap-frozen mastectomy specimens.

Results: Processing tissue through RNALater preserves tissue architecture when biopsies are washed for 5 min on ice with ice-cold PBS before histopathological analysis. Cell margins are clear, tissue folding and fragmentation are not observed, and integrity of the cores is maintained, allowing optimal pathological interpretation and preservation of important diagnostic information. Adequate concentrations of high-quality RNA are recovered; 51 of 55 biopsies produced a median of 1.34 µg of total RNA (range, 100 ng to 12.60 µg). Snap-freezing or the use of RNALater does not affect RNA recovery or the molecular profiles obtained from biopsies. The neural network predictors accurately discriminate between predominantly cancer and noncancer breast biopsies.

Conclusions: The approaches generated in these studies provide a simple, safe, and effective method for prospectively acquiring and processing breast core needle biopsies for gene expression studies. Gene expression data from these studies can be used to build accurate predictive models that separate different molecular profiles. The data establish the use and effectiveness of these approaches for future prospective studies.

Received 11/27/01; revised 2/4/02; accepted 2/15/02.

The costs of publication of this article were defrayed in part by the payment of page charges. This article must therefore be hereby marked advertisement in accordance with 18 U.S.C. Section 1734 solely to indicate this fact.

¹ Supported by USPHS from National Cancer Institute Grants 5R33CA83231 (to Y. W.), R01-CA/AG58022 (to R. C.), P50-CA58185 (to R. C.), and K12-CA76903 (to M. L.), the Department of Defense Grants BC980629 (to R. C.) and BC990358 (to R. C.), and C1-3 Cancer Research Fund-Lilly Clinical Investigator Award of the Damon Runyon-Walter Winchell Foundation (to V. S., D. F. H.).

² Present address: Breast Cancer Program, 25105, The Morris Building, Duke University Medical Center, Durham, NC 27710.

³ Present address: Department of Medicine, 3110 Taubman Centre, University of Michigan, Ann Arbor, MI 48109.

⁴ To whom requests for reprints should be addressed, at Department of Oncology, Georgetown University School of Medicine, W405A Research Building, 3970 Reservoir Road NW, Washington, DC 20007. Phone: (202) 687-3755; Fax: (202) 687-7505; E-mail: clarke@georgetown.edu.

INTRODUCTION

The emerging gene microarray technologies provide powerful new methodologies with which to address several important issues in breast cancer research. For example, it should be possible to define gene expression patterns that can identify specific phenotypes (diagnosis), establish a patient's expected clinical outcome (prognosis), and indicate the likelihood of a beneficial effect of a specific therapy (prediction; Refs. 1 and 2). Gene microarray technologies are performed on chips, glass slides, or filters and allow the comparison of gene expression profiles from two or more tissues or the same tissue in different biological states (3). The technologies continue to develop, with considerable discussion regarding which technology has the greatest potential to address the molecular profiling of tumors. Each of the major approaches has advantages and disadvan-

tages, but the most important consideration is the ability of the technology to address the chosen hypothesis (4). Overall, there is no compelling evidence of major differences in the accuracy or reproducibility of the various microarray platforms (4–6). Studies that directly compare the nylon-based cDNA arrays with either glass slide cDNA arrays and/or oligonucleotide chips consistently report that these platforms produce comparable data (5–8).

Because gene expression technologies provide an assessment of mRNA abundance in a sample, all require the production of a probe, labeled with either a radioactive nucleotide or fluorescent molecule, generated from either the total or polyadenylate RNA isolated from the sample. Currently, it is not possible to isolate adequate concentrations of high-quality RNA from what would otherwise be the most abundant source: the formalin-fixed, paraffin-embedded tumor specimens available in established tumor banks. Only fresh or appropriately frozen tissues provide the necessary quality of RNA for the preparation of probes to hybridize to existing gene expression microarrays.

Whereas many institutions have frozen tumor banks, these may be of limited use in obtaining reproducible gene expression profiles for some breast cancers. For example, most are heavily biased toward large breast tumors (T₃–T₄). These tumors are poorly representative of the small tumors now seen in many patients for initial diagnosis (9). A further concern with existing frozen tissue banks is the frequent lack of a standardized approach for tissue acquisition and processing. Tissue handling between excision and freezing can vary considerably. For example, some tumors are frozen within seconds of excision, and others are placed on wet or dry ice after excision, whereas some may stand for many minutes at room temperature before being placed in liquid nitrogen. The importance of tissue processing is often critical for assessing various end points and can affect both RNA stability for RNA *in situ* hybridizations and antigen stability/accessibility for immunohistochemistry (10).

The effect of tissue acquisition and processing on gene microarray data has not been widely addressed. Nonetheless, this is likely to be important for at least two critical parameters. First is preservation of high-quality RNA. Most investigators acknowledge the importance of using only pure, high-quality RNA for gene microarray studies (11). The second factor is maintenance of a tissue's gene expression profile. For example, hypoxia- or stress-induced responses can be induced in metabolically active cells. Oxygen deprivation begins with the loss of tissue perfusion occurring upon excision. This deprivation can trigger a hypoxic response, characterized by the altered expression of specific genes (12, 13). Several of these genes are transcription factors that further affect the expression of their target genes (13).

One problem with these two factors is that both can affect a sample, but RNA could still be obtained, a probe could still be generated, and a molecular profile could still be obtained after hybridization to a gene expression microarray. Subtle changes that are time, temperature, pH, and/or oxygen dependent could occur with sufficient variability that they are almost impossible to detect reproducibly. Some tumors with high metabolic activity may be more sensitive to hypoxia, producing a statistically valid and biologically plausible clustering that could have re-

Table 1 Experimental conditions for xenograft study

All samples were processed in duplicate.

Temperature of 72 h storage	Wash solution	Wash time
4°C	1:6 (RNALater:PBS)	5 min
4°C	1:9 (RNALater:PBS)	5 min
4°C	1:12 (RNALater:PBS)	5 min
4°C	PBS	5 min
4°C	No wash	No wash
4°C	1:6 (RNALater:PBS)	120 min
4°C	1:9 (RNALater:PBS)	120 min
4°C	1:12 (RNALater:PBS)	120 min
4°C	PBS	120 min
Room temperature	No wash	No wash
–20°C	No wash	No wash

sulted more from tissue processing rather than tissue biology. Where such changes are subtle, expression profiles might still appear grossly similar, complicating an assessment of tissue processing artifacts.

Given the bias of existing banks and the potential differences in tissue processing, many important questions in breast cancer biology may require prospective study designs. Such study designs are more valid for the exploration or validation of new predictive and prognostic factors. Whereas optimized tissue acquisition and processing strategies for prospective studies offer the opportunity for greater control of tissue quality than retrospective studies, these strategies have not been described. In this study, we wished to develop a standard tissue acquisition/processing method for prospective core needle breast biopsy sampling. This method should avoid the initial use of liquid nitrogen, preserve tissue architecture, and provide adequate concentrations of high-quality RNA for microarray analysis. We now report a simple tissue processing approach using a commercially available reagent (RNALater) that is applicable to prospective studies on core needle biopsies. RNA obtained from this approach was compared with RNA from snap-frozen human breast biopsies of neoplastic and nonneoplastic tissues, gene expression microarray data were obtained, and an accurate neural network capable of discriminating between these tissues was built and validated in an independent data set.

MATERIALS AND METHODS

Breast Cancer Xenograft Studies. MDA-MB-231 cells were inoculated into athymic nude mice as described previously (14, 15). Mice were sacrificed, and tumor tissue was obtained using sterile scissors and forceps. Needle biopsies were taken from the excised xenografts and placed into separate tubes containing 0.5 ml of RNALater (Ambion, Austin, TX) at room temperature. Samples were stored at various temperatures for 72 h and subsequently processed according to the scheme in Table 1. Each experimental condition was explored in duplicate samples. Tissues were embedded in OCT (BDH; Poole, Dorset, United Kingdom), and standard frozen sections were prepared from each sample. Subsequently, sections were stained with H&E and evaluated by the study pathologist. The remainder of the core was stored at –80°C, and total RNA was extracted for evaluation. All animal studies were performed under protocols approved

by the Georgetown University Animal Care and Use Committee.

Patient Population. Patients undergoing a diagnostic core needle or excisional biopsy at Georgetown University Hospital were eligible for the tissue acquisition protocol, in which additional cores were obtained for study purposes. All patients signed a written consent form approved by the Georgetown University Medical Center Institutional Review Board. Core biopsies provided by the radiologists were obtained with either mammographic or ultrasound guidance. Core biopsies obtained by the surgeons were obtained either after surgical exposure of the tumor or during a routine needle biopsy. A total of 1–4 cores were obtained from each patient for study purposes, depending on the size of the breast lesion. In addition, nine frozen breast tumor specimens were obtained from the Department of Oncology, University of Edinburgh (Edinburgh, Scotland, United Kingdom) for use in testing the neural networks for accuracy in identifying tissues as malignant or non-malignant. These samples were collected after appropriate patient consent and consistent with the relevant United Kingdom legislation. In this study, the pathologist was blinded to all clinical information on all samples.

Collection and Handling of Human Breast Core Biopsies for Microarray Analysis. Generally, 1–4 core needle biopsies (14-gauge needle) were obtained from each consenting patient. Random cores were immediately snap-frozen in liquid nitrogen; others were individually placed in separate cryo-tubes containing 0.5 ml of *RNALater* solution. Snap-frozen tissues were placed directly in liquid nitrogen from the core biopsy needle, immediately upon removal from the patient. For the *RNALater* samples, core biopsies were placed in 500 μ l of *RNALater* and maintained at 4°C for 24 h before snap-freezing. Each tube was labeled with the patient's name, hospital number, and study number. Frozen samples were transferred to the Lombardi Cancer Center's Tissue and Histopathology Shared Resource (Washington, DC) for processing.

Before removing the samples from the tube for frozen section preparation, each sample was washed for 5 min on ice with 500 μ l of ice-cold sterile PBS (RNase free); otherwise, samples in *RNALater* will not freeze in the cryostat. Each core biopsy sample was then embedded separately in an OCT block. A frozen section was taken, stained with H&E, and examined by the study pathologist. OCT-embedded samples were maintained frozen at -70°C until the analysis of the main tumor mass was complete.

The study pathologist evaluated all biopsies to determine the presence of invasive cancer and to estimate the relative amounts of normal epithelium, stroma, and fat. Because samples were to be used for microarray analysis, the percentage of invasive cancer, normal epithelium, stroma, and fat was estimated relative to cell nuclei only. Provided this histological review offered no new clinical information important for patient care, biopsies suitable for microarray were identified. In this manner, tissue for expression microarray analysis was ensured to be of no new diagnostic relevance. This determination is important because RNA extraction destroys tissue architecture. If the samples had contained information that modified the surgical pathology diagnosis, these biopsies would not have been used. This situation did not occur in this study.

Once released for study, all patient identifiers were removed from each sample. The link between patient identifiers and study identifiers was held in a confidential database. Access to this database was reserved only for the clinical study principal investigator and the data entry technician. The frozen clinical material, mostly frozen in OCT, was directly provided to the research laboratory for storage and/or processing. Upon receipt in the research laboratory, tissue was either stored at -80°C or processed immediately for RNA extraction.

Preparation and Quality Assessment of RNA from Frozen Tissues. Frozen tissue was placed in a 1 \times 1-inch plastic bag on dry ice and pulverized, and lysis buffer from the Qiagen RNeasy kit was added (Qiagen, Inc., Valencia, CA). Each sample was then transferred to a 1.5-ml centrifuge tube, homogenized with a 1-ml syringe and an 18-gauge needle, added to the Qiagen spin column, and centrifuged to bind the RNA to the matrix. The column was washed with the buffers provided in the kit, and the RNA was finally eluted with distilled H₂O. RNA concentrations were determined by comparing the absorbance ratios ($A_{260\text{ nm}}/A_{280\text{ nm}}$) obtained spectrophotometrically using a Beckman DU640 Spectrophotometer (Beckman, Fullerton, CA).

Because using standard gel electrophoresis to assess RNA quality would require almost the entire RNA sample, we used an Agilent 2100 analyzer and RNA 6000 LabChip kits (RNA microelectroseparation and analysis; Agilent Technologies, New Castle, DE). A total of 100 ng of each RNA sample was loaded/well. The analyzer allows for visual examination of both the 18S and 28S rRNA bands as a measure of RNA integrity.

Probe Generation for Gene Microarray Hybridizations. Probes were generated as described previously (16). This method radiolabels both the sense and antisense probe strands and further increases probe-specific activity by incorporating two radiolabeled nucleotides. Thus, tumors can be arrayed on nylon filter arrays with as little as 100 ng of total RNA and without RNA amplification (7, 16). Whereas an adequate signal is generated with 100 ng of total RNA, the use of very low RNA concentrations will likely affect the ability to adequately and reproducibly detect many lower abundance mRNAs. We used 500 ng of total RNA, which is sufficient to allow the use of approximately 70% of breast needle biopsies without either RNA amplification or pooling. None of the RNAs was amplified or pooled in the current study.

To synthesize the labeled cDNA probe, 500 ng of total RNA were incubated at 70°C for 10 min with 2 mg of oligodeoxythymidine and then chilled on ice for 2 min. The primed DNA was incubated at 37°C for 90 min in a solution containing 1× first strand, 3 mM DTT, 1 mM dGTP/dTTP, 300 units of reverse transcriptase, 50 mCi of [³²P]dCTP, and 50 mCi of [³²P]dATP. The second strand was synthesized by adding 1× reaction buffer, 100 units of DNA polymerase I, 500 ng of random primers, 1 mM dGTP/dTTP, 50 mCi of [³²P]dCTP, and 50 mCi of [³²P]dATP. The reaction was incubated for 2 h at 16°C. A radiolabeled probe was purified using a BioSpin-6 chromatography column (Bio-Rad) and denatured by boiling for 3 min. A purified probe was added to the hybridization roller tube containing the prehybridized GeneFilter and incubated for 12–18 h at 42°C in a Robin Scientific Roller Oven. For these studies, the NamedGenes

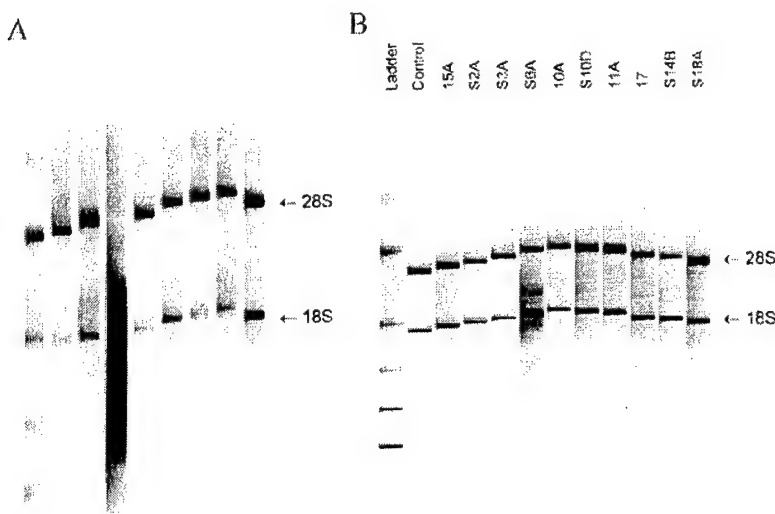


Fig. 1 The quality of RNA recovered from human core breast needle biopsies. RNA was evaluated using an Agilent 2100 analyzer. *A*, xenografts; *B*, breast core needle biopsies arrayed in Figs. 5 and 6 and further characterized in Table 4. In the images displayed, fluorescence scales are not equivalent between lanes but have been normalized for clarity.

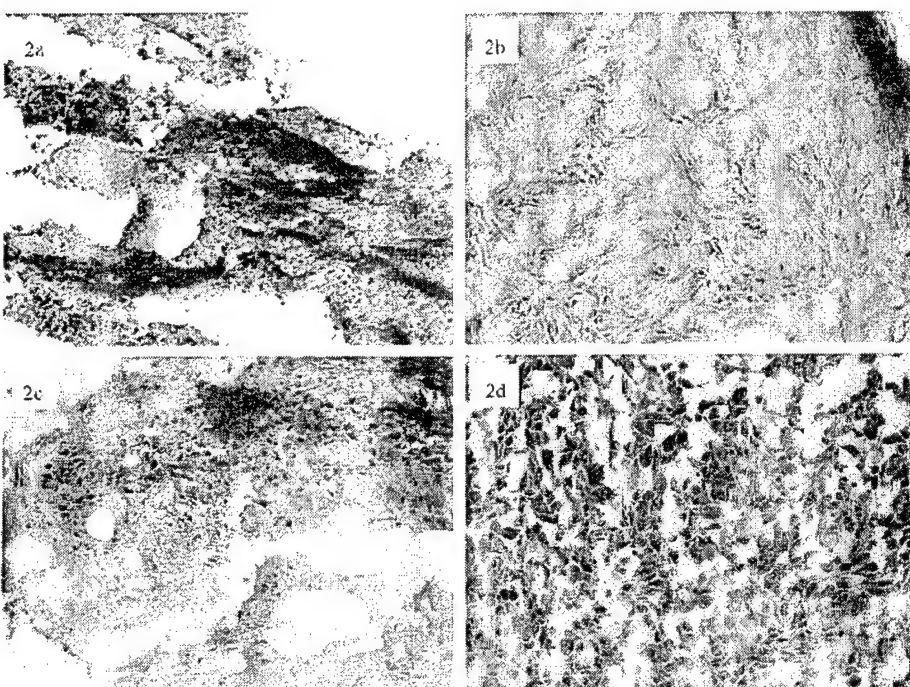


Fig. 2 MDA-MB-231 human breast tumor xenografts processed for frozen tissue sectioning in RNALater. *A*, no wash; *B*, washed in PBS:RNALater (1:6; v/v) for 2 h at 4°C; *C*, washed in PBS:RNALater (1:6; v/v) for 5 min at 4°C; *D*, washed in PBS for 5 min on ice.

filters (Research Genetics, Inc., Huntsville, AL) were used. These filters contain 4032 known genes, 192 housekeeping genes, and 192 control genes on each filter. Each hybridized GeneFilter was washed twice in 2× SSC, 1% SDS at 50°C for 20 min and once at 55°C in 0.5× SSC, 1% SDS for 15 min. Hybridization signals were detected by phosphorimaging using a Molecular Dynamics Storm PhosphorImager (Molecular Dynamics, Sunnyvale, CA). The sensitivity and reproducibility of these and other nylon filter-based cDNA microarrays have been widely reported (7, 17–20).

Normalization of Data. Pathways software algorithms (Research Genetics, Inc.) were used to correct for nonspecific binding of the probe to filter (background correction). Approaches for signal normalization, intended to correct for differences in probe specific activities, hybridizations, and other interexperiment variables, are diverse (11). In the present study, the average of all data points was used to calculate a normalization factor; the normalized intensity value for each spot was obtained by multiplying the normalization factor by the raw intensity (11).

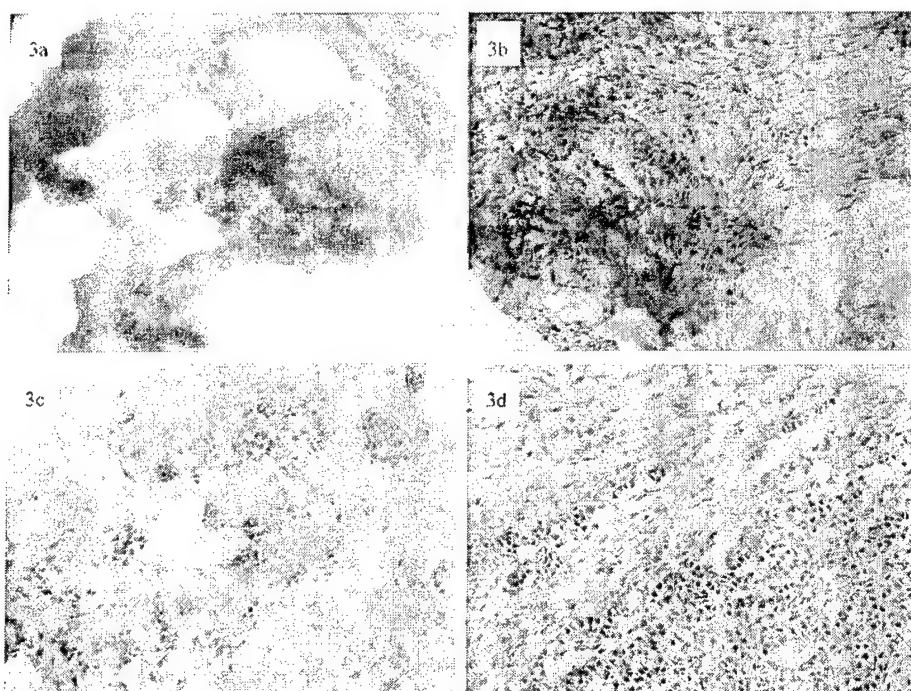


Fig. 3 Human breast needle biopsies processed for frozen tissue sectioning in RNALater. *A*, no wash; *B*, washed in PBS:RNALater (1:6; v/v) for 2 h at 4°C; *C*, washed in PBS:RNALater (1:6; v/v) for 5 min at 4°C; *D*, washed in PBS for 5 min on ice.

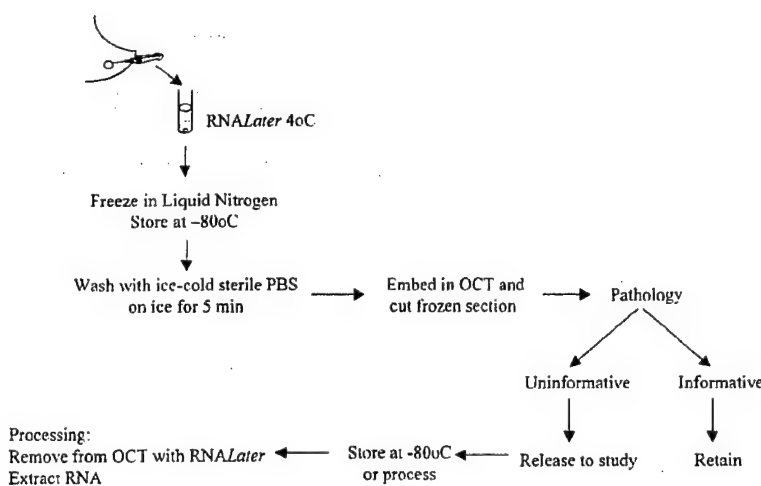


Fig. 4 Optimized tissue acquisition/processing procedure for breast needle biopsies.

Analysis of Gene Microarray Data. The optimal approach for analyzing the high dimensional gene expression data generated by gene microarray studies remains unclear. The high dimensionality of these data are problematic, with most existing analyses functioning more accurately in low dimensionality (21). However, rather than making statistical inference for identifying and studying functionally relevant genes, the study goal was to validate the tissue acquisition and processing methods and demonstrate the applicability of this approach for building clinically relevant predictive models.

Recently, we devised a simple approach to the exploration

of small studies with two experimental groups.⁵ Our approach used simple statistical analyses to reduce data dimensionality and identify subsets of discriminant genes. This approach is similar in principle to that used by Hedenfalk *et al.* (22). Because the class of each sample (cancer *versus* noncancer) is

⁵ Z. Gu. Association of interferon regulatory factor-1, nucleophosmin, nuclear factor-kappa-B and cAMP binding with acquired resistance to Faslodex (ICI 182,780), submitted for publication.

Table 2 Concentration of RNA recovered from breast needle biopsies

Biopsies	RNA ≥ 100 ng ^a	Total RNA recovered ($\bar{x} \pm SE$)	Range (>100 ng)
<i>n</i> = 55 ^b	51/55 (93%)	3.63 \pm 0.48 μ g; median = 1.34 μ g	100 ng to 12.60 μ g
<i>n</i> = 25	Snap-frozen	2.04 \pm 0.51 μ g; median = 1.32 μ g	100 ng to 9.00 μ g ^c
<i>n</i> = 21	RNA _{Later}	3.49 \pm 0.78 μ g; median = 2.70 μ g	100 ng to 12.60 μ g

^a Number producing ≥ 100 ng of RNA, the minimum useful concentration of RNA without amplification, irrespective of the tissue acquisition and processing method applied.

^b We did not have complete data on processing for the first 9 of the 55 samples.

^c *P* = 0.13; Mann-Whitney rank-sum test; RNA_{Later} versus snap-frozen tissue.

Table 3 Characteristics of breast needle biopsy material

A. Biopsy	Source	ER/PR ^a	% Cancer	% Normal	% Fat	% CT	RNA (μ g) ^b
15A ^c	Radiology	ND	0%	70%	0%	30%	3.28
S6A ^c	Surgery	ND	0%	0%	100%	0%	2.49
10A	Radiology	ND	0%	5%	45%	50%	2.07
11A	Radiology	ND	0%	20%	40%	40%	1.36
17 ^c	Radiology	ND	2%	0%	90%	8%	6.70
S2A	Surgery	++	90%	0%	5%	5%	3.20
S3A ^c	Surgery	++	90%	0%	0%	10%	2.70
S10D ^c	Surgery	++	80%	0%	0%	20%	6.50
S14B ^c	Surgery	--	80%	0%	0%	20%	4.20
S18A	Surgery	+-	90%	0%	0%	10%	1.70

B. RNA recovered from biopsies used in this study ($\bar{x} \pm SE$) ^d							
No RNA _{Later}							2.21 \pm 0.52 μ g total RNA ^d
RNA _{Later}							3.83 \pm 0.73 μ g total RNA
Overall RNA recovered							3.10 \pm 1.60 μ g total RNA

C. Case	Biopsies	Pathological diagnosis
S2	S2A	Invasive adenocarcinoma
	S2B	Invasive adenocarcinoma
	S2C	Invasive adenocarcinoma
S6	S6A	No cancer
	S6B	No cancer
	S6C	No tissue
	S10A	No cancer
S10	S10B	Possible DCIS
	S10C	No cancer
	S10D	Invasive adenocarcinoma

^a PR, progesterone receptor; CT, connective tissue; DCIS, ductal carcinoma *in situ*; ND, not determined.

^b Total RNA recovered from each needle biopsy. Five hundred ng of each RNA population were used to generate the probes hybridized to obtain the data presented in Fig. 5.

^c Biopsies processed in RNA_{Later}.

^d *P* = 0.129; Student's *t* test; RNA_{Later} versus no RNA_{Later}.

known from the histopathological analyses, dimensionality can be reduced in a supervised manner by performing a series of statistical tests. The major purpose of performing these tests was only to select a group of genes that would be used for data visualization and analysis. Student's *t* test and a *t* test for unequal variances (each assumes normal distribution of the data) and a nonparametric (distribution-free) Wilcoxon test were used. Whereas the inflated type I error will overestimate significant differences, the incidence of false negative estimates should be smaller. Because the distribution of the data among and within replicate experiments and for individual genes cannot be determined (23), both logarithm-transformed and non-transformed data were compared.

Two reduced dimensional data sets were selected; one comprising genes with *P*s < 0.05, and one comprising genes

with *P*s < 0.02. Because of their marked biological differences, these phenotypes should be easily separable. Thus, the data were visualized using our Fisher separability-based multidimensional scaling approach that projects high dimensional data into three-dimensional data space (24, 25). Because it has become widely used, visualization using the simple hierarchical clustering described by Eisen *et al.* (26) is also presented.

Generation and Testing of a Neural Network. To determine whether the genes we selected could be used to separate cancer from noncancer tissues, a neural network was trained using the gene expression microarray data from five cancer biopsies and five noncancer biopsies. Neural networks can be considered as parallel computing systems consisting of many simple processors with many interconnections. The main advantages of neural networks are that they can learn complex non-

linear input-output relationships, use sequential training procedures, and adapt themselves to the data (27, 28).

The learning process involves updating network architecture and connection weights so that the predictive model can efficiently perform a specific classification task. We used a multilayer perceptron to design a nonlinear neural classifier, using each of the gene's expression levels in the tissue samples as the input and the cancer *versus* noncancer phenotype of each sample as the output. Consequently, the network output comes to approximate the posterior Bayesian probabilities of a sample being either cancer or noncancer given its gene expression profile (27, 29, 30). Three experimental configurations were tested, with either the top 40, 80, and 103 dimensions (data set selecting the top 103 genes; $P < 0.05$) or 10, 20, and 30 dimensions (data set selecting the top 30 genes; $P < 0.02$). These top genes were selected based on their fold difference between cancer and noncancer and their respective P s. Two prediction models were built, one with 3 hidden nodes and 8 inputs and one with 5 hidden nodes and 18 inputs. Mean-squared error estimates were used to explore network performance. The "leave-one-out" method was used for the initial testing and training of each neural network (27, 29, 30).

RESULTS

RNA Quality and Tissue Architecture from Xenograft Tissues Processed Using RNALater. Recovery of high-quality RNA was optimal when OCT-embedded tissue samples were removed from frozen blocks using a small volume of RNALater, which thawed and softened the embedding medium before tissue extraction from the blocks. Thus, the frozen block was placed in a small plastic tray, with the embedded tissue facing up, and 500 μ l of RNALater were pipetted on top. Using this method, seven of eight samples yielded high-quality RNA (Fig. 1A; RNA integrity analyzed using the Agilent 2100 bioanalyzer and RNA 6000 LabChip kit). In previous experiments, where the OCT block was dissolved by vigorous shaking in a large volume of PBS and tissue fragments were recovered with a strainer, only 6 of 12 samples yielded fully intact RNA (data not shown).

Pathology was not interpretable from material frozen directly in RNALater and transferred to OCT without wash steps (Fig. 2A). This reflects inadequate freezing in the cryostat and consequent tissue folding during the cutting process. When washed in PBS:RNALater (1:6) for 2 h at 4°C, the tissue did not fold on cutting, but cell outlines appeared blurred, making pathological interpretation difficult (Fig. 2B). Washing in PBS:RNALater (1:6) for 5 min at 4°C also eliminated tissue folding, but now the cell outlines appeared distinct. Nonetheless, tissue fragmentation occurred in some specimens, making pathological interpretation suboptimal (Fig. 2C). Optimal preservation of tissue architecture was obtained by washing tissue for 5 min on ice with ice-cold PBS. Cell margins were clear, tissue folding and fragmentation were not observed, and the integrity of the cores was maintained, allowing optimal pathological interpretation (Fig. 2D). Similar data were obtained from a human breast core biopsy released to this study (Fig. 3A–D). A scheme of the optimized tissue acquisition protocol is shown in Fig. 4.

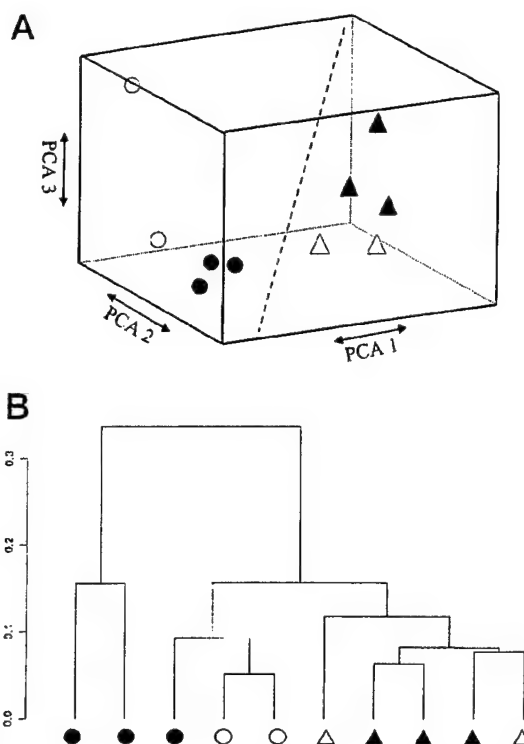


Fig. 5 Structure of the gene expression data using the top 103 genes. *A*, projection from top 103 genes (103 dimensions), selected by t test comparisons of \log_{10} -transformed gene expression data ($P \leq 0.05$) and projected into three dimensions; *B*, hierarchical clustering of samples in 2 dimensions based on 1-Pearson's coefficient matrix of the top 103 genes. Snap-frozen tissue: ○, noncancer; △, cancer. RNALater-processed tissue: ●, noncancer; ▲, cancer.

Recovery of High-quality RNA from Human Breast Biopsies for Gene Microarray Studies. Cores were removed from OCT by placing the frozen block in a small plastic tray, with the embedded tissue facing up, and pipetting 500 μ l of RNALater on top. Intact cores were easily picked out of the OCT, which remained semisolid, using a sterile pipette tip. From a study of 55 breast needle biopsies, we obtained ≥ 100 ng of RNA on almost all samples (Table 2). The median value (1.34 μ g) shows that most biopsies produce sufficient RNA to generate data using 500 ng of total RNA. There was no significant difference between frozen and RNALater-processed biopsies in the mean concentrations of total RNA recovered (Tables 2 and 3). Thus, prospectively collected breast needle biopsies, either directly snap-frozen or processed in RNALater, can produce adequate RNA concentrations for use in gene microarray studies.

A further requirement of gene expression microarray experiments is the isolation of high-quality RNA (11). Sufficient RNA was not recovered to allow for an assessment of RNA quality by both standard gel electrophoresis methods and gene microarray studies on the same samples. Because gel electrophoresis requires ~ 1 μ g of RNA, the Agilent 2100 "lab-on-a-chip" technology was used to assess RNA quality. This technology requires only 100 ng of RNA to determine quality, with

Table 4 Genes comprising the 30-dimensional data set

Gene	C:NC ^a	P			Wilcoxon
		t test ^b	Unequal	t test log ₁₀	
<i>BTTF-2</i>	3.2	0.010	0.026	0.001	0.008
<i>p160</i>	3.1	0.016	0.030	0.027	0.095
<i>spr2</i>	3.0	0.006	0.013	0.007	0.008
<i>Interferon inducible 9-27</i>	2.9	0.007	0.019	0.003	0.008
<i>Human surface antigen</i>	2.7	0.018	0.035	0.023	0.056
<i>Grb14</i>	2.6	0.004	0.011	0.001	0.008
<i>gp250 precursor</i>	2.6	0.008	0.009	0.002	0.016
<i>TAK1-binding protein</i>	2.4	0.014	0.010	0.002	0.008
<i>Myosin-binding protein H</i>	2.3	0.016	0.022	0.011	0.032
<i>RP3</i>	2.3	0.006	0.008	0.004	0.016
<i>α-Catenin</i>	2.3	0.001	0.004	0.001	0.008
<i>T3 receptor cofactor-1</i>	2.3	0.005	0.006	0.015	0.016
<i>DAP-3</i>	2.2	0.017	0.021	0.025	0.032
<i>Selenoprotein-W (selW)</i>	2.1	0.015	0.023	0.018	0.056
<i>Ferroxidase</i>	2.1	0.007	0.011	0.008	0.016
<i>Cytochrome c</i>	2.1	0.017	0.017	0.044	0.032
<i>RAN-BP8</i>	2.1	0.017	0.018	0.016	0.032
<i>Aspartate aminotransferase-1</i>	1.9	0.010	0.011	0.009	0.032
<i>unc-18 homologue</i>	1.9	0.007	0.010	0.005	0.008
<i>Phosphethanolamine cytidylyltransferase</i>	1.9	0.007	0.007	0.001	0.016
<i>Frizzled (fre)</i>	1.9	0.016	0.024	0.014	0.016
<i>Interferon α-induced 11.5 kDa</i>	1.8	0.017	0.019	0.017	0.032
<i>Ubiquitin activating enzyme E1</i>	1.8	0.015	0.015	0.011	0.032
<i>Macrophage-stimulating 1</i>	1.8	0.014	0.014	0.022	0.032
<i>Ah receptor</i>	1.8	0.002	0.004	0.002	0.008
B. Genes that appear up-regulated in noncancer tissues					
Gene	C:NC ^a	t test ^b	Unequal	t test log ₁₀	Wilcoxon
<i>Neurofibromin 2</i>	0.6	0.005	0.005	0.006	0.008
<i>Frizzled-related protein</i>	0.5	0.016	0.025	0.015	0.031
<i>Type II keratin</i>	0.4	0.006	0.007	0.027	0.008
<i>CAGH4</i>	0.4	0.004	0.006	0.003	0.008
<i>Dihydroguanosine triphosphatase</i>	0.3	0.014	0.033	0.002	0.008

^a C:NC, ratio of expression level in cancer *versus* noncancer. Genes were selected on the basis of C:NC ≥ 1.8 (approximately 2-fold); $P \leq 0.02$ (estimated to three significant figures) in Student's *t* test.

^b *t* tests used are: *t* test, Student's (untransformed data); Unequal, unequal variance (untransformed data); *t* test log₁₀, Student's *t* test on log₁₀-transformed data; Wilcoxon, Wilcoxon rank-sum test (nonparametric).

specificity comparable with or better than that obtained from standard gel electrophoresis. Consequently, RNA quality can be assessed on samples that will later be subjected to gene microarray analysis. As is evident from Fig. 1B, >90% of representative biopsies produced high-quality RNA.

Analysis of Core Needle Breast Biopsies and Visualization of Gene Expression Data. To assess the applicability of the tissue processing procedure, we obtained total RNA from five random breast cancer biopsies and five random biopsies of noncancer tissue (Table 3). All tissues were evaluated by the study pathologist before release for our studies to ensure that the investigational cores contained no diagnostically useful information. Both biopsies processed in RNALater and biopsies frozen without RNALater were analyzed. These biopsies were approximately equally represented in each group (RNALater processed: cancer = 3; noncancer = 3). RNA was prepared, and probes were generated as described above. The mean RNA concentrations recovered by both methods were comparable

(see also Table 2). Probes were hybridized to NamedGene filters, and signal was measured using a Molecular Dynamics Storm PhosphorImager. Digitized representations of the hybridized filter signals were imported into the Pathways software for background correction and normalization.

Normalized gene expression data were imported into the visualization algorithm, and scatter plots of the gene expression data were generated. We first reduced dimensionality by eliminating noninformative genes. Hence, we excluded those genes whose expression was not likely to be different between the cancer and noncancer groups (multiple *t* tests, $P > 0.05$). A total of 103 genes met this criterion and were used to generate a three-dimensional (from 103-dimensional) plot of the data (Fig. 5A). The three axes are the first three principal components fitted to the cancer and noncancer molecular profile data. The cumulative proportion of the variance captured by each principal component axis is: (a) principal component axis 1, 55%; (b) principal component axis 2, 72%; and (c) principal component

axis 3, 79%. We also applied hierarchical clustering, similar to approaches used by others (26), based on Euclidean space analysis (1-Pearson's correlation coefficient matrix). The latter approach could not completely separate two cancers from the clusters of noncancers (Fig. 5B). PCA⁶-based multidimensional scaling visualization separated breast cancers (triangles) and noncancer tissue (circles) into linearly separable gene expression data space. However, it should be noted that neither approach provides a statistical assessment of separability, only a visualization of data structure. Whereas the number of data points is limited, the multidimensional scaling visualization is consistent with our ability to identify a putative molecular profile that can separate neoplastic from nonneoplastic tissues.

This subset of genes is expected to include some false positives, reflecting the type 1 error associated with the selection. Consequently, data dimensionality was further reduced using more conservative criteria ($P \leq 0.02$ and regulation ≥ 1.8 -fold). We chose this fold regulation to include all ≤ 2 -fold differences in mean gene expression levels between cancer and noncancer tissues. The analysis produced a 30-dimensional data set; 25 signals (genes) were up-regulated in the neoplastic biopsies (Table 4A), and 5 signals were up-regulated in the nonneoplastic biopsies (Table 4B). The ability of this subset to separate cancer from noncancer was also evaluated using both our PCA-based multidimensional scaling approach and simple hierarchical clustering. The cumulative proportion of the variance captured by each principal component axis is: (a) principal component axis 1, 64%; (b) principal component axis 2, 75%; and (c) principal component axis 3, 82%. Neoplastic and nonneoplastic tissues (Table 3) were now linearly separable in gene expression data space by both visualization methods (Fig. 6, A and B).

Neural Network Predictors of Biopsy Phenotypes. Having reduced the dimensionality, it was necessary to assess whether the expression patterns of remaining genes in the 103 and 30 dimensions contained useful discriminatory information. Thus, the ability of various gene subsets to train accurate neural network predictors that could predominantly separate cancer from noncancer tissues was assessed. The three configurations tested (1–3 hidden nodes) for genes within the 30- and 103-dimensional data sets are described in "Materials and Methods." All were evaluated using the leave-one-out method. Whereas the number of microarrays from which the data are obtained is small ($n = 10$), each configuration achieved a 0% misclassification rate (network training) for cancer *versus* noncancer, whether in 103 or 30 dimensions and with either \log_{10} or nontransformed gene expression data.

Because the initial training and testing were done on the original data set from the Georgetown University samples, we tested the neural networks against an independent data set of nine frozen breast specimens from the University of Edinburgh. These were snap-frozen mastectomy specimens rather than core needle breast biopsies, but they should contain a mixture of cancer and noncancer cells and provide a strong and independent

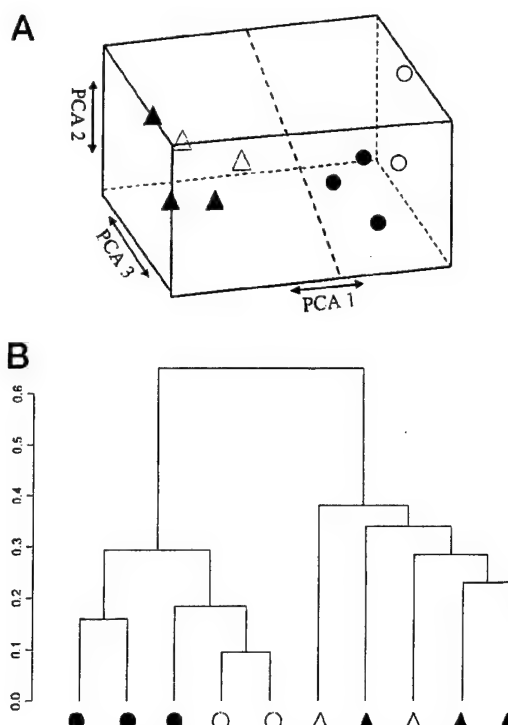


Fig. 6. Structure of the gene expression data using the top 30 genes. *A*, projection from top 30 genes (30 dimensions), selected by *t* test comparisons of \log_{10} -transformed gene expression data ($P \leq 0.02$; ≥ 1.8 -fold difference) and projected into three dimensions; *B*, hierarchical clustering of samples in 2 dimensions based on 1-Pearson's coefficient matrix of the top 30 genes. Snap-frozen tissue: ○, noncancer; △, cancer; RNALater-processed tissue: ●, noncancer; ▲, cancer.

challenge for the neural network. The neural network model should accurately predict as cancer any biopsy comprising $>80\%$ cancer tissue.

Gene expression data were generated using the same Research Genetics filter technology and queried in the predictive model. For both the 103 and 30 gene data sets, the nontransformed data provided the more accurate models. Both models predicted that all nine samples should be cancer and not noncancer. The pathologist who evaluated the samples for the training set subsequently performed histopathological analysis of stored samples of these tissues. All nine samples were confirmed as $\geq 80\%$ cancer specimens. Thus, no samples in the independent test data set were misclassified, demonstrating the neural network's predictive accuracy. When the \log_{10} data were used, the models misclassified 1 of 9 tumors (30 dimensions; 89% accurate) and 2 of 9 tumors (103 dimensions; 78% accurate). The lower classification rate with the 103 genes probably reflects the increased type 1 error associated with this data set and the failure to exclude some uninformative genes.

Genes Differentially Expressed between Breast Cancer and Noncancer Tissues. The data in Table 4 show that the choice of *t* test has only a marginal effect on data selection for supervised dimension reduction. If we make no assumption regarding distribution of the data, approximately 1 in 3 genes

⁶ The abbreviations used are: PCA, principal component analysis; ER, estrogen receptor.

Table 5 Function of selected genes

Gene name(s)	UniGene no. ^a	Function	Ref. no.
<i>BTF2</i> (butyrophilin)	Hs.167741	Glycoprotein component of human milk fat globule membranes; membrane-associated receptor for association of cytoplasmic droplets with the apical plasma membrane	35 and 41
<i>grb14</i> (growth factor receptor-bound protein 14)	Hs.83070	Member of the grb7 family; phosphorylated by a PDGF-regulated serine kinase; expression correlates with ER expression	37
<i>TAB1; TAK1</i> (MAPKKK; TGF β -activated kinase-1) binding protein-1	Hs.31472	Stimulates NF κ B activation; implicated in signaling in response to TGF- β and TNF- α ; activates plasminogen activator inhibitor 1	42 and 43
α -Catenin	Hs.178452	Cell adhesion molecule; binds E-cadherin; associated with tumor grade and ER expression	38 and 44
<i>DAP3</i> (death-associated protein-3) <i>Ceruloplasmin; ferroxidase</i>	Hs.159627 Hs.28896	Proapoptotic, nucleotide-binding protein Copper transport protein; present in breast milk; serum levels are elevated in breast cancer patients with progressive disease but not in patients in remission or those with benign breast lesions	45 and 46 33, 34, and 47
<i>Ah receptor</i> (aryl hydrocarbon receptor)	Hs.172287	Binds environmental toxins; interacts with ER; can block the transcriptional activity of ER; binds ER co-regulators ERAP140 and SMRT	36, 48, and 49
<i>NF2</i> (neurofibromatosis-2) <i>Frizzled-related gene</i>	Hs.902 Hs.7306	Tumor suppressor; rarely mutated in breast cancer Secreted protein; lost in ~80% of breast cancers; apoptosis related gene, induced by Adriamycin	50 and 51 52 and 53

^a The UniGene databases can be found at <http://www.ncbi.nlm.nih.gov/UniGene/Hs.Home.html>.

^b PDGF, platelet-derived growth factor; NF κ B, nuclear factor κ B; TGF, transforming growth factor; TNF, tumor necrosis factor.

would be rejected by relying solely on the nonparametric analyses, a ≥ 1.8 -fold differential expression, and a cutoff of $P \leq 0.02$. The 30 target cDNAs comprising the 30-dimensional data set are presented in Table 4.

DISCUSSION

Generally, prospective study designs are more valid for the exploration or validation of new predictive and prognostic factors. Retrospective breast cancer studies may be compromised by the bias toward larger tumors in many existing frozen tumor banks, whereas the average size of most newly diagnosed breast tumors continues to decrease (9). Thus, many studies into the molecular biology of such early lesions may need to be done prospectively. Investigators at single academic institutions can often prospectively obtain frozen samples under a rigorous collection protocol. However, the ability to do so at multiple institutions or when local clinics and community physicians are also involved can be problematic. A rapid, standard tissue processing approach should allow for the use of tissues from multiple institutions in a controlled manner. For example, it should be possible to reduce possible changes in molecular profiles associated with differences in tissue acquisition and processing. Whereas these concerns have not been explored in detail experimentally, tissue processing clearly affects the performance of other molecular biological technologies applied to human biopsies and tumor tissues (10).

To address these issues, we conducted studies to identify an optimal tissue acquisition, processing, and analysis procedure for exploring the gene expression profiles of prospectively accrued breast core needle biopsies. Because RNA extraction destroys tissue architecture, we developed a novel method for tissue processing that would allow us to obtain

samples in a uniform manner, preserve RNA quality/quantity, and, most importantly, retain all potentially diagnostically relevant information.

Tissue placed in *RNALater* can be left at room temperature for up to 1 h at 37°C, 1 week at 25°C, and ≥ 1 month at 4°C and retain fully intact RNA (31). Our data show that biopsies processed immediately in either liquid nitrogen or *RNALater* can produce sufficient concentrations of high-quality RNA for nylon filter microarray analysis without RNA amplification. This amount of RNA is also adequate for amplification for use with other gene expression microarray technologies (32). If processed carefully, tissue architecture can be maintained from biopsies collected in *RNALater*. This is clearly important because some small breast lesions can be completely removed by the biopsy procedure. These core biopsies should not be used for studies if critical diagnostic information could be lost. We estimate that, using the approaches described in this study, approximately 90% of suitable core needle breast biopsies should produce sufficient material for gene expression microarray studies.

Our studies demonstrate that the RNA recovered can be used to generate relevant gene expression microarray information. Relevance is evident from our abilities to identify differentially expressed genes associated with breast cancer cells and to build accurate neural network predictors that can identify cancer from noncancer samples based solely on their gene expression profiles.

Among the differentially expressed genes in the reduced 30-dimensional space, we would expect to find either some genes already implicated in breast cancer or known to be expressed in normal or neoplastic breast tissues. Consistent with this expectation, several genes of potential relevance were iden-

tified. For example, ceruloplasmin is up-regulated in neoplastic breast tissues, and elevated serum levels of ceruloplasmin are associated with recurrent breast cancers (33, 34). The BT2 glycoprotein is a milk protein (35) and might be expected to be expressed in tissues predominately composed of breast epithelial cells.

ER protein status is determined routinely for cancer but not noncancer biopsies. Because four of the five tumor biopsies were ER positive, we also would expect to find genes with expression patterns known either to be associated with ER or to modulate ER function. At least three genes meet these criteria. The aryl hydrocarbon receptor is known to interact with ER and affect its function (36), and the expression of both grb14 and α -catenin is associated with ER expression in breast tumors (Refs. 37 and 38; Table 5).

The discriminant power of the genes selected is evident from the accuracy of the neural networks built using the data from the initial five cancer and five noncancer biopsies. The ability to accurately identify independent samples as cancer shows that the genes of interest are expressed or repressed in both patterns and at levels consistent with the model. This is an appropriate and rigorous test of the approach because the goal was to build molecular predictors, rather than to identify functionally relevant genes. Building a predictor is also a much more efficient test of the selected genes than would be obtained by simply confirming expression gene by gene in more standard assays: Northern blot, RNase protection, or real-time PCR. Confirming the differential expression of each gene is unnecessary for building clinically relevant predictive models. Unlike studies to identify functionally relevant genes, the discriminant power of each signal from the target cDNAs on the array is independent of whether that signal originates from hybridization to its expected mRNA.

The gene expression profile data and neural network performance suggest that, at least for samples of very different biologies, contamination of samples with $\geq 80\%$ of other cell types may not confound analyses for molecular profiling. Whether this observation can be extrapolated to other studies remains to be further established. Nonetheless, the resource intensive requirements of microdissection and RNA amplification may not be absolute requirements for all molecular profiling studies.

The tissue acquisition and processing methods, dimension reduction, data visualization approaches, and neural network analyses we describe may be useful in the design of larger prospective studies. We continue to develop other data visualization, normalization, and exploration algorithms that also may be of use in the analysis of gene expression microarray studies (24, 25, 39, 40).

REFERENCES

1. Hayes, D. F., Bast, R. C., Desch, C. E., Fritzsche, H., Kemeny, N. E., Jessup, J. M., Locker, G. Y., MacDonald, J. S., Mennel, R. G., Norton, L., Ravdin, P. M., Taube, S., and Winn, R. J. Tumor marker utility grading system: a framework to evaluate clinical utility of tumor markers. *J. Natl. Cancer Inst. (Bethesda)*, 88: 1456–1466, 1996.
2. Hayes, D. F., Trock, B., and Harris, A. Assessing the clinical impact of prognostic factors: when is "statistically significant" clinically useful? *Breast Cancer Res. Treat.*, 52: 305–319, 1998.
3. Marx, J. DNA arrays reveal cancer in its many forms. *Science (Wash. DC)*, 289: 1670–1672, 2000.
4. Carulli, J. P., Artinger, M., Swain, P. M., Root, C. D., Chee, L., Tulig, C., Guerin, J., Osborne, M., Stein, G., Lian, J., and Lomedico, P. T. High throughput analysis of differential gene expression. *J. Cell. Biochem.*, 30–31: 286–296, 1998.
5. Richmond, C. S., Glasner, J. D., Mau, R., Jin, H., and Blattner, F. R. Genome-wide expression profiling in *Escherichia coli* K-12. *Nucleic Acids Res.*, 27: 3821–3835, 1999.
6. Cox, J. M. Applications of nylon membrane arrays to gene expression analysis. *J. Immunol. Methods*, 250: 3–13, 2001.
7. Bertucci, F., Bernard, K., Loriod, B., Chang, Y. C., Granjeaud, S., Birnbaum, D., Nguyen, C., Peck, K., and Jordan, B. R. Sensitivity issues in DNA array-based expression measurements and performance of nylon microarrays for small samples. *Hum. Mol. Genet.*, 8: 1715–1722, 1999.
8. Granjeaud, S., Bertucci, F., and Jordan, B. R. Expression profiling: DNA arrays in many guises. *Bioessays*, 21: 781–790, 1999.
9. Morrow, M., Schnitt, S. J., and Harris, J. R. *In situ* carcinomas. In: J. R. Harris, M. E. Lippman, M. Morrow, and S. Hellman (eds.), *Diseases of the Breast*, pp. 355–373. Philadelphia: Lippincott-Raven, 1996.
10. Zeller, R. *In situ* hybridization and immunohistochemistry. In: F. M. Ausbel, R. E. Brent, R. E. Kingston, D. D. Moore, J. G. Seidman, J. A. Smith, and K. Struhl (eds.), *Current Protocols in Molecular Biology*, pp. 14.1.1–14.14.8. New York: John Wiley & Sons, Inc., 2001.
11. Schuchhardt, J., Beule, D., Malik, A., Wolski, E., Eickhoff, H., Lehrach, H., and Herzel, H. Normalization strategies for cDNA microarrays. *Nucleic Acids Res.*, 28: E47, 2000.
12. Wang, G. L., and Semenza, G. L. General involvement of hypoxia-inducible factor 1 in transcriptional response to hypoxia. *Proc. Natl. Acad. Sci. USA*, 90: 4304–4308, 1993.
13. Wenger, R. H., Rolfs, A., Marti, H. H., Bauer, C., and Gassmann, M. Hypoxia, a novel inducer of acute phase gene expression in a human hepatoma cell line. *J. Biol. Chem.*, 270: 27865–27870, 1995.
14. Leonessa, F., Green, D., Licht, T., Wright, A., Wingate-Legette, K., Lippman, J., Gottesman, M. M., and Clarke, R. MDA435/LCC6 and MDA435/LCC6^{MDR1}: ascites models of human breast cancer. *Br. J. Cancer*, 73: 154–161, 1996.
15. Clarke, R. Human breast cancer cell line xenografts as models of breast cancer: the immunobiology of recipient mice and the characteristics of several tumorigenic cell lines. *Breast Cancer Res. Treat.*, 39: 69–86, 1996.
16. Sgroi, D. C., Teng, S., Robinson, G., LeVangie, R., Hudson, J. R., and Elkahloun, A. G. *In vivo* gene expression profile analysis of human breast cancer progression. *Cancer Res.*, 59: 5656–5661, 1999.
17. Walker, J., and Rigley, K. Gene expression profiling in human peripheral blood mononuclear cells using high-density filter-based cDNA microarrays. *J. Immunol. Methods*, 239: 167–179, 2000.
18. McCormick, S. M., Eskin, S. G., McIntire, L. V., Teng, C. L., Lu, C. M., Russell, C. G., and Chittur, K. K. DNA microarray reveals changes in gene expression of shear stressed human umbilical vein endothelial cells. *Proc. Natl. Acad. Sci. USA*, 98: 8955–8960, 2001.
19. Herwig, R., Aanstad, P., Clark, M., and Lehrach, H. Statistical evaluation of differential expression on cDNA nylon arrays with replicated experiments. *Nucleic Acids Res.*, 29: E117, 2001.
20. Carlisle, A. J., Prabhu, V. V., Elkahloun, A., Hudson, J., Trent, J. M., Linehan, W. M., Williams, E. D., Emmert-Buck, M. R., Liotta, L. A., Munson, P. J., and Krizman, D. B. Development of a prostate cDNA microarray and statistical gene expression analysis package. *Mol. Carcinog.*, 28: 12–22, 2000.
21. Hinneburg, A., and Keim, D. A. Optimal grid-clustering: toward breaking the curse of dimensionality in high-dimensional clustering. In: M. P. Atkinson, M. E. Orlowska, P. Valdoriez, S. B. Zdonik, and M. L. Brodie (eds.), *Proceedings of the 25th Conference on Very Large Databases*, pp. 506–517. San Francisco: Morgan Kaufman, 1999.

22. Hedenfalk, I., Duggan, D., Chen, Y., Radmacher, M., Bittner, M., Simon, R., Meltzer, P., Gusterson, B., Esteller, M., Kallioniemi, O. P., Wilfond, B., Borg, A., and Trent, J. Gene-expression profiles in hereditary breast cancer. *N. Engl. J. Med.*, **344**: 539–548, 2001.
23. Witten, J., and Friedman, H. P. Searching for evidence of altered gene expression: a comment on statistical analysis of microarray data. *J. Natl. Cancer Inst. (Bethesda)*, **91**: 400–401, 1999.
24. Wang, Y., Lin, S. H., Li, H., and Kung, S. Y. Data mapping by probabilistic modular networks and information theoretic criteria. *IEEE Trans. Signal Processing*, **46**: 3378–3397, 1998.
25. Wang, Y., Luo, L., Freedman, M. T., and Kung, S. Y. Probabilistic principal component subspaces: a hierarchical finite mixture model for data visualization. *IEEE Trans. Neural Net.*, **11**: 635–646, 2000.
26. Eisen, M. B., Spellman, P. T., Brown, P. O., and Botstein, D. Cluster analysis and display of genome-wide expression patterns. *Proc. Natl. Acad. Sci. USA*, **95**: 14863–14868, 1998.
27. Haykin, S. *Neural Networks: A Comprehensive Foundation*. Upper Saddle River, NJ: Prentice Hall, Inc., 1999.
28. Jain, A. K., Duin, R. P. W., and Mao, J. Statistical pattern recognition: a review. *IEEE Trans. Pattern Anal. Machine Intell.*, **22**: 4–37, 2000.
29. Adali, T., Wang, Y., and Li, H. Neural networks for biomedical signal processing. In: Y.-H. Hu and J.-N. Huang (eds.), *Handbook of Neural Network Signal Processing*, in press. Boca Raton, FL: CRC Press, Inc., 2001.
30. Ripley, B. *Pattern Recognition and Neural Networks*. Cambridge, U.K.: Cambridge University Press, 1996.
31. RNALater Tissue Collection. RNA Stabilization Solution. In: Ambion Protocols and Manuals. Austin, TX: Ambion, 2001.
32. Eberwine, J. Amplification of mRNA populations using aRNA generated from immobilized oligo(dT)-T7 primed cDNA. *Biotechniques*, **20**: 584–591, 1996.
33. Ozyilkan, O., Baltali, E., Ozyilkan, E., Tekuzman, G., Kars, A., and Firat, D. Ceruloplasmin level in women with breast disease. Preliminary results. *Acta Oncol.*, **31**: 843–846, 1992.
34. Schapira, D. V., and Schapira, M. Use of ceruloplasmin levels to monitor response to therapy and predict recurrence of breast cancer. *Breast Cancer Res. Treat.*, **3**: 221–224, 1983.
35. Peterson, J. A., Hamosh, M., Scallan, C. D., Ceriani, R. L., Henderson, T. R., Mehta, N. R., Armand, M., and Hamosh, P. Milk fat globule glycoproteins in human milk and in gastric aspirates of mother's milk-fed preterm infants. *Pediatr. Res.*, **44**: 499–506, 1998.
36. Klinge, C. M., Kaur, K., and Swanson, H. I. The aryl hydrocarbon receptor interacts with estrogen receptor α and orphan receptors COUP-TFI and ERR α 1. *Arch. Biochem. Biophys.*, **373**: 163–174, 2000.
37. Daly, R. J., Sanderson, G. M., Janes, P. W., and Sutherland, R. L. Cloning and characterization of GRB14, a novel member of the *GRB7* gene family. *J. Biol. Chem.*, **271**: 12502–12510, 1996.
38. Gonzalez, M. A., Pinder, S. E., Wencyk, P. M., Bell, J. A., Elston, C. W., Nicholson, R. I., Robertson, J. F., Blamey, R. W., and Ellis, I. O. An immunohistochemical examination of the expression of E-cadherin, α - and β -catenins, and α_2 - and β_1 -integrins in invasive breast cancer. *J. Pathol.*, **187**: 523–529, 1999.
39. Wang, Y., Lu, J., Lee, R. Y., and Clarke, R. Iterative normalization of cDNA microarray data. *IEEE Trans. Inf. Technol. Biomed.*, **6**: 29–37, 2002.
40. Lu, J., Wang, Y., Xuan, J., Kung, S. Y., Gu, Z., and Clarke, R. Discriminative mining of gene microarray data. *Proc. IEEE Neural Net. Signal Processing*, **11**: 218–227, 2001.
41. Heid, H. W., Winter, S., Bruder, G., Keenan, T. W., and Jarisch, E. D. Butyrophilin, an apical plasma membrane-associated glycoprotein characteristic of lactating mammary glands of diverse species. *Biochim. Biophys. Acta*, **728**: 228–238, 1983.
42. Sakurai, H., Miyoshi, H., Toriumi, W., and Sugita, T. Functional interactions of transforming growth factor β -activated kinase 1 with I κ B kinases to stimulate NF- κ B activation. *J. Biol. Chem.*, **274**: 10641–10648, 1999.
43. Shibuya, H., Yamaguchi, K., Shirakabe, K., Tonegawa, A., Gotoh, Y., Ueno, N., Irie, K., Nishida, E., and Matsumoto, K. TAB1: an activator of the TAK1 MAPKKK in TGF- β signal transduction. *Science (Wash. DC)*, **272**: 1179–1182, 1996.
44. Bokhholm, I. K., Nesland, J. M., and Borresen-Dale, A. L. Reexpression of E-cadherin, α -catenin and β -catenin, but not of γ -catenin, in metastatic tissue from breast cancer patients. *J. Pathol.*, **190**: 15–19, 2000.
45. Berger, T., Brigl, M., Herrmann, J. M., Vielhauer, V., Luckow, B., Schlondorff, D., and Kretzler, M. The apoptosis mediator mDAP-3 is a novel member of a conserved family of mitochondrial proteins. *J. Cell Sci.*, **113**: 3603–3612, 2000.
46. Levy-Strumpf, N., and Kimchi, A. Death-associated proteins (DAPs): from gene identification to the analysis of their apoptotic and tumor suppressive functions. *Oncogene*, **17**: 3331–3340, 1998.
47. Kunapuli, S. P., Singh, H., Singh, P., and Kumar, A. Ceruloplasmin gene expression in human cancer cells. *Life Sci.*, **40**: 2225–2228, 1987.
48. Trombino, A. F., Near, R. I., Matulka, R. A., Yang, S., Hafer, L. J., Toselli, P. A., Kim, D. W., Rogers, A. E., Sonenshein, G. E., and Sherr, D. H. Expression of the aryl hydrocarbon receptor/transcription factor (AhR) and AhR-regulated *CYP1* gene transcripts in a rat model of mammary tumorigenesis. *Breast Cancer Res. Treat.*, **63**: 117–131, 2000.
49. Nguyen, T. A., Hoivik, D., Lee, J. E., and Safe, S. Interactions of nuclear receptor coactivator/corepressor proteins with the aryl hydrocarbon receptor complex. *Arch. Biochem. Biophys.*, **367**: 250–257, 1999.
50. Yaegashi, S., Sachse, R., Ohuchi, N., Mori, S., and Sekiya, T. Low incidence of a nucleotide sequence alteration of the *neurofibromatosis 2* gene in human breast cancers. *Jpn. J. Cancer Res.*, **86**: 929–933, 1995.
51. Kanai, Y., Tsuda, H., Oda, T., Sakamoto, M., and Hirohashi, S. Analysis of the neurofibromatosis 2 gene in human breast and hepatocellular carcinomas. *Jpn. J. Clin. Oncol.*, **25**: 1–4, 1995.
52. Preiherr, J., Hildebrandt, T., Klostermann, S., Eberhardt, S., Kaul, S., and Weidle, U. H. Transcriptional profiling of human mammary carcinoma cell lines reveals PKW, a new tumor-specific gene. *Anticancer Res.*, **20**: 2255–2264, 2000.
53. Ugolini, F., Adelaide, J., Charafe-Jauffret, E., Nguyen, C., Jacquemier, J., Jordan, B., Birnbaum, D., and Pebusque, M. J. Differential expression assay of chromosome arm 8p genes identifies Frizzled-related (FRP1/FRZB) and fibroblast growth factor receptor 1 (FGFR1) as candidate breast cancer genes. *Oncogene*, **18**: 1903–1910, 1999.

Block principal component analysis with application to gene microarray data classification

Aiyi Liu^{1,*†}, Ying Zhang¹, Edmund Gehan¹ and Robert Clarke²

¹ Biostatistics Unit, Lombardi Cancer Center, Georgetown University Medical Center, 3800 Reservoir Road, NW, Washington, DC 20007, U.S.A.

² Department of Oncology, Lombardi Cancer Center, Georgetown University Medical Center, Washington, DC 20007, U.S.A.

SUMMARY

We propose a block principal component analysis method for extracting information from a database with a large number of variables and a relatively small number of subjects, such as a microarray gene expression database. This new procedure has the advantage of computational simplicity, and theory and numerical results demonstrate it to be as efficient as the ordinary principal component analysis when used for dimension reduction, variable selection and data visualization and classification. The method is illustrated with the well-known National Cancer Institute database of 60 human cancer cell lines data (NCI60) of gene microarray expressions, in the context of classification of cancer cell lines. Copyright © 2002 John Wiley & Sons, Ltd.

KEY WORDS: principal component analysis; grouping of variables; similarity; gene expression; microarray data analysis

1. INTRODUCTION

Principal component analysis is one of the most common techniques of exploratory multivariate data analysis. It is a method of transforming a set of p correlated variables $\mathbf{x} = (x_1, x_2, \dots, x_p)$ to a set of p uncorrelated variables $\mathbf{y} = (y_1, y_2, \dots, y_p)$ that are linear functions of the x 's, referred to as p principal components of \mathbf{x} , such that the variances of the y 's are in descending order with respect to the variation among the x 's. Usually the first several components explain most of the variation among the x 's. In addition to many other applications, principal component analysis has been shown to be a useful tool in reducing data dimension and extracting information, in seeking important regressors in regression analysis, and in effectively visualizing and clustering subjects, when measurements on a large number of variables are collected from each subject. The book by Jolliffe [1] provides excellent reading on this topic, although other textbooks on multivariate data analysis do also (for

* Correspondence to: Aiyi Liu, Biostatistics Unit, Lombardi Cancer Center S112, Georgetown University Medical Center, 3800 Reservoir Road, Washington, DC 20007, U.S.A.

† E-mail: Liua1@georgetown.edu

example, references [2] and [3]). Recently, principal component analysis has found application in the analysis of microarray gene expressions [4], a growing technology in human genome studies [5, 6].

When dealing with an extremely large number of variables (for example, 500 or more), deriving principal components can be computationally intensive, since it involves finding the eigenvectors (and eigenvalues) of a matrix with large dimensions. Moreover, a linear combination of such a large number of variables becomes less meaningful to the investigators since the high dimensionality makes it hard to extract useful information and to interpret the combination. In one microarray technology, cDNA clone inserts are printed onto a glass slide and then hybridized to two differentially fluorescently labelled probes. The final gene expression profile contains fluorescent intensities and ratio information of many hundreds or thousands of genes. If one intends to apply principal component analysis directly to extract gene expression information for these genes from a certain group of subjects, then one has to deal with a matrix with huge dimensions.

In dealing with such high dimensional data, we propose to perform the principal component analysis in a 'stratified' way. We first group the original variables into several 'blocks' of variables, in the sense that each block contains variables (genes in the microarray experiments) that are similar; variables from the same block are more correlated than variables from different blocks. We then perform principal component analysis within each block and obtain a small number of variance-dominating principal components. Combining these principal components obtained from each block forms a new database from which we can then extract information by performing a new principal component analysis. We term this procedure as '*block principal component analysis*'. Dominating principal components obtained from the final stage can then be used in various data exploratory analyses such as clustering and visualization.

The proposed 'block principal component analysis' method also enables us to reduce the number of variables effectively. Within each block, when principal component analysis is conducted and dominating linear combinations of variables are examined, only those variables that have relatively large coefficients are retained. We will examine this variable selection procedure in detail using the gene microarray example.

After a brief review of the mathematical derivation of principal components and their applications in Section 2, we introduce in Section 3 the method of 'block principal component analysis'. In Section 4, we investigate the efficiency of block principal components in the reduction of data dimension with respect to the amount of variance explained. It is shown that the proposed procedure can be as efficient as the ordinary principal component analysis. We then discuss the selection of informative variables using block principal component analysis. In Section 5 we apply the method to the problem of classification of microarray data from the well-known National Cancer Institute database of 60 human cancer cell lines (NCI60), each of which has gene microarray expression of more than 1000 genes [7]. Some discussion is given in Section 6.

2. PRINCIPAL COMPONENTS

We start with a brief mathematical derivation of principal components. More details can be found in references [1] or [2] and [3]. Throughout, vectors are viewed as column vectors, and A' is the transpose of a matrix A .

Consider a p -variate random vector \mathbf{X} with mean vector μ and positive definite covariance matrix Σ . Let $\lambda_1 \geq \lambda_2 \geq \dots \geq \lambda_p (> 0)$ be the eigenvalues of Σ and let $\mathbf{W} = (\mathbf{w}_1, \dots, \mathbf{w}_p)$ be a $p \times p$ orthogonal matrix such that

$$\mathbf{W}'\Sigma\mathbf{W} = \Lambda = \text{diag}(\lambda_1, \dots, \lambda_p) \quad (1)$$

so that \mathbf{w}_i is an eigenvector of Σ corresponding to the eigenvalue λ_i . Now put $\mathbf{U} = \mathbf{W}'\mathbf{X} = (U_1, \dots, U_p)'$; then $\text{cov}(\mathbf{U}) = \Lambda$, so that U_1, \dots, U_p are all uncorrelated, and $\text{var}(U_i) = \lambda_i$, $i = 1, \dots, p$. The linear components U_1, \dots, U_p are called principal components of \mathbf{X} . The first principal component is $U_1 = \mathbf{w}_1' \mathbf{X}$ and its variance is λ_1 ; the second principal component is $U_2 = \mathbf{w}_2' \mathbf{X}$ with variance λ_2 ; and so on. These p principal components have the following key property. The first principal component U_1 is the normalized (unit length) linear combination of the components of \mathbf{X} with the largest variance, and its maximum variance is λ_1 ; then out of all normalized linear combinations of the components of \mathbf{X} which are uncorrelated with U_1 , the second principal component U_2 has maximum variance λ_2 . In general, the k th principal component U_k has maximum variance λ_k , among all normalized linear combinations of the components of \mathbf{X} which are uncorrelated with U_1, \dots, U_{k-1} .

Very often these principal components are referred to as population principal components. In practice Σ is not known and has to be estimated from the sample, yielding the sample principal components. We do not distinguish these two definitions here.

Once the p principal components are derived, then we can conduct various statistical analyses using only the first $q (< p)$ principal components which account for most of the variance of \mathbf{X} . For example, we can plot the first two (three) principal components in a two- (three-) dimensional space to seek interesting patterns among the data, or perform clustering analysis on subjects in order to search for clusters among the data. We can also use these leading principal components as regressors in a regression analysis to find prognostic factors for clinical outcomes (for example, drug response or resistance). See reference [1] for various other applications of principal component analysis.

Derivation of principal components involves computation of eigenvalues and eigenvectors of the $p \times p$ matrix Σ (or its sample estimate). When p is very large, the computation will become extremely extensive. Moreover, it is always the interest of the investigators to examine the first several leading principal components in order to find useful information. With a linear combination of a large number of variables, this becomes extremely difficult and results are hard to interpret. To deal with these problems, we develop the 'block principal component analysis' method to be discussed in the following sections.

3. BLOCK PRINCIPAL COMPONENT ANALYSIS

Ordinary principal component analysis needs to find an orthogonal matrix \mathbf{W} such that $\mathbf{W}'\Sigma\mathbf{W}$ is diagonal. In a very extreme case when all of the components of \mathbf{X} are independent, the p principal components are the p components of \mathbf{X} , and \mathbf{W} is merely some permutation of the identity matrix, rearranging the components of \mathbf{X} according to their variances. If the random vector \mathbf{X} can be partitioned into k uncorrelated random subvectors, so that Σ has diagonal blocks, then performing principal component analysis with \mathbf{X} is equivalent to performing principal component analysis with each subvector and then combining all the principal components

from all subvectors. This simple fact leads to the consideration of 'block principal component analysis' even when \mathbf{X} does not have uncorrelated partitions.

Let \mathbf{X} be partitioned as $\mathbf{X} = (\mathbf{X}'_1, \dots, \mathbf{X}'_k)'$ with \mathbf{X}_i being p_i -dimensional, where $p_1 + \dots + p_k = p$, and Σ be partitioned accordingly as

$$\Sigma = \begin{pmatrix} \Sigma_{11} & \Sigma_{12} & \dots & \Sigma_{1k} \\ \vdots & \ddots & \ddots & \vdots \\ \vdots & \ddots & \ddots & \vdots \\ \Sigma_{k1} & \Sigma_{k2} & \dots & \Sigma_{kk} \end{pmatrix} \quad (2)$$

Let $\mathbf{W}_i = (\mathbf{w}_{i1}, \dots, \mathbf{w}_{ip_i})$, $i = 1, \dots, k$, be an $p_i \times p_i$ orthogonal matrix such that

$$\mathbf{W}'_i \Sigma_{ii} \mathbf{W}_i = \Lambda_i = \text{diag}(\lambda_{i1}, \dots, \lambda_{ip_i}), \quad \lambda_{i1} \geq \dots \geq \lambda_{ip_i} \quad (3)$$

so that \mathbf{w}_{ij} , $j = 1, \dots, p_i$, is an eigenvector of Σ_{ii} corresponding to the eigenvalue λ_{ij} . Put $\mathbf{U}_i = \mathbf{W}'_i \mathbf{X}_i = (U_{i1}, \dots, U_{ip_i})'$, then the p_i components U_{ij} , $j = 1, \dots, p_i$, of \mathbf{U}_i define the p_i principal components, referred to as 'block' principal components, with respect to the random vector \mathbf{X}_i , the i th block of variables of \mathbf{X} .

Now define

$$\mathbf{Q} = \text{diag}(\mathbf{W}_1, \dots, \mathbf{W}_k) \quad (4)$$

also an orthogonal matrix, and

$$\mathbf{Y} = \mathbf{Q}' \mathbf{X} = (\mathbf{U}'_1, \dots, \mathbf{U}'_k)' \quad (5)$$

a random vector combining all 'block' principal components, then

$$\text{cov}(\mathbf{Y}) = \Omega = \mathbf{Q}' \Sigma \mathbf{Q} = \begin{pmatrix} \Lambda_1 & \mathbf{W}'_1 \Sigma_{12} \mathbf{W}_2 & \dots & \mathbf{W}'_1 \Sigma_{1k} \mathbf{W}_k \\ \vdots & \vdots & \ddots & \vdots \\ \mathbf{W}'_k \Sigma_{k1} \mathbf{W}_1 & \mathbf{W}'_k \Sigma_{k2} \mathbf{W}_2 & \dots & \Lambda_k \end{pmatrix} \quad (6)$$

Note that Ω and Σ have the same eigenvalues, and in particular, $\text{tr}(\Omega) = \text{tr}(\Sigma)$, where tr stands for the trace (sum of all diagonal elements) of a matrix. Hence \mathbf{X} and \mathbf{Y} have equal total variance. Let \mathbf{W} be defined as in (1), and

$$\mathbf{R} = \mathbf{Q}' \mathbf{W} \quad (7)$$

then \mathbf{R} is also an orthogonal matrix and

$$\mathbf{R}' \text{cov}(\mathbf{Y}) \mathbf{R} = \mathbf{W}' \Sigma \mathbf{W} = \text{diag}(\lambda_1, \dots, \lambda_p) \quad (8)$$

that is, the p principal components of \mathbf{Y} are identical to those of \mathbf{X} .

Hence, we can obtain the principal components of a random vector \mathbf{X} by two steps. In the first step, we group the variables in \mathbf{X} into several blocks, and then derive principal components for each block of variables. In the second step, we define a new random vector \mathbf{Y} by combining all the 'block' principal components and then obtain the principal components of \mathbf{Y} , which are identical to the principal components of \mathbf{X} .

The geometrical interpretation of block principal component analysis is quite clear. The p -dimensional random vector \mathbf{X} represents the p axes in a p -dimensional space. The p principal components rotate the \mathbf{X} -space to one whose axes are defined by the p principal components. In order to rotate the original space to its desired direction, we can first group the axis and rotate the axis within each group and then do an overall rotation to achieve the desired direction.

From the mathematical derivation above, we notice that this procedure always yields the principal components of \mathbf{X} , regardless of how the blocks are defined. The choice of blocks, however, does have effects on several aspects. First, if the \mathbf{X} can be divided into uncorrelated blocks, then the components in \mathbf{Y} are the principal components of \mathbf{X} , and there is no need to orthogonalize \mathbf{Y} . Second, even when \mathbf{X} cannot be partitioned into uncorrelated blocks, if the off-diagonal terms $\mathbf{W}_i'\Sigma_{ij}\mathbf{W}_j$ are relatively small, as measured, say, by a matrix norm (for example, squared sum of squares of all elements), then without losing much information, we can still use the components of \mathbf{Y} as approximation to the principal components of \mathbf{X} . Third, when reduction in dimension and in the number of variables is conducted within each block, which will be discussed in the next section, we would expect that variables within each block are much more correlated than variables from two different blocks, so that selection of dimensions and of variables from one block will not be much affected by selection of variables from another block. For these reasons, we recommend grouping the variables into blocks according to their correlation. This can be achieved by clustering the variables using a proper function of Pearson's correlation coefficient as the measure of similarity between variables; one such measure is given in Section 5 of the paper.

4. DIMENSION REDUCTION AND VARIABLE SELECTION

4.1. Dimension reduction

A major application of principal component analysis is to reduce data dimension so that the data structures can be explored or even visualized in a low-dimensional space. When data dimension is extremely high, block principal component analysis allows us to reduce data dimension more effectively without losing much information. We propose the following procedure to achieve low dimension. Suppose k blocks, \mathbf{X}_i , with dimension p_i and covariance matrix Σ_{ii} , $i = 1, \dots, k$, of the original variables \mathbf{X} , are determined according to the correlation between variables. For each block \mathbf{X}_i we derive the p_i principal components, and retain only the first q_i ($< p_i$) principal components, say, U_{ij} , $j = 1, \dots, q_i$, so that the total variance explained by these q_i principal components is $\pi_i \text{tr}(\Sigma_{ii})$, where $0 < \pi_i < 1$. Now define

$$\hat{\mathbf{Y}} = (U_{11}, \dots, U_{1q_1}, \dots, U_{k1}, \dots, U_{kq_k})' \quad (9)$$

a variable combining all principal components selected from each block. We then obtain the principal components of $\hat{\mathbf{Y}}$, and choose the first f principal components, say Z_1, \dots, Z_f , which explain a high percentage of $100\hat{\pi}$ per cent (for example, $\hat{\pi} = 95$ per cent) of the total variance of $\hat{\mathbf{Y}}$. Data visualization and classification with the original variable \mathbf{X} is then conducted based on these f principal components.

These block principal components preserve many optimal properties of the ordinary principal components: (i) Z_1, \dots, Z_f are uncorrelated; and (ii) $\text{var}(Z_1) \geq \dots \geq \text{var}(Z_f)$. However, these variances are no longer the eigenvalues of Σ , the covariance matrix of the original

variables \mathbf{X} . Instead, they are the eigenvalues of the covariance matrix of $\tilde{\mathbf{Y}}$; (iii) the total variance of Z_1, \dots, Z_f is

$$\tilde{\pi} \operatorname{tr}[\operatorname{cov}(\tilde{\mathbf{Y}})] = \tilde{\pi} \sum_{i=1}^k \left[\sum_{j=1}^{q_i} \operatorname{var}(U_{ij}) \right] = \tilde{\pi} \sum_{i=1}^k \pi_i \operatorname{tr}(\Sigma_{ii})$$

which accounts for 100π per cent of the total variance of \mathbf{X} , where

$$\pi = \frac{\tilde{\pi} \sum_{i=1}^k \pi_i \operatorname{tr}(\Sigma_{ii})}{\operatorname{tr}(\Sigma)} = \frac{\tilde{\pi} \sum_{i=1}^k \pi_i \operatorname{tr}(\Sigma_{ii})}{\sum_{i=1}^k \operatorname{tr}(\Sigma_{ii})}$$

We hence have

$$\pi \geq \tilde{\pi} \min\{\pi_i\} \quad (10)$$

When using principal components to explore (for example, cluster, visualize) the data, we expect that the leading components explain most of the variance so that they will reveal the true nature of the data structure; (10) asserts that block principal components Z_1, \dots, Z_f will retain most of the variance if, within each block and for the final principal component analysis, the selected principal components explain most of the variance. For example, if $\pi_i \geq 95$ per cent, $i = 1, \dots, k$ and $\tilde{\pi} > 95$ per cent, then $\pi > 90$ per cent.

4.2. Variable selection

When the number p of variables is very large, many variables can be highly correlated with each other and some may become redundant when the rest are being used to explore data structure. For example, in a gene microarray experiment where gene expression of a large number of genes is obtained for a number of tissues, tissue classification based on all genes may be quite similar to that based on a small group of genes. If this is the case, then with respect to tissue classification, only these genes are informative and the rest become redundant, assuming that using all the genes indeed captures the real structure of the data. It is therefore important to select variables that contain almost all information, with respect to certain statistical properties, that all variables would contain.

Block principal component analysis can be used to select these variables. We propose the following two steps:

- Step 1. Divide the original variable \mathbf{X} into k blocks, \mathbf{X}_i , $i = 1, \dots, k$, according to correlation between variables.
- Step 2. For each block \mathbf{X}_i , conduct principal component analysis and select the first q_i leading principal components such that the total variance of \mathbf{X}_i is explained by a satisfactory amount, say, at least 95 per cent. Examine the coefficients (or loadings in many principal component analysis literatures) of the variables in \mathbf{X}_i in these q_i leading components and retain only those variables with large coefficients. Combine all the variables selected from each block and then use only these variables for further analysis.

A third step may also be useful if the number of variables selected is still too large:

- Step 3. Conduct principal component analysis again, but based only on the variables selected in step 2. Select the first several leading principal components to explain most of the

variance. Then examine the variables again and retain those with large coefficients in these leading combinations.

There is no universal criterion for how many and which variables should be selected from the leading principal components. Jolliffe [1] recommended choosing a variable from each leading principal component with the largest absolute coefficient, if the variable has not been selected from previous leading components. In practice some modifications of Jolliffe's procedure may also be effective. For example, one can choose several variables from each leading principal component with the largest absolute coefficients. For more discussion, see reference [1].

In the next section, we demonstrate the block principal component analysis method using the well-known NCI60 human cancer cell-line data [7] to select a group of genes to visualize/cluster the cell lines. The result shows such selection to be quite effective.

5. APPLICATION TO GENE MICROARRAY ANALYSIS: AN EXAMPLE

The NCI60 database contains expression of more than 9000 genes of 60 human cancer cell lines from nine types of cancer including colorectal, renal, ovarian, breast, prostate, lung and central nervous system, as well as leukaemia and melanomas. Gene expression levels are expressed as $-\log(\text{ratio})$, where ratio = the red/green fluorescence ratio after computational balancing of the two channels. Readers are referred to reference [7] for more details. The data have been made public for analysis on the authors' web site <http://discover.nci.nih.gov>. To get familiar with the DNA microarray technology, readers are referred to references [5] and [6] for more information.

One of the objectives of this study is to explore the relationship between gene profiles and cancer phenotypes. Scherf *et al.* [7] used a clustering analysis method to study the relationship. They provide the clustering tree of the 60 cell lines, based on 1376 genes, and showed that most of the cell lines cluster together according to their phenotypes (see Figure 2a of reference [7].) One important question is whether a smaller group of genes can preserve the same relationship structure.

We use a selection method based on block principal component analysis, as described in Section 4, to tackle this issue. For simplicity, we study only cell lines from three types of cancer, colorectal (7 cell lines), leukaemia (6 cell lines) and renal (8 cell lines); each cell line has microarray expression of the same 1416 genes. The data set of interest, 21 cell lines (being the subjects) and 1416 genes (being the variables), hence form a 21×1416 matrix, representing 21 data points (21 rows of the matrix) in a 1416-dimensional data space. The complete-linkage clustering tree based on these 1416 genes is shown in Figure 1(a). The dendrogram is consistent with that in reference [7], and shows clearly that the 21 cell lines cluster according to their cancer phenotypes. The readers are reminded that phenotype information is not used in the clustering, but only to validate the clustering results. One renal cell line marked as 'RE8', which is farther from the rest of renal cell lines, has been recognized to have some special feature (see reference [7] for detail).

We now seek to determine the blocks for the 1416 genes. Figure 2 shows a plot of semi-partial R^2 versus the number of clusters using complete-linkage algorithm and $d_{ij} = \arccos(|\rho_{ij}|)$ as a measure of dissimilarity between gene i and gene j , where ρ_{ij} is the Pearson correlation

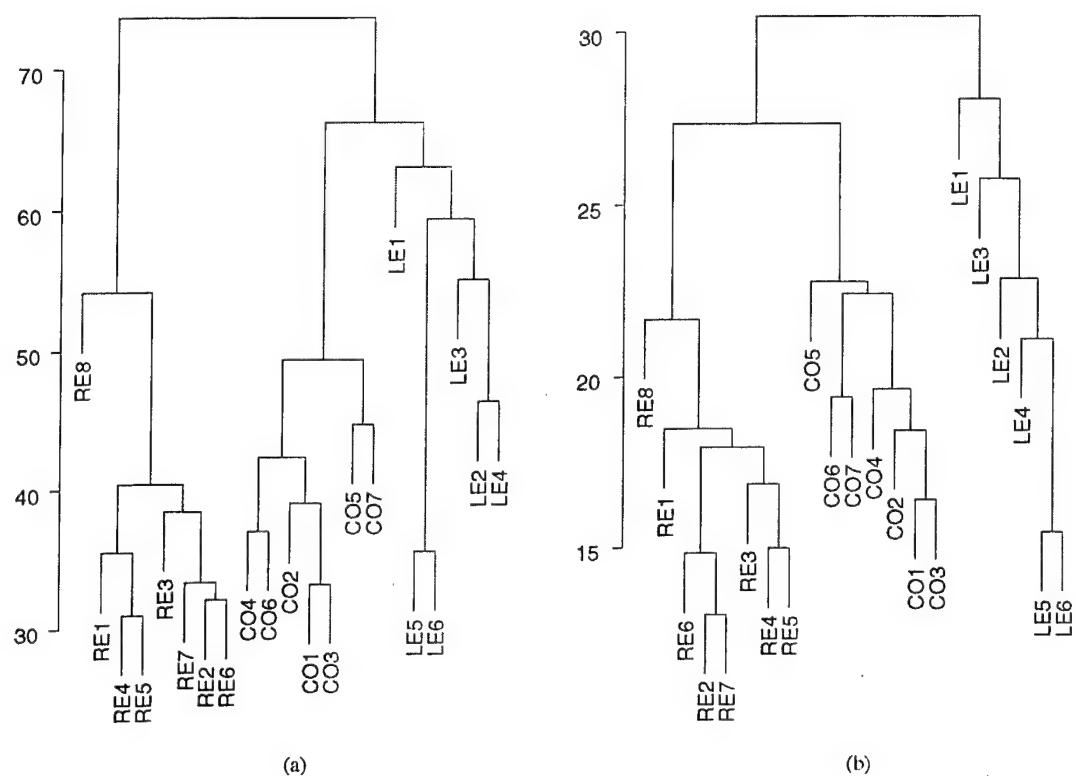


Figure 1. Dendrogram of complete linkage hierarchical clustering of 21 cell lines: (a) tree based on 1416 genes; (b) tree based on 200 genes. CO is colorectal, LE is leukaemia and RE is renal.

coefficient. The semi-partial R^2 measures the loss of homogeneity when two clusters are merged. Define SS_T as the corrected total sum of squares of all subjects and summed over all variables. For a certain cluster C , let SS_C be the corrected total sum of squares of all subjects in cluster C summed over all variables. Then the semi-partial R^2 for combining two clusters C_1 and C_2 into one cluster C is $(SS_C - SS_{C_1} - SS_{C_2})/SS_T$. A large semi-partial R^2 indicates significant decrease in homogeneity. Since subjects within the same cluster should be similar, two clusters should not be combined as one cluster if the semi-partial R^2 is large. In practice we determine the number of clusters by minimizing the semi-partial R^2 ; a plot of the semi-partial R^2 versus the number of clusters is extremely helpful. More discussion and computation of semi-partial R^2 can be found in reference [8]. Other statistics can also be used to determine the number of clusters in the data. Milligan and Cooper [9] examined 30 procedures for determining the number of clusters, including several variations based on sum of squares.

For the cancer cell-line microarray data, the semi-partial R^2 becomes nearly flat after 14 clusters. This indicates that the 1416 genes can be approximately divided into 14 clusters; further dividing the data gains little in reducing heterogeneity. These clusters of genes determine the blocks within each of which principal component analysis will be conducted. The number of genes in the blocks ranges from 43 to 158 (Table I). Principal component analysis

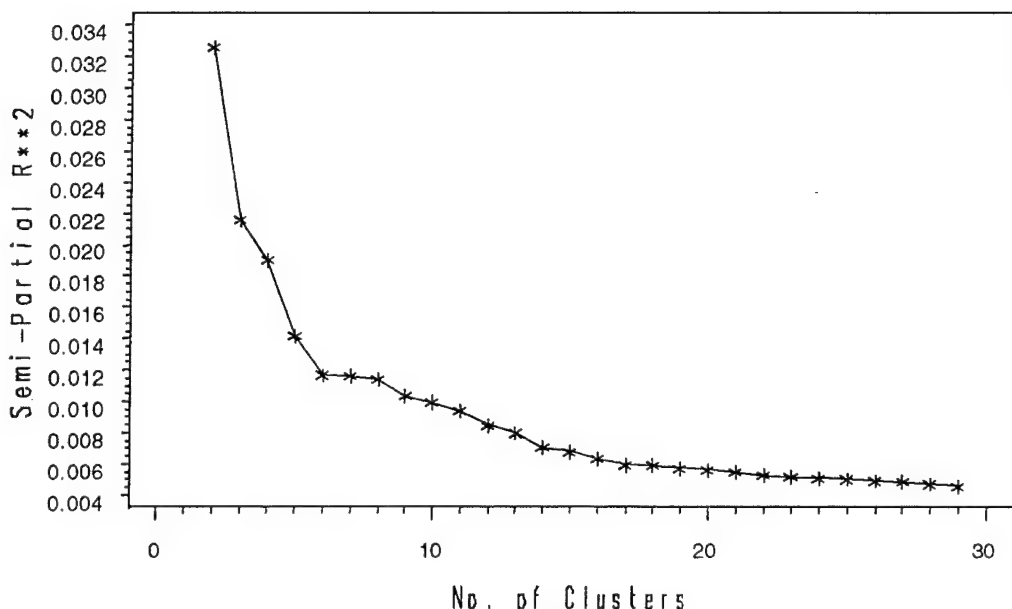
Figure 2. Determining number of blocks: plot of semi-partial R^2 .

Table I. Summary of 14 gene blocks.

	Block													
	1	2	3	4	5	6	7	8	9	10	11	12	13	14
Number of genes	107	154	88	158	68	152	84	136	44	84	143	82	73	43
Number of PCs	14	13	15	15	14	15	14	15	14	16	16	14	14	11
Per cent variance	95.6	95.3	95.2	95.3	95.2	96	95.1	95.2	96	96	95.1	96	95.6	95.6

is conducted within each block, and the first several leading principal components are then selected, resulting in a total of 200 principal components. For each block, selected principal components explain >95 per cent of total variance in that block. For each block, Table I lists the number of genes, the number of selected principal components and the percentage of total variance explained by these leading components.

For each block, genes with largest coefficients in the selected leading principal components are retained, using Jolliffe's one variable per leading component method. This yields a total of 200 genes for further analysis.

The first three leading principal components, computed based on the 1416 genes, explain only 49 per cent of the total variance. Two- or three-dimensional visualization of the data based on these principal components can be very misleading. We validate these selected 200 genes by deriving a hierarchical clustering tree for the 21 cell lines based on gene expressions. The dendrogram is shown in Figure 1(b). It is remarkably similar to the one based on all 1416 genes (Figure 1(a)). Both illustrate that cell lines with the same phenotype are more similar than those from different phenotypes. This shows that a much smaller number of genes

can provide the same insight for the data as the whole set of genes, and block principal component analysis provides an effective way to achieve this. Note that a hierarchical clustering dendrogram, obtained based on a set of variables, is essentially the same as the hierarchical clustering dendrogram obtained based on leading principal components, provided that these leading components explain most of the variation among the variables. The remarkable resemblance between Figure 1(a) and Figure 1(b) further demonstrates the effectiveness of the block principal component analysis method, as compared to the ordinary principal component analysis.

6. DISCUSSION

In this paper we show that a much smaller number of genes can provide the same insight for the cancer phenotypes as the whole set of genes. We demonstrate that block principal component analysis is an effective way to select these genes. This kind of analysis is 'unsupervised', a term popular in neural network/pattern recognition [10]; cancer phenotypes are used only to validate the algorithm and analysis.

Selection of informative genes in the microarray setting, and other settings as well, is by no means an easy task, especially when the analysis is unsupervised. Very likely the choices of genes are not unique; there might exist several groups of genes that provide the same classification. Biostatisticians should provide every potential group of genes to the medical investigators and hopefully a meaningful group of genes can be determined by combining the statistical guidance and biological knowledge. Indeed, some preliminary selection of genes based on biological knowledge is extremely valuable, even before any statistical analysis is conducted. It should be noted, however, that genes that are biologically similar/dissimilar may not be statistically similar (correlated)/dissimilar (uncorrelated).

ACKNOWLEDGEMENTS

The authors would like to thank the editor and three anonymous referees for their valuable comments and suggestions, which have improved the manuscript.

REFERENCES

1. Jolliffe IT. *Principal Component Analysis*. Springer-Verlag: New York, 1986.
2. Anderson TW. *An Introduction to Multivariate Statistical Analysis*. 2nd edn. Wiley: New York, 1984.
3. Rencher AC. *Methods of Multivariate Analysis*. Wiley: New York, 1995.
4. Hilsenbeck SG, Friedrichs WE, Schiff R, O'Connell P, Hansen RK, Osborne CK, Fuqua SA. Statistical analysis of array expression data as applied to the problem of tamoxifen resistance. *Journal of the National Cancer Institute* 1999; **91**:453–459.
5. Cheung VG, Morley M, Aguilar F, Massimi A, Kucherlapati R, Childs G. Making and reading microarrays. *Nature Genetics Supplement* 1999; **21**:15–19.
6. Brown PO, Botstein D. Exploring the new world of the genome with DNA microarrays. *Nature Genetics Supplement* 1999; **21**:33–37.
7. Scherf W, Ross DT, Waltham M, Smith LH, Lee JK, Tanabe L, Kohn KW, Reinhold WC, Myers TG, Andrews DT, Scudiero DA, Eisen MB, Sausville EA, Pommier Y, Botstein D, Brown PO, Weinstein JN. A gene expression database for the molecular pharmacology of cancer. *Nature Genetics* 2000; **24**:236–244.
8. Khattree R, Naik DN. *Multivariate Data Reduction and Discrimination with SAS Software*. SAS Institute Inc.: Cary, NC, 2000.
9. Milligan G, Cooper MC. An examination of procedures for determining the number of clusters in a data set. *Psychometrika* 1985; **50**:159–179.
10. Ripley RD. *Pattern Recognition and Neural Networks*. Cambridge University Press: Cambridge (UK), 1996.

C-7 Analogues of Progesterone as Potent Inhibitors of the P-Glycoprotein Efflux Pump

Fabio Leonessa,¹ Ji-Hyun Kim,¹ Alem Ghiorghis,¹ Robert J. Kulawiec,¹ Charles Hammer,¹ Abdelhossein Talebian,^{1,8} and Robert Clarke*,^{1,7}

Departments of Oncology, Physiology and Biophysics, and Lombardi Cancer Center, Georgetown University School of Medicine, 3970 Reservoir Road Northwest, Washington, DC 20007, and Department of Chemistry, Georgetown University, 37th and O Streets Northwest, Washington, DC

Received March 20, 2001

The P-glycoprotein product (Pgp) of the MDR1 gene has been implicated in the multiple drug resistance phenotype expressed by many cancers. Functioning as an efflux pump, P-glycoprotein prevents the accumulation of high intracellular concentrations of substrates. We have taken a rational approach to designing inhibitors of P-glycoprotein function, selecting a natural substrate (progesterone) as our lead compound. We hypothesized that progesterone, substituted at C-7 with an aromatic moiety(s), would exhibit reduced Pgp affinity, significantly increased antiPgp activity, and reduced affinity for progesterone receptors (PGR). We synthesized 7 α -[4'-aminophenyl]thio]pregna-4-ene-3,20-dione (2), which comprises a C-7 α thiol bridge linking an aminophenyl moiety to progesterone, from pregn-4,6-diene-3,20-dione (1). The subsequent addition reaction of 2 with the appropriate isocyanate produced an initial series of compounds (3–6). Compounds 3–5 (respectively, $-\text{CH}_2\text{CH}_2\text{Cl}$; $-\text{CH}_2\text{CH}_3$; and $-\text{CH}(\text{CH}_3)\text{C}_6\text{H}_5$) exhibit a significantly increased ability to inhibit P-glycoprotein. Potency for restoring doxorubicin accumulation in MDR1-transduced human breast cancer cells is increased up to 60-fold as compared with progesterone. Compound 5 has greater potency than verapamil and is equipotent with cyclosporin A, for inhibiting P-glycoprotein function. Furthermore, 5 does not bind to PGR, implying a potential reduction in *in vivo* toxicity. These data identify C-7-substituted progesterone analogues and 5, in particular, as rationally designed antiPgp compounds worthy of further evaluation/development.

Introduction

While many cancers are initially responsive to cytotoxic chemotherapy, most acquire a resistant phenotype. This phenotype is often characterized by crossresistance to structurally unrelated drugs to which the tumor has not been exposed. The precise genes that confer this multidrug resistance phenotype are unknown, but there are several strong single-gene candidates. These include several ABC transporters including the P-glycoprotein product of the MDR1 gene (Pgp; gp170),¹ the lung resistance protein,² the breast cancer resistance protein,³ and several members of the multidrug resistance associated protein family.^{4,5} The precise contribution of each potential multidrug resistance mechanism is unclear. Indeed, more than one mechanism may operate, either within the same tumor cell subpopulation and/or within different subpopulations of the same tumor.

We have chosen to study Pgp-mediated multiple drug resistance. Pgp confers resistance to drugs by preventing their accumulation within the cell. Pgp's efflux capabilities appear to reflect its ability to bind substrates within the inner leaflet of the plasma membrane.⁶ Subsequently, and in a potentially adenosine 5'-triphosphate (ATP)-dependent manner, substrates are

expelled from the cell.⁷ We have shown by meta analysis that Pgp expression is detected in $\geq 50\%$ of breast cancers and that this expression is associated with prior chemotherapy, a worse than partial response to chemotherapy, and *in vitro* resistance to Pgp substrates.⁸ These data suggest that where Pgp expression is detected, it likely contributes to multiple drug resistance in some breast cancers. Nonetheless, the likely role of Pgp in conferring drug resistance remains controversial.

The poor activity of current antiPgp agents in patients has been attributed to the presence of resistance factors in addition to Pgp, inappropriate design of clinical trials, toxicity, and/or lack of specificity of antiPgp reagents. The ability of reversing agents to alter the pharmacokinetics of the coadministered cytotoxic drugs, and an inability to achieve adequate levels of some reversing agents, also are problematic.⁹ The absence of a series of nontoxic drugs, specifically designed to reverse Pgp, limits the design of clinical trials to reverse this form of multidrug resistance.

One aspect of the controversy regarding the role of Pgp comes from the relatively poor activity of those few Pgp reversing agents evaluated in clinical trials. Most attention has focused on the Pgp reversing agents verapamil, cyclosporin A, and its nonimmunosuppressive analogue PSC833 (valsphodar), but the activity of other drugs also has been studied in patients. Few of these compounds were designed as Pgp inhibitors. Thus, severe side effects, often related to either the "normal" function of these agents and/or their ability to influence

* To whom correspondence should be addressed. Tel: (202)687-3755. Fax: (202)687-7505. E-mail: clarke@georgetown.edu.

¹ Departments of Oncology, Physiology and Biophysics, and Lombardi Cancer Center, Georgetown University School of Medicine.

² Department of Chemistry, Georgetown University.

³ Deceased.

additional targets, may be induced at concentrations required to affect Pgp function. Many antiPgp drugs affect the pharmacokinetics of the substrate, significantly increasing cytotoxic drug-induced toxicity.¹⁰ Other antiPgp agents cannot readily be delivered at doses that produce adequate serum levels. For example, the serum levels of verapamil required to produce *in vitro* reversal of Pgp resistance are rarely achieved in patients, despite administering sufficient doses of verapamil to induce significant cardiotoxicity.^{9,11,12} Adequate serum trifluoperazine levels are not reached in patients at doses that induce dose-limiting toxicities.^{9,13} Peak plasma levels of the stereoisomer of *cis*-flupenthixol (*trans*-flupenthixol) are 1000-fold less than that necessary to achieve full chemosensitization *in vitro*.^{14,15} Several clinical studies have used patient populations where tumor Pgp expression is unknown, complicating a clear determination of its contribution to multiple drug resistance.

Previously, we have established cellular breast cancer models in which to study Pgp-mediated efflux and evaluate inhibitors of this activity. These models have been generated by inducing a constitutive expression of Pgp, following transduction with retroviral gene expression vectors.^{16,17} The major advantage of these models is that unlike cells selected for resistance *in vitro*, Pgp expression is the only mechanism present to produce the multiple drug resistance phenotype. For example, the widely used MCF7^{ADR} cells, which were selected *in vitro* for resistance to doxorubicin (DOX) and recently redesignated NCI/ADR-RES,¹⁸ exhibit increased glutathione transferase and topoisomerase II activities.^{19,20} Differences in the potency of isomers of flupenthixol identified in MCF7^{ADR} cells could not be confirmed in MDR1-transfected NIH 3T3 cells.¹⁵

Using our cellular models, we now describe an initial series of progesterone analogues that exhibit significantly increased antiPgp activity as compared with progesterone and verapamil and comparable to that seen with cyclosporin A. Importantly, the most potent of these analogues has lost its ability to activate progesterone receptors (PGR) and is predicted to exhibit relatively low intrinsic toxicity *in vivo*.

Chemistry

Conceptualization and Design. We wished to take a rational, structure-function-based approach to design inhibitors of Pgp function. Initially, we hypothesized that a natural substrate for the pump could provide an ideal candidate for rational drug design, since it is likely that Pgp evolved specifically to efflux such molecules. Evidence shows that several molecules with a steroid nucleus are Pgp substrates.^{21–23} Pgp is expressed in the uterus^{23,24} and the placenta,²⁵ suggesting a natural role for protecting secretory cells from the toxic effects of high local concentrations of steroids. Progesterone is the most potent of the steroids, including progesterone's metabolites, for reversing the effects of Pgp expression.^{23,26,27} Progestins have intrinsically lower toxicity than other reversing agents and are orally active. In addition, progesterone is readily available and cheap, and the chemistry for generating several structural modifications is relatively straightforward.^{28,29} Thus, we chose progesterone as our lead compound.

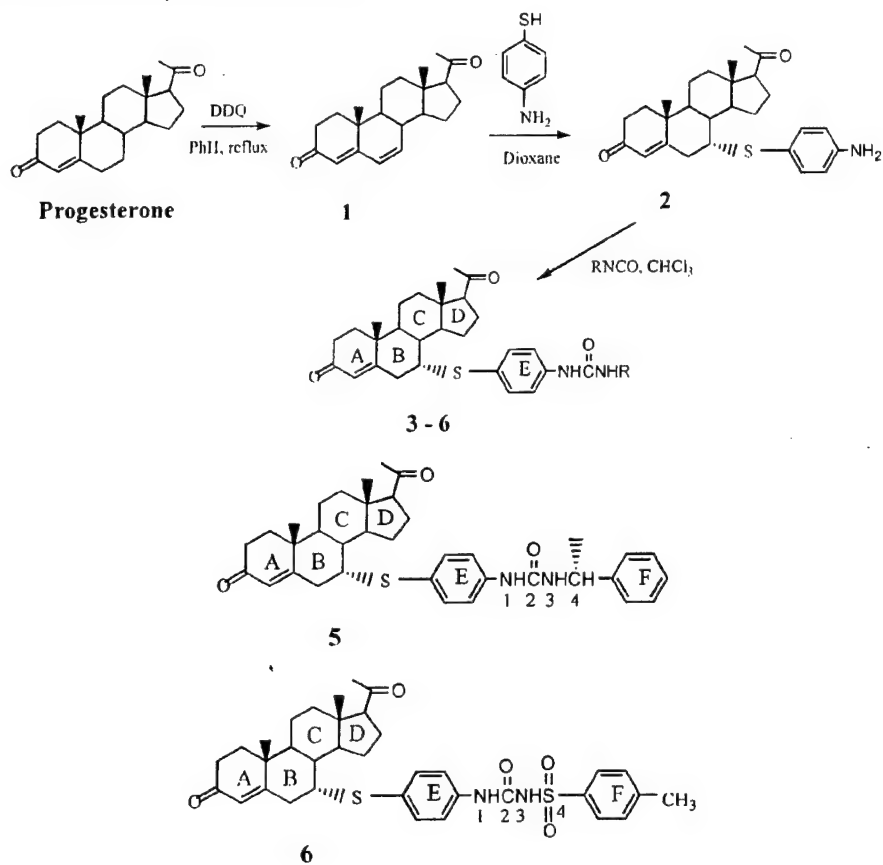
The major beneficial properties we wished to confer included but were not restricted to (i) improved potency for Pgp reversal, (ii) either no change or a reduction in affinity for PGR, and (iii) no agonist (mitogenic) activities. Concurrently, we wished to avoid either a substantial increase in PGR binding or a loss of Pgp reversing potency.

Unfortunately, the precise structure-function characteristics of Pgp reversing agents are unknown. This is not surprising, given the remarkable structural diversity of Pgp substrates.³⁰ Nonetheless, several characteristics are apparent, providing generic guidelines for the design of Pgp reversing agents. Lipophilicity appears central, with increased lipophilicity strongly associated with increased antiPgp activity.^{31–37} Planar aromatic rings are commonly found in substrates, and these may contribute to lipophilicity.³⁷ Amphipathicity also is common, as is the presence of a basic amine, where primary amines appear most effective.^{31,33,35,36,38} Size, for example, as determined by calculated molar refractivity, appears an important factor in several classes of compounds.^{32,35,39} C21-aminosteroids have a structural similarity to progesterone, and in these compounds, the steroid moiety, lipophilicity, and amphipathicity are considered important attributes.⁴⁰ For compounds composed of two structures joined by a molecular spacer, the length of the spacer seems important.^{15,31,34,41,42} This suggests that some part of the molecule may be oriented into a "pocket" in Pgp.³¹ This pocket may have specific requirements for lipophilicity, size, and charge.

A C-7 addition to the steroid 17 β -estradiol, as occurs in the antiestrogens ICI 182,780 and ICI 164,384, produces compounds with low toxicity and potentially appropriate pharmacokinetics.^{43,44} Limited evidence suggests that ICI 164,384 can reverse Pgp-mediated resistance,⁴⁵ despite the apparent inability of 17 β -estradiol to do so.²³ Thus, a bulky C-7 substitution on a steroid nucleus might increase antiPgp activity. C-7-substituted progesterone analogues were synthesized 20 years ago, but several exhibit antiprogestational activity.⁴⁶ Data from these studies suggest that bulky additions at C-7, when these include an aromatic ring, reduce PGR affinity by approximately 10–1000-fold.⁴⁶ Consequently, it may be possible to reduce the endogenous toxicity of progesterone by reducing/eliminating its ability to bind PGR.

On the basis of the various structure-function observations noted above, we hypothesized that progesterone, substituted at C-7 with an aromatic moiety(s), would exhibit both reduced Pgp affinity and significantly increased antiPgp activity. Thus, we designed an initial compound from which we could derive an appropriate series of progesterone analogues for evaluation. This compound, 7 α -[4'-(aminophenyl)thio]pregna-4-ene-3,20-dione (2), has a C-7 thiol bridge linking an aminophenyl moiety to progesterone. Subsequent additions to the amine with the appropriate isocyanate generated the corresponding Pgp analogues. For our initial series of compounds, we selected isocyanates that would provide analogues with predicted differences in the size, lipophilicity, and charge of their C-7 additions.

Synthesis. Compound 1 (Scheme 1) was prepared from progesterone by a modified Turner and Ringold's

Scheme 1. Synthesis of C-7 Progesterone Analogues**Table 1.** Structure and Physical Properties of C-7 Progesterone Analogues^a

compd	R	mp (deg)	R _f ^b
2	N/A	228–230	0.23
3	–CH ₂ CH ₂ Cl	137–141	0.47
4	–CH ₂ CH ₃	130–135	0.36
5	–CH(CH ₃)C ₆ H ₅	146–149	0.46
6	–SO ₂ C ₆ H ₄ CH ₃	128–132	0.29

^a See Scheme 1 for the structures of 2–6. ^b R_f in hexane–ethyl acetate (2:3).

method,^{47–49} using 2,3-dichloro-5,6-dicyano-1,4-benzoquinone (DDQ) as an oxidizing agent and *p*-toluenesulfonic acid (*p*-TsOH) in refluxing benzene via Dean–Stark distillation. Purification of the crude 1 on silica gel gives 6-dehydroprogesterone (1) as a yellow solid (35%, R_f = 0.44, 2:3 hexanes–ethyl acetate, mp = 143–145 °C). Reaction of compound 1 with 4-aminothiophenol and NaOH pellets, in degassed dioxane as solvent for 6 days at 74 °C, provided 7α-[4'-aminophenyl]thio]pregna-4-ene-3,20-dione (2) as an ivory solid. Crude crystals of 2 were precipitated from a mixture of hexanes–ethyl acetate and purified by flash column chromatography to yield 790 mg of white solid (61%, R_f = 0.23, 2:3 hexanes–ethyl acetate, mp = 228–230 °C).

The additional C-7 progesterone analogues (3–6) were obtained by reacting compound 2 with the appropriate isocyanate (Table 1). The general reaction was performed under a N₂ atmosphere for 12 h, until no 2 was detected by thin-layer chromatography (TLC), and the solvent was removed under reduced pressure. All crude

analogues were purified by flash column chromatography to yield the corresponding ureas as a white solid (40–83%). The physical properties of these analogues are provided in Table 1 as mp and R_f on silica gels (2:3 hexanes–ethyl acetate).

Results and Discussion

Substrate Accumulation Studies. Because Pgp is an efflux pump, we measured the ability of our compounds to influence the intracellular accumulation of the cytotoxic drugs vinblastine (VBL) and DOX. Both drugs are widely used clinically and are efficiently effluxed by Pgp.⁵⁰ Activity was evaluated in MDR1-transduced human breast cancer cells (MDA435/LCC6^{MDR1}), using the parental cells (MDA435/LCC6) as the Pgp-negative control. Potency of the compounds was compared with that of progesterone and the established Pgp inhibitors verapamil and cyclosporin A. VBL content in Pgp-positive cells, exposed to media containing 5 nM [³H] VBL, was approximately 6-fold lower than in parental Pgp-negative cells. Cellular content of DOX, in cells exposed to 4 μM DOX, was about 8-fold lower in the presence than in the absence of Pgp.

Results of VBL and DOX accumulation studies, summarized in terms of EC₅₀, are presented in Table 2. Because these data were estimated from dose response curves, representative curves are shown in Figure 1. Treatment with progesterone analogues 3–6 reverses the difference in VBL and DOX content between Pgp-positive and Pgp-negative cells. Analogues 3–5 exhibit significantly increased antiPgp potency as compared

Table 2. Potency of C-7 Progesterone Analogues, Progesterone, Verapamil, and Cyclosporin A in Reversing the Difference in VBL and DOX Accumulation between Pgp-Negative and Pgp-Positive Cells

compd	reversal of [³ H] VBL accumulation		reversal of DOX accumulation	
	EC ₅₀ μ M ^a (relative potency) ^b	Pgp-specific EC ₅₀ μ M (relative potency)	EC ₅₀ μ M (relative potency)	Pgp-specific EC ₅₀ μ M (relative potency)
progesterone	18.7 \pm 3.7 ^d (1)	21.0 \pm 4.2 (1)	22.3 \pm 2.0 (1)	42.2 \pm 7.2 (1)
3	0.8 \pm 0.2 (22.5)	0.9 \pm 0.2 (23.5)	0.6 \pm 0.1 (40.5)	0.7 \pm 0.2 (60.2)
4	1.3 \pm 0.1 (14.2)	1.5 \pm 0.2 (14.0)	0.7 \pm 0.07 (31.3)	1.0 \pm 0.06 (42.7)
5	0.8 \pm 0.2 (24.5)	0.7 \pm 0.2 (28.2)	0.6 \pm 0.07 (37.2)	0.9 \pm 0.09 (44.8)
6	34.8 \pm 8.6 (0.5)	33.4 \pm 5.2 (0.6)	14.7 \pm 3.2 (1.5)	37.0 \pm 6.5 (1.1)
verapamil	1.2 \pm 0.2 (16.1)	3.1 \pm 0.9 (6.8)	2.4 \pm 0.3 (9.2)	4.1 \pm 0.5 (10.2)
cyclosporin A	0.6 \pm 0.06 (32.5)	0.6 \pm 0.06 (32.5)	0.5 \pm 0.1 (41.9)	0.7 \pm 0.2 (60.6)

^a EC₅₀ = drug concentration that reduces the difference in drug accumulation between MDA435/LCC6 and MDA435/LCC6^{MDR1} cells by 50%; obtained by interpolation on dose response curves. Representative curves are shown in Figures 1 ([³H] VBL) and 2 (DOX). ^b Values in parentheses represent the potency of each compound relative to the lead compound progesterone. ^c Pgp-specific EC₅₀ = data corrected for any effect of test compound on drug accumulation in MDA435/LCC6 (Pgp-negative) cells. ^d Values represent the mean \pm SE obtained from at least three independent experiments.

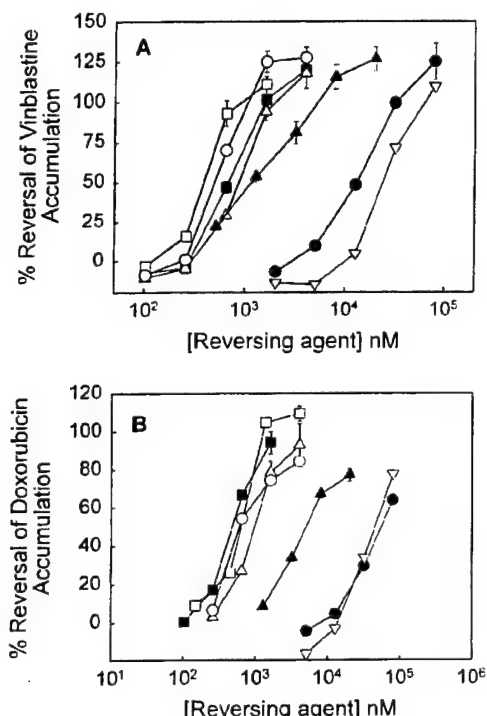


Figure 1. Ability of C-7 progesterone analogues to affect [³H] VBL accumulation (A) and DOX accumulation (B) in MDA435/LCC6 and MDA435/LCC6^{MDR1} cells. Data (mean \pm SE) are from one of three or more representative experiments used to obtain the ED₅₀ values presented in Table 2. Progesterone = ●, cyclosporin A = ○, verapamil = ▲, 3 = ■, 4 = △, 5 = □, and 6 = ▽.

with progesterone, being 14–60-fold more potent. In marked contrast, **6** is only equipotent with progesterone. Three compounds (**3–5**) are significantly more potent than verapamil, when Pgp-specific EC₅₀s are compared for both VBL and DOX accumulation. Compounds **3** and **5** were equipotent with cyclosporin A ($p > 0.05$ for all comparisons). Recently, we have established a chromatographic approach for assessing relative Pgp binding affinities.^{51,52} Studies to measure the affinity of these analogues are in progress.

While **3** and **5** tend to be slightly more potent than **4**, the difference is not statistically significant. This suggests that addition of either a Cl (**3**) or a second aromatic ring (**5**) does not further increase activity. In marked contrast, the presence of the sulfonyl group in **6** elimi-

nates the gain in activity conferred by the C-7 moiety. Thus, the increased activity in **5** is not simply due to the presence of an aromatic F ring (Scheme 1). Further structural modifications will allow us to test further the structure–activity relationships of C-7 progesterone analogues for Pgp reversal.

A major problem with many existing antiPgp compounds is their intrinsic toxicity. We wished to obtain an *in vitro* assessment of the toxicity of our compounds relative to progesterone, verapamil, and cyclosporin A. We used our breast cancer cell models because they do not express PGR and would provide a simple model for assessing PGR-independent cytotoxicity. Furthermore, any reduction in toxicity seen in the MDA435/LCC6^{MDR1} cells, as compared with the MDA435/LCC6 cells (relative resistance of Pgp-positive cells in Table 3), would suggest that the compounds were Pgp substrates, not simply Pgp inhibitors. Results are summarized in terms of IC₅₀ in Table 3; representative dose response curves are shown in Figure 2.

To estimate relative activity, each drug's intrinsic cytotoxicity was expressed relative to its antiPgp activity (IC₅₀/EC₅₀; Table 3). We did not detect cytotoxicity for compounds **4** and **5**, due to their low solubility, rendering our ratios underestimates based on the highest (noncytotoxic) concentration tested. Nonetheless, **4** produces ~40% inhibition of proliferation at 20 μ M. In marked contrast, 20 μ M **5** does not inhibit proliferation significantly in either untreated cells or MDA435/LCC6 and MDA435/LCC6^{MDR1} cells.

When adjusted for cytotoxicity, cyclosporin A and progesterone exhibit approximately equivalent relative activities. The low estimates for cyclosporin A reflect its substantial toxicity. Compound **6** is the least active compound, and **5** is the most active despite the overestimation of its cellular toxicity. While VBL and DOX may have different recognition sites in Pgp,⁵³ **5** shows broadly comparable activity against both drugs, as does cyclosporin A.

Having established that the C-7 addition significantly increased antiPgp activity, we wished to evaluate the PGR activity of our best compound. Overall, **3** and **5** have antiPgp activity comparable to cyclosporin A. Because **3** exhibits significant cellular toxicity, we chose to evaluate the relative affinity of **5** for binding to PGR. We compared the ability of **5**, progesterone, and unlabeled ORG2058, a synthetic progestin, to compete with [³H] ORG2058 for binding to PGR. The data in Figure

Table 3. Growth Inhibitory Activity of C-7 Progesterone Analogue, Progesterone, Verapamil, and Cyclosporin A on MDA435/LCC6 (Pgp Positive) and MDA435/LCC6^{MDR1} (Pgp Negative) Human Breast Cancer Cells

compd	IC ₅₀ μ M		relative resistance of Pgp-positive cells ^b	IC ₅₀ /EC ₅₀ ^c	
	MDA435/LCC6 (relative cytotoxicity) ^a	MDA435/LCC6 ^{MDR1} (relative cytotoxicity)		VBL activity	DOX activity
progesterone	27.4 \pm 7.9 ^d (1.0)	36.4 \pm 8.3 (1.0)	1.4 \pm 0.09	1.3	0.6
3	3.2 \pm 0.09 (8.5)	7.3 \pm 2.5 (5.0)	2.2 \pm 0.7	3.6	3.2
4	>20.0 (ND) ^e	>20.0 (ND)	ND	>13.3	>20.0
5	>20.0 (ND)	>20.0 (ND)	ND	>28.6	>22.2
6	22.1 \pm 1.6 (1.2)	38.2 \pm 0.2 (1.0)	1.7 \pm 0.1	0.7	0.6
verapamil	65.8 \pm 0.04 (0.4)	63.4 \pm 1.2 (0.6)	1.0 \pm 0.02	21.2	16.0
cyclosporin A	1.0 \pm 0.5 (26.9)	1.1 \pm 0.2 (33.6)	1.3 \pm 0.4	1.7	1.4

^a Relative cytotoxicity = ability of compounds to inhibit cell growth relative to progesterone. ^b Relative resistance of Pgp-positive = ratio of toxicity in resistant and control cells. Relative resistance > 1 suggests that the compound is at least partly effluxed by Pgp. ^c This ratio relates the effect of each drug on either VBL or DOX accumulation to its intrinsic cellular toxicity; higher ratios suggest a greater degree of safety. ^d Values represent the mean \pm SE obtained from at least three independent experiments. ^e ND = no data; an IC₅₀ was not reached at the highest concentration tested (limited by solubility). Some values (>) are underestimates based on nontoxic concentrations.

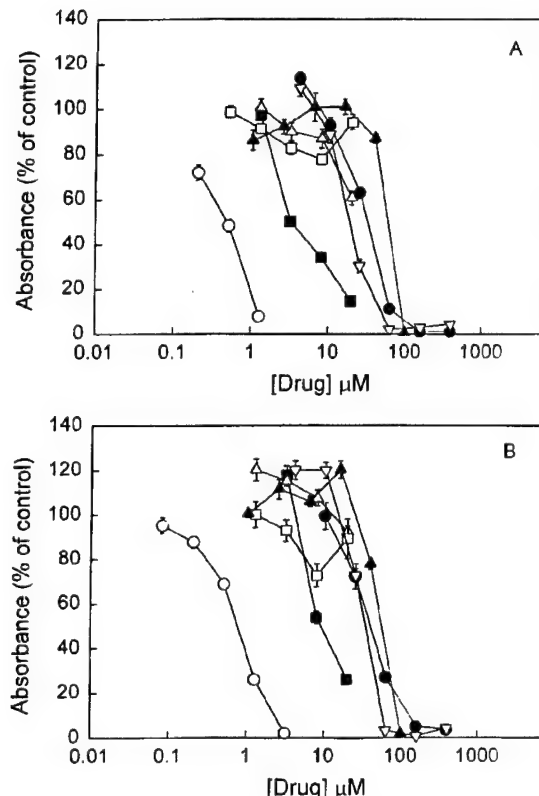


Figure 2. Cytotoxicity of progesterone analogues in MDA435/LCC6 (A) and MDA435/LCC6^{MDR1} cells (B). Data (mean \pm SE) are from one of three or more representative experiments used to obtain the IC₅₀ values presented in Table 3. Progesterone = ●, cyclosporin A = ○, verapamil = ▲, 3 = ■, 4 = △, 5 = □, and 6 = ▽.

3 show that **5**, at concentrations up to its EC₅₀, does not significantly compete with ORG2058. This represents a reduction of >100-fold in its PGR affinity as compared with ORG2058. Thus, **5** has antiPgp activity comparable to cyclosporin A, exhibits potentially low intrinsic cellular toxicity, and does not bind to its predicted cellular target (PGR) at its EC₅₀ for inhibition of Pgp activity.

Conclusions

While we cannot draw definitive structure-activity conclusions, some potentially useful preliminary obser-

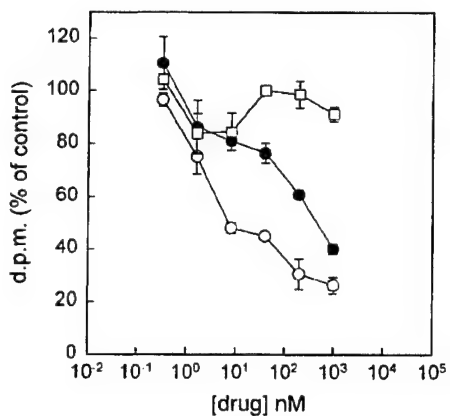


Figure 3. Competitive binding of progesterone, ORG2058, and 5 to PGR. [³H] ORG2058 was used as the radiolabeled ligand. Progesterone = ●, ORG2058 = ○, and 5 = □.

vations can guide future studies. The molecules are clearly amphiphatic, with lipophilicity greatest around the "E" and/or "F" rings and the polarity greatest around C-17–C-21. These observations suggest that effective substrates may concurrently interact with both hydrophilic and hydrophobic regions. However, it is not clear whether these are both in Pgp as previously suggested³¹ or whether they represent pockets at the plasma membrane/Pgp interface. The possibility that drugs are removed from within the plasma membrane⁶ may favor the model that invokes a plasma membrane component to the binding interaction.

Compounds **3–5** are significantly more potent than progesterone at specifically increasing Pgp substrate accumulation. These observations are consistent with our initial hypothesis that aromatic C-7 substitutions of progesterone will increase activity and with the known contribution of aromatic moieties in other modulating agents.^{37,42} Compound **6** also contains a C-7 aromatic addition but is essentially equipotent with progesterone. Perhaps the simplest explanation is that this compound is the least lipophilic of the analogues, since lipophilicity appears to be a major factor in the activity of other Pgp substrates.^{31–35}

The significant increase in potency observed with compounds **3–5** supports our initial structure–function-based hypothesis, based on previous published observations. The activity of our existing compounds already compares well with that of cyclosporin A. C-7 progest-

erone analogues have the potential to provide more potent, selective, and safe inhibitors of Pgp function than others that have currently completed clinical trials. We believe that the observations reported here, combined with the lack of receptor binding activity, identify **5** as the next logical lead compound for further development and provide valuable clues for the further optimization of this structure. We are currently synthesizing a larger series of compounds to further optimize the MDR1 reversing potency and effectively define the structure-activity relationships of these compounds.

Our ability to increase the potency of progesterone up to 60-fold (**3**; Pgp-specific EC₅₀ for DOX accumulation) supports the use of relatively limited structure-function data in the design of effective antiPgp compounds. Furthermore, by including structure-activity information on the binding characteristics of the lead's natural intracellular target (PGR) in our conceptualization, we reduced affinity of **5** for a target that could produce toxicity in normal cells. We are now poised to evaluate our compounds *in vivo*, to pursue further modifications that may increase antiPgp activity, and to explore the structure-activity relationship for C-7 progestrone analogues in detail. Overall, the data in this study identify C-7-substituted progestrone analogues and **5**, in particular, as rationally designed antiPgp compounds worthy of further evaluation/development.

Experimental Section

Chemistry. General Procedures. All reactions were carried out under an atmosphere of nitrogen using standard Schlenk techniques.⁵⁴ Benzene and chloroform were distilled from CaH₂, stored over 3D molecular sieves, and deaerated by purging with nitrogen immediately before use. TLC was performed using Merck glass plates precoated with F₂₅₄ silica gel 60; compounds were visualized by UV and/or with *p*-anisaldehyde stain solution. Flash chromatography was performed using EM Science silica gel 60, following the procedure of Still,⁵⁵ with the solvent mixtures indicated. Melting points were measured on a Thomas-Hoover capillary melting point apparatus and are uncorrected (Table 1). The broad melting points for compounds **3–6** suggest the presence of minor impurities. All reagents were purchased from commercial suppliers and used as received unless indicated otherwise. Dioxane was purchased from Aldrich in Sure-Seal bottles.

Nuclear magnetic resonance (NMR) spectra were measured on Nicolet NT 270 and Varian Mercury 300 MHz instruments at the Georgetown NMR Facility. Chemical shifts are reported in units of parts per million relative to Me₄Si. All spectra are recorded in CDCl₃. Significant ¹H NMR data are tabulated in the following order: multiplicity (s, singlet; d, doublet; t, triplet; q, quartet; m, multiplet), coupling constants in Hertz, and number of protons. ¹³C NMR spectra were recorded at frequencies of 67.9 and 75.6 MHz. Infrared (IR) spectra were measured on a MIDAC Corp. or a Mattson Galaxy 2020 Series FTIR, as neat films; absorption bands are reported in cm⁻¹. Low-resolution mass spectra were measured on a Fisons Instruments MD 800 quadrupole mass spectrometer, with 70 eV electron ionization and a GC 8000 Series gas chromatograph inlet, and using a J & W Scientific DB-5MS column (15 m length, 0.25 mm internal diameter, 0.25 μ m film thickness). Mass spectra data are given as mass-to-charge ratio, with the relative peak height following in parentheses. All new compounds were characterized by ¹H NMR, IR, and ¹³C NMR spectroscopies. Fast atom bombardment mass spectra (FABMS) were recorded at the University of Maryland College Park of Mass Spectrometry Facility. Literature references are given for all known compounds, except for those that are commercially available; all known compounds were identified by

¹H NMR spectroscopy. Elemental analysis was performed by Atlantic Microlab (Norcross, GA).

Pregna-4,6-diene-3,20-dione (1). Compound **1** was prepared by the method of Tuner and Ringold.^{47,49} Thus, *p*-TsOH monohydrate (11.0 g, 63.9 mmol) was dehydrated in freshly distilled benzene (320 mL) by azeotropic refluxing using a Dean-Stark trap. After 1 h, the solution was cooled for 0.5 h, and progesterone (5.0 g, 15.9 mmol) and DDQ (4.6 g, 20.3 mmol) were added. The olive mixture was refluxed for 3 h and then filtered through a pad of Celite. The filtrate was washed with saturated NaCl (5 \times 20 mL) followed by 1% NaOH solution until it gave clear solution and dried over anhydrous MgSO₄. Solvent was removed under reduced pressure, and the filtrate was purified by chromatography; 1.69 g of product (35%, *R*_f = 0.44, 2:3 hexanes-ethyl acetate); yellow solid (mp = 143–145 °C). ¹H NMR: δ 6.12 (s, 1H), 5.69 (s, 1H), 2.84–1.12 (complex, 12H), 2.17 (s, 3H), 2.14 (s, 3H), 1.12 (s, 3H), 1.10 (s, 1H), 1.00 (s, 1H), 0.72 (s, 3H). IR: 3855, 3745, 3678, 2953, 1700, 1663, 1457, 1361, 1223, 875, 754.

7a-[4'-(Aminophenyl)thio]pregna-4-ene-3,20-dione (2). We obtained **2** using the method of Brueggemeier et al.⁵⁶ Briefly, **1** (1.65 g, 5.28 mmol), 4-aminothiophenol (1.32 g, 10.56 mmol), and NaOH (pellet, 116 mg, 2.9 mmol) were placed in a Schlenk tube, which was purged with a constant flow of N₂(g). Deoxygenated anhydrous dioxane (25 mL) was added and heated at 74 °C for 6 days. The mixture was concentrated under reduced pressure and purified by chromatography; 790 mg white solid (61%, *R*_f = 0.23, 2:3 hexanes-ethyl acetate); mp = 228–230 °C. ¹H NMR: δ 7.26–7.21 (q, *J* = 8.5 Hz, 2H), 6.64–6.61 (q, *J* = 8.5 Hz, 2H), 5.73 (s, 1H), 3.77 (s, 2H), 3.24 (s, 1H), 2.14 (s, 3H), 2.63–1.10 (complex, 11H), 1.19 (s, 3H), 0.69 (s, 3H). IR: 3420, 3360, 3250, 2930, 1700. ¹³C NMR: δ 209.3, 199.0, 167.6, 147.1, 136.6, 127.3, 121.2, 115.7, 63.4, 17.7, 13.1.

General Procedure for the Preparation of Progesterone Analogues. A suspension of **2** in degassed chloroform was treated with the appropriate isocyanates under N₂. The mixture was stirred for 12 h and then chromatographed directly on silica gel to afford the corresponding ureas as oil. The resulting oil was stirred in anhydrous ether until white powder came out.

7a-[4'-(N-Chloroethylaminoacylaminophenyl)thio]pregna-4-ene-3,20-dione (3). Reaction of **2** (0.10 g, 0.23 mmol) with 2-chloroethylisocyanate (38 μ L, 0.46 mmol) in CHCl₃ (3.0 mL) for 12 h gave 50 mg of product (40%, mp = 137–141 °C, *R*_f = 0.47, 2:3 hexanes-ethyl acetate). ¹H NMR: δ 7.34–7.25 (m, 4H), 5.69 (s, 1H), 5.18 (s, 1H), 3.68–3.62 (m, 4H), 3.38 (s, 1H), 2.64–0.84 (complex, 18H), 2.14 (s, 3H), 1.19 (s, 3H), 0.69 (s, 3H). IR: 3312, 2964, 1700, 1630, 1587, 1517, 1488, 1449, 1394, 1238, 1013, 831, 734. ¹³C NMR: δ 231.5, 210.3, 196.2, 193.9, 181.9, 156.5, 149.3, 146.4, 141.4, 132.9, 125.1, 119.5, 118.5, 103.2, 94.2, 75.9, 75.8, 71.9, 69.3, 49.0, 35.8, 24.2, 14.4. MS: *m/e* = 543 (24, M⁺ + 1), 507 (10), 313 (27), 230 (23), 185 (50), 149 (69), 125 (57), 119 (23), 107 (38), 105 (48), 91 (50), 81 (50), 57 (73), 55 (100). HRMS: calcd for C₃₀H₄₃N₂O₃SCl [M + H]⁺, 543.24481; found, 543.24248. Anal. Calcd for (C₃₀H₄₄O₃N₂SCl): C, 66.22; H, 7.41; N, 8.82; S, 6.52. Found: C, 66.38; H, 7.27; N, 8.78; S, 6.28.

7a-[4'-(N-Ethylaminoacylaminophenyl)thio]pregna-4-ene-3,20-dione (4). Reaction of **2** (0.10 g, 0.23 mmol) with ethylisocyanate (37 μ L, 0.46 mmol) in CHCl₃ (3.0 mL) for 12 h gave 78 mg of product (67%, mp = 130–135 °C, *R*_f = 0.36, 2:3 hexanes-ethyl acetate). ¹H NMR: δ 7.36–7.25 (m, 4H), 6.38 (s, 1H), 5.69 (s, 1H), 4.18–4.03 (m, 2H), 3.38–3.26 (m, 2H), 2.67–0.68 (complex, 17H), 2.14 (s, 3H), 2.05 (s, 2H), 1.20 (s, 3H), 0.69 (s, 3H). IR: 3855, 3745, 3678, 3373, 2953, 2359, 1700, 1663, 1539, 1457, 1223. ¹³C NMR: δ 228.5, 222.5, 193.9, 171.5, 141.5, 135.0, 128.3, 127.0, 123.4, 118.5, 108.7, 96.2, 84.5, 69.3, 67.7, 66.0, 62.6, 52.2, 48.4, 46.3, 43.9, 39.8, 34.1, 22.9, 21.2, 13.4. MS: *m/e* = 509 (62, M⁺ + 1), 438 (8), 313 (32), 196 (47), 125 (100), 117 (57), 97 (52), 95 (85), 79 (68), 71 (59). HRMS: calcd for C₃₀H₄₄N₂O₃SCl [M + H]⁺, 509.28378; found, 509.28372. Anal. Calcd for (C₃₀H₄₅O₃N₂S): C, 70.69; H, 8.11; N, 5.49; S, 6.29. Found: C, 70.46; H, 8.06; N, 5.52; S, 6.20.

7 α -[4'-(*N*- α -(+)-Methylbenzylaminoacylaminophenyl)-thio]pregna-4-ene-3,20-dione (5). Reaction of 2 (0.10 g, 0.23 mmol) with (*R*)-(+)- α -methylbenzylisocyanate (66 μ L, 0.46 mmol) in CHCl₃ (3.0 mL) for 12 h gave 56 mg of product (46%, mp = 146–149 °C, R_f = 0.46, 2:3 hexanes–ethyl acetate). ¹H NMR: δ 7.32–7.25 (m, 5H), 5.79–5.77 (m, 1H), 5.70–5.68 (s, 1H), 4.97–4.92 (m, 1H), 4.13–4.06 (m, 1H), 3.28 (s, 1H), 2.64–1.49 (complex, 7H), 2.14 (s, 3H), 1.45 (d, J = 9.3 Hz, 3H), 1.19 (s, 3H), 0.68 (s, 3H). IR: 3353, 3273, 2949, 2854, 2362, 2340, 1700, 1653, 1595, 1539, 1457, 1460, 1376, 1343, 1159, 1089, 916. ¹³C NMR: δ 209.4, 199.0, 167.6, 147.0, 136.6, 127.2, 121.2, 115.8, 63.4, 17.7, 13.1. MS: m/e = 585 (11, M⁺ + 1), 135 (12), 125 (20), 105 (100), 103 (22), 91 (29), 77 (22), 55 (26). HRMS: calcd for C₃₆H₄₄N₂O₃S [M + H]⁺, 585.31506; found, 585.31501. Anal. Calcd for (C₃₆H₄₅O₃N₂S): C, 73.81; H, 7.74; N, 4.78; S, 5.47. Found: C, 73.76; H, 7.79; N, 4.81; S, 5.39.

7 α -[4'-(*N*-*p*-Toluenesulfonylaminoacylaminophenyl)-thio]pregna-4-ene-3,20-dione (6). Reaction of 2 (0.10 g, 0.23 mmol) with *p*-toluenesulfonylisocyanate (59 μ L, 0.46 mmol) in CHCl₃ (3.0 mL) for 12 h gave 120 mg of product (83%, mp = 128–132 °C, R_f = 0.29, 2:3 hexanes–ethyl acetate). ¹H NMR: δ 8.38 (s, 1H), 7.88 (d, J = 8.4 Hz, 2H), 7.80 (d, J = 8.3 Hz, 2H), 7.37–7.25 (m, 4H), 5.70 (s, 1H), 3.36 (s, 1H), 2.67–1.13 (complex, 20H), 2.41 (s, 3H), 2.15 (s, 3H), 1.55 (m, 2H), 1.20 (s, 3H), 0.69 (s, 3H). IR: 3855, 3745, 2359, 1700, 1539, 1457, 1160, 1086, 668. ¹³C NMR: δ 198.6, 148.6, 141.4, 136.6, 134.6, 129.9, 129.7, 129.6, 127.7, 127.2, 126.4, 120.5, 118.5, 92.4, 76.1, 69.3, 63.3, 52.1, 51.1, 47.0, 46.3, 39.8, 39.4, 38.5, 38.1, 35.4, 34.0, 31.6, 23.7, 22.9, 21.8, 21.1, 17.9, 13.4. MS: m/e = 635 (29, M⁺ + 1), 313 (39), 155 (33), 135 (36), 125 (65), 119 (64), 91 (100), 85 (92), 77 (47), 59 (50), 47 (45). HRMS: calcd for C₃₅H₄₂N₂O₅S₂ [M + H]⁺, 635.26135; found, 635.26130. Anal. Calcd for (C₃₅H₄₃O₅N₂S₂): C, 66.11; H, 6.82; N, 4.41; S, 10.09. Found: C, 66.05; H, 6.79; N, 4.45; S, 10.02.

Pharmacology. Cell Lines. For the studies of antiPgp activity, we used cells transduced with a retroviral vector directing the constitutive expression of the Pgp gene (MDA435/LCC6^{MDR1}) and their parental, Pgp-negative, MDA435/LCC6 human breast cancer cells.¹⁷ Both MDA435/LCC6 and MDA435/LCC6^{MDR1} cells are estrogen receptor and PGR negative and grow as monolayer cultures in vitro and as rapidly proliferating solid tumors and malignant ascites in vivo in nude mice.¹⁷ We used MCF-7 human breast cancer cells⁵⁷ to measure binding to PGR. These cells were routinely grown in vitro in Improved Minimal Essential Media (Bioscience) containing 5% fetal bovine serum in a 5% CO₂/95% air atmosphere.

Substrate Accumulation Assays. Pgp reversing activity of all test agents was evaluated by measuring the ability of the agents to affect accumulation of DOX and VBL in MDA435/LCC6^{MDR1} (resistant) and MDA435/LCC6 (control) cells. Cells were plated at 2.5 \times 10⁵ cells/well into 24 well culture dishes, in routine growth media, and incubated at 37 °C. Forty-eight hours after they were plated, cells were treated by replacing growth media with media containing the test compounds at five different concentrations and either DOX (4 μ M) or [³H]VBL (5 nM). All treatments were carried out in triplicate. After 3 h of incubation, treatments were stopped by washing each well with 0.5 mL of ice-cold NaCl (0.15 M). Cells from reference wells in each plate were counted to enable accumulation to be corrected for cell number.

For the DOX accumulation assays, DOX was extracted from cell monolayers by adding 1.5 mL of 20% trichloroacetic acid to each well and incubating overnight at 4 °C in the dark. DOX concentrations in the extracts were evaluated fluorometrically. Thus, extracts were transferred into 13 mm \times 100 mm borosilicate glass tubes, placed in the 10 \times 10 rack of a Hitachi A3000 Autosampler and connected to a Hitachi F-4500 fluorescence spectrophotometer. Fluorescence was read at 500 nm excitation and 580 nm emission wavelengths. Concentrations of DOX were obtained by interpolation on a DOX standard curve and normalized on the extraction volume and number of cells per well. For the VBL accumulation assays, at the end of treatment, wells were rinsed with phosphate-buffered saline (0.5 mL/well) and left to dry at room temperature. Cell

monolayers were removed by trypsinization and diluted with 10 mL of scintillation fluid (Ultima Gold XR, Packard Bioscience, Meriden, CT). Drug accumulation was radiometrically assessed by scintillation spectrometry.

Results of substrate accumulation assays were plotted as cellular concentration of substrate against the concentration of the respective test compound. Pgp reversing potency was expressed as the EC₅₀, defined as the concentration of a test drug that reduced the difference in substrate accumulation between Pgp-negative and Pgp-positive cells by 50%. Progesterone and the standard Pgp reversing agents verapamil and cyclosporin A were used as positive controls and as a reference to establish relative potency.

Cytotoxicity. Twenty-four hours after they were plated in 96 well plates, MDA435/LCC6 and MDA435/LCC6^{MDR1} cells were exposed to growth media containing different concentrations of the test agents for 5 days. Cell cultures were then fixed/stained by incubation in a 0.5% (w/v) crystal violet solution in 25% methanol (v/v). After plates had dried, the dye was extracted in 0.1 M sodium citrate in 25% methanol (v/v) and absorbance was read at 540 nm using a microplate spectrophotometer. Absorbance directly correlates with cell number in this assay.⁵⁰ Cell survival curves were obtained by plotting absorbance values (as percent of untreated controls) against drug concentration. The toxicity of each drug was expressed as an IC₅₀, defined as the concentration inhibiting cell density by 50% at the end of the treatment period. To estimate the extent of resistance conferred by Pgp, the ratio of each drug's IC₅₀ in MDA435/LCC6^{MDR1} and MDA435/LCC6 cells (relative resistance of Pgp-positive cells) was used for those drugs that produced a detectable IC₅₀ value.

Radioligand Binding Studies. These were performed as previously described, using a whole cell competitive binding assay.^{57,58} Briefly, MCF-7 cells were grown in 24 well dishes and incubated at 37 °C with 100 nM hydrocortisone for 30 min, before determining PGR binding, to eliminate residual binding to glucocorticoid receptors. Subsequently, cells were incubated for 60 min at 37 °C with 5 nM [³H] ORG2058 (specific activity 50.6 Ci/mmol) in the absence or presence of increasing concentrations of unlabeled competitor (0.5 nM–1 μ M; progesterone, ORG2058, 5). Radioactivity was extracted into ethanol and measured in a liquid scintillation spectrometer.

Data Analysis. DOX accumulation and cytotoxicity dose response data were processed and graphed using SigmaPlot 4.0 (SPSS Science, Chicago, IL). EC₅₀ (DOX accumulation assays) and IC₅₀ values (cytotoxicity assays) were calculated by interpolation on the respective dose response curves. The EC₅₀ and IC₅₀ values reported in Tables 2 and 3 represent the mean and standard error (SE) obtained from at least three independent experiments. Descriptive statistics were obtained using SigmaStat 2.0 (SPSS Science).

Acknowledgment. This work was supported in part by the Department of Defense, United States Army Medical Research and Materiel Command, Award RP950649, and by a grant from the Susan G. Komen Breast Cancer Foundation, Award PDF 2000 186.

References

- Ueda, K.; Clark, D. P.; Chen, C. J.; Roninson, I. B.; Gottesman, M. M.; Pastan, I. The human multidrug resistance (MDR1) gene: cDNA cloning and transcription initiation. *J. Biol. Chem.* **1987**, *262*, 505–508.
- Pohl, G.; Filipits, M.; Suchomel, R. W.; Stranzl, T.; Delpisch, D.; Pirkner, R. Expression of the lung resistance protein (LRP) in primary breast cancer. *Anticancer Res.* **1999**, *19*, 5051–5055.
- Doyle, L. A.; Yang, W.; Abruzzo, L. V.; Krogmann, T.; Gao, Y.; Rishi, A. K.; Ross, D. D. A multidrug resistance transporter from human MCF-7 breast cancer cells. *Proc. Natl. Acad. Sci. U.S.A.* **1998**, *95*, 15665–15670.
- Noeter, K.; de la Riviere, B. G.; Look, N. P.; van Wingerden, K. E.; Henzen-Logmans, S. C.; Schepen, R. J.; Flens, M. J.; Klijn, J. G. M.; Stoter, G.; Fockens, J. A. The prognostic significance of expression of the multidrug resistance-associated protein (MRP) in primary breast cancer. *Br. J. Cancer* **1997**, *76*, 486–493.

- (5) Borst, P.; Evers, R.; Kool, M.; Wijnholds, J. A family of drug transporters: the multidrug resistance-associated proteins. *J. Natl. Cancer Inst.* **2000**, *92*, 1295–1302.
- (6) Raviv, Y.; Pollard, H. B.; Bruggemann, E. P.; Pastan, I.; Gottesman, M. M. Photosensitized labeling of a functional multidrug transporter in living drug-resistant tumor cells. *J. Biol. Chem.* **1990**, *265*, 3975–3980.
- (7) Nuti, S. L.; Mehdi, A.; Rao, U. S. Activation of the human P-glycoprotein ATPase by trypsin. *Biochemistry* **2000**, *39*, 3424–3432.
- (8) Trock, B. J.; Leonessa, F.; Clarke, R. Multidrug resistance in breast cancer: a meta analysis of MDR1/gp170 expression and its possible functional significance. *J. Natl. Cancer Inst.* **1997**, *89*, 917–931.
- (9) Murren, J. R.; Hait, W. N. Why have not we cured multidrug resistant tumors? *Oncol. Res.* **1992**, *1*, 1–6.
- (10) Horton, J. K.; Thimmaiah, K. N.; Houghton, J. A.; Horowitz, M. E.; Houghton, P. J. Modulation by verapamil of vincristine pharmacokinetics and toxicity in mice bearing human tumor xenografts. *Biochem. Pharmacol.* **1989**, *38*, 1727–1736.
- (11) Miller, T. P.; Grogan, T. M.; Dalton, W. S.; Speir, C. M.; Schepner, R. J.; Salmon, S. E. P-glycoprotein expression in malignant lymphoma and reversal of clinical drug resistance with chemotherapy plus high-dose verapamil. *J. Clin. Oncol.* **1991**, *9*, 17–24.
- (12) Dalton, W. S.; Grogan, T. M.; Meltzer, P. S.; Schepner, R. J.; Durie, B. G. M.; Taylor, C. W.; Miller, T. P.; Salmon, S. E. Drug-resistance in multiple myeloma and non-Hodgkin's lymphoma: detection of P-glycoprotein and potential circumvention by addition of verapamil to chemotherapy. *J. Clin. Oncol.* **1989**, *7*, 415–424.
- (13) Miller, R. L.; Bukowski, R. M.; Budd, G. T.; Purvis, J.; Weick, J. K.; Shepard, K.; Midha, K. K.; Ganapathi, R. Clinical modulation of doxorubicin resistance by the calmodulin-inhibitor, trifluoperazine: a phase I/II trial. *J. Clin. Oncol.* **1988**, *6*, 880–888.
- (14) Jorgenson, A.; Fredricson, O. K. Clopenthixol and flupenthixol depot preparations in outpatient schizophrenics. III. Serum levels. *Acta Psychiatr. Scand.* **1980**, *279*, 41–54.
- (15) Ford, J. M.; Bruggemann, E. P.; Pastan, I.; Gottesman, M. M.; Hait, W. N. Cellular and biochemical characterization of thioxanthenes for reversal of multidrug resistance in human and murine cell lines. *Cancer Res.* **1990**, *50*, 1748–1756.
- (16) Clarke, R.; Currier, S.; Kaplan, O.; Lovelace, E.; Boulay, V.; Gottesman, M. M.; Dickson, R. B. Effect of P-glycoprotein expression on sensitivity to hormones in MCF-7 human breast cancer cells. *J. Natl. Cancer Inst.* **1992**, *84*, 1506–1512.
- (17) Leonessa, F.; Green, D.; Licht, T.; Wright, A.; Wingate-Legette, K.; Lippman, J.; Gottesman, M. M.; Clarke, R. MDA435/LCC6 and MDA435/LCC6MDR¹: ascites models of human breast cancer. *Br. J. Cancer* **1996**, *73*, 154–161.
- (18) Scudiero, D. A.; Monks, A.; Sausville, E. A. Cell line designation change: multidrug-resistant cell line in the NCI anticancer screen. *J. Natl. Cancer Inst.* **1998**, *90*, 862–863.
- (19) Batist, G.; Tuple, A.; Sinha, B. K.; Katki, A. G.; Myers, C. E.; Cowan, K. H. Overexpression of a novel anionic glutathione transferase in multidrug-resistant human breast cancer cells. *J. Biol. Chem.* **1986**, *261*, 15544–15549.
- (20) Sinha, B. K.; Mimnaugh, E. G.; Rajagopalan, S.; Myers, C. E. Adriamycin activation and oxygen free radical formation in human breast tumor cells: protective role of glutathione peroxidase in adriamycin resistance. *Cancer Res.* **1989**, *49*, 3844–3848.
- (21) van Kalken, C. K.; Broxterman, H. J.; Pinedo, H. M.; Feller, N.; Dekker, H.; Larkelman, J.; Giaccone, G. Cortisol is transported by the multidrug resistance gene product P-glycoprotein. *Br. J. Cancer* **1993**, *67*, 284–289.
- (22) Wolf, D. C.; Horwitz, S. B. P-glycoprotein transports corticosterone and is photoaffinity-labeled by the steroid. *Int. J. Cancer* **1992**, *52*, 141–146.
- (23) Yang, C.-P. H.; DePinho, S. G.; Greenberger, L. M.; Arceci, R. J.; Horwitz, S. B. Progesterone interacts with P-glycoprotein in multidrug-resistant cells and in the endometrium of gravid uterus. *J. Biol. Chem.* **1989**, *264*, 782–788.
- (24) Arceci, R. J.; Croop, J. M.; Horwitz, S. B.; Housman, D. The gene encoding multidrug resistance is induced and expressed at high levels during pregnancy in the secretory epithelium of the uterus. *Proc. Natl. Acad. Sci. U.S.A.* **1988**, *85*, 4350–4354.
- (25) MacFarland, A.; Abramovich, D. R.; Ewen, S. W.; Pearson, C. K. Stage-specific distribution of P-glycoprotein in first-trimester and full-term human placenta. *Histochem. J.* **1994**, *26*, 417–423.
- (26) Naito, M.; Yusa, K.; Tsuruo, T. Steroid hormones inhibit binding of Vinca alkaloid to multidrug resistance related P-glycoprotein. *Biochem. Biophys. Res. Commun.* **1989**, *158*, 1066–1071.
- (27) Ichikawa-Igarashi, M.; Sumizawa, T.; Yoshimura, A.; Furukawa, T.; Hiramoto, S.; Sugita, M.; Akiyama, S.-I. Progesterone and its metabolites: the potent inhibitors of the transporting activity of P-glycoprotein in the adrenal gland. *Biochim. Biophys. Acta* **1993**, *1158*, 201–208.
- (28) Neef, G.; Beier, S.; Elger, W.; Henderson, D.; Wiechert, R. New steroids with antiprogestational and antiglucocorticoid activities. *Steroids* **1984**, *44*, 349–372.
- (29) Teutsch, G.; Philibert, D. History and perspectives of anti-progestins from the chemist's point of view. *Hum. Reprod.* **1994**, *9* (Suppl. 1), 12–31.
- (30) Ford, J. M.; Hait, W. N. Pharmacology of drugs that alter multidrug resistance in cancer. *Pharmacol. Rev.* **1990**, *42*, 155–199.
- (31) Hait, W. N.; Aftab, D. T. Rational design and pre-clinical pharmacology of drugs for reversing multidrug resistance. *Biochem. Pharmacol.* **1992**, *43*, 103–107.
- (32) Zamora, J. M.; Pearce, H. L.; Beck, W. T. Physical-chemical properties shared by compounds that modulate multidrug resistance in human leukemic cells. *Mol. Pharmacol.* **1988**, *33*, 454–462.
- (33) Granzen, B.; Graves, D. E.; Baguley, B. C.; Danks, M. K.; Beck, W. T. Structure–activity studies of amsacrine analogues in drug resistant human leukemia cell lines expressing either altered DNA topoisomerase II or P-glycoprotein. *Oncol. Res.* **1992**, *4*, 489–496.
- (34) Ford, J. M.; Prozialeck, W. C.; Hait, W. N. Structural features determining activity of phenothiazines and related drugs for inhibition of cell growth and reversal of multidrug resistance. *Mol. Pharmacol.* **1988**, *35*, 105–115.
- (35) Tang-Wai, D. F.; Brossi, A.; Arnold, L. D.; Gros, P. The nitrogen of the acetamido group of colchicine modulates P-glycoprotein-mediated multidrug resistance. *Biochemistry* **1993**, *32*, 6470–6476.
- (36) Klopman, G.; Srivastava, S.; Kolossvary, J.; Epand, R. F.; Ahmed, N.; Epand, R. M. Structure–activity study and design of multidrug reversal compounds by a computer automated structure evaluation methodology. *Cancer Res.* **1992**, *52*, 4121–4129.
- (37) Dellingen, M.; Pressman, B. C.; Calderon-Higginson, C.; Savaraj, N.; Tapiero, H.; Kolonias, D.; Lampidis, T. J. Structural requirements of simple cations for recognition by multidrug-resistant cells. *Cancer Res.* **1992**, *52*, 6385–6389.
- (38) Nogae, I.; Kohno, K.; Kikuchi, J.; Kuwano, M.; Akiyama, S.-I.; Kiue, A.; Suzuki, K.-I.; Yoshida, Y.; Cornwell, M.; Pastan, I.; Gottesman, M. M. Analysis of structural features of dihydro pyridine analogues needed to reverse multidrug resistance and to inhibit photoaffinity labeling of P-glycoprotein. *Biochem. Pharmacol.* **1989**, *38*, 519–527.
- (39) Horton, J. K.; Thimmaiah, K. N.; Harwood, F. C.; Kuttessch, J. F.; Houghton, P. J. Pharmacological characterization of N-substituted phenoxazines directed toward reversing *Vinca* alkaloid resistance in multidrug-resistance cancer cells. *Mol. Pharmacol.* **1993**, *44*, 552–559.
- (40) Abraham, I.; Wolf, C. L.; Sampson, K. E. Nonglucocorticoid steroid analogues (21-aminosteroids) sensitize multidrug-resistant cells to vinblastine. *Cancer Chemother. Pharmacol.* **1993**, *32*, 116–122.
- (41) D'hainaut, A.; Régnier, G.; Atassi, G.; Pierré, A.; Léonce, S.; Kraus-Berthier, L.; Prost, J.-F. New triazine derivatives as potent modulators of multidrug resistance. *J. Med. Chem.* **1992**, *35*, 2481–2496.
- (42) Pearce, H. L.; Safa, A. R.; Bach, N. J.; Winter, M. A.; Cirtain, M. C.; Beck, W. T. Essential features of the P-glycoprotein pharmacophore as defined by a series of reserpine analogues that modulate multidrug resistance. *Proc. Natl. Acad. Sci. U.S.A.* **1989**, *86*, 5128–5132.
- (43) Wakeling, A. E.; Dukes, M.; Bowler, J. A potent specific pure antiestrogen with clinical potential. *Cancer Res.* **1991**, *51*, 3867–3873.
- (44) Wakeling, A. E.; Bowler, J. Novel antiestrogens without partial agonist activity. *J. Steroid Biochem.* **1988**, *31*, 645–653.
- (45) Hu, X. F.; Nadalin, G.; De Luise, M.; Martin, T. J.; Wakeling, A.; Huggins, R.; Zaleberg, J. R. Circumvention of doxorubicin resistance in multi-drug resistant human leukaemia and lung cancer cells by the pure antiestrogen ICI 164384. *Eur. J. Cancer* **1991**, *27*, 773–777.
- (46) Beyer, B.; Terenius, L.; Counsell, R. E. Synthesis of potential anti-progestins. *Steroids* **1980**, *35*, 481–488.
- (47) Turner, A. B.; Ringold, H. J. Applications of high-potential quinones: the mechanism of dehydrogenation of steroid ketones by 2,3-dichloro-5,6-dicyanobenzoquinone. *J. Chem. Soc.* **1967**, (C), 1720–1730.
- (48) Darby, M. V.; Lovett, J. A.; Brueggemeier, R. W.; Groziak, M. P.; Counsell, R. E. 7a-substituted derivatives of androstanedione as inhibitors of estrogen biosynthesis. *J. Med. Chem.* **1985**, *28*, 803–807.

(49) Haynex, R. K.; Jackson, W. R.; Stragalinon, S. Conversion of enone into diones via allylpalladium complexes. *Aust. J. Chem.* **1980**, *33*, 1537–1544.

(50) Leonessa, F.; Jacobson, M.; Boyle, B.; Lippman, J.; McGarvey, M.; Clarke, R. The effect of tamoxifen on the multidrug resistant phenotype in human breast cancer cells: isobogram, drug accumulation and gp-170 binding studies. *Cancer Res.* **1994**, *54*, 441–447.

(51) Zhang, Y.; Leonessa, F.; Clarke, R.; Wainer, I. W. Development of an immobilized P-glycoprotein stationary phase for on-line liquid chromatographic determination of drug binding affinities. *J. Chromatogr., B* **2000**, *739*, 33–37.

(52) Lu, L.; Leonessa, F.; Clarke, R.; Wainer, I. W. Competitive and allosteric interactions in ligand binding to P-glycoprotein as observed on an immobilized P-glycoprotein liquid chromatographic stationary phase. *Mol. Pharmacol.* **2001**, *59*, 62–68.

(53) Gros, P.; Dhir, R.; Croop, J.; Talbot, F. A single amino acid substitution strongly modulates the activity and substrate specificity of the mouse mdr1 and mdr3 drug efflux pumps. *Proc. Natl. Acad. Sci. U.S.A.* **1991**, *88*, 7289–7293.

(54) Shriner, D. F.; Drezdon, M. A. *The Manipulation of Air-Sensitive Compounds*; Wiley: New York, 1986.

(55) Still, W. C.; Kahn, M.; Mitra, A. Rapid chromatographic technique for preparative separations with moderate resolution. *J. Org. Chem.* **1978**, *43*, 3, 2923–2925.

(56) Brueggemeier, R. W.; Floyd, E. E.; Counsell, R. E. Synthesis and biochemical evaluation of inhibitors of estrogen biosynthesis. *J. Med. Chem.* **1978**, *21*, 1007–1011.

(57) Clarke, R.; Brünner, N.; Katzenellenbogen, B. S.; Thompson, E. W.; Norman, M. J.; Koppi, C.; Paik, S.; Lippman, M. E.; Dickson, R. B. Progression from hormone dependent to hormone independent growth in MCF-7 human breast cancer cells. *Proc. Natl. Acad. Sci. U.S.A.* **1989**, *86*, 3649–3653.

(58) Clarke, R.; Morwood, J.; van den Berg, H. W.; Nelson, J.; Murphy, R. F. The effect of cytotoxic drugs on estrogen receptor expression and response to tamoxifen in MCF-7 cells. *Cancer Res.* **1986**, *46*, 6116–6119.

JM010126M